MOBILE MEASUREMENTS OF ULTRAFINE PARTICLES NEAR AN URBAN, ELEVATED, HIGH-TRAFFIC ROADWAY

A Thesis

Presented to the Faculty of the Graduate School

of Cornell University

In Partial Fulfillment of the Requirements for the Degree of

Master of Science in Atmospheric Science

by

Verena Mireille Joerger

May 2017

ABSTRACT

Ultrafine particles (UFP) have both health and climate impacts and are emitted in large quantities by vehicles. To further our understanding of how high-traffic roadways contribute to urban UFP concentrations, a mobile sampling strategy is developed to measure UFP on a perpendicular transect near interstate 81 (I-81) in Syracuse, New York. Measurements are taken during morning rush hour and non rush hour using a bicycle-mounted TSI Nanoscan scanning mobility particle sizer capable of measuring particles with diameters of 10 – 420 nm. UFP concentrations near I-81 are considerably lower and more variable than reported in previous studies. The spatial decay of UFP with distance from I-81 is examined, and a linear mixed-effects model is generated to determine the variables that influence near I-81 UFP concentrations. Temperature, sampling time, and distance are important predictors of near-I-81 UFP concentrations, but local UFP sources are evident and identification of such sources is explored.

BIOGRAPHICAL SKETCH

Verena Joerger was born in Newark, Delaware, USA and spent her formative years (kindergarten – 8th grade) at an alternative school, Newark Center for Creative Learning where her curiosity and love of learning were fostered. She attended Conrad Schools of Science in Wilmington, Delaware for high school, and completed an honors degree in environmental science (B.S.) from Sweet Briar College in Sweet Briar, Virginia, where she was awarded high honors for her thesis entitled, "Environmental Controls on Atmospheric New Particle Formation in Central Virginia". Following her interest in aerosols, Verena accepted an offer to study atmospheric science at Cornell University as a Master's student. Verena's passion for protecting the environment and people's health has motivated her to pursue a career at the Environmental Protection Agency, despite the current tumultuous and uncertain political climate.

ACKNOWLEDGMENTS

I am grateful for the guidance provided by my committee members, Sara C. Pryor, and Tom Whitlow. I would like to thank the Syracuse Center of Excellence, especially Chetna Chianese and Ed Bogucz for providing me with a desk space while doing fieldwork in Syracuse and for being so welcoming and supportive. Special thanks also goes out to Pat McHale at SUNY ESF for providing me with meteorological data from the Syracuse Center of Excellence tower, and Erika Mudrak in the Cornell Statistical Consulting Unit for her advice and input concerning some of the statistical tests used in this thesis. In addition, I would like to acknowledge funding support provided by the Cornell University Program in Cross-Scale Biogeochemistry and Climate, which is supported by NSF-IGERT and the Atkinson Center for a Sustainable Future, as well as NSF grants 1517365 and 1502400 (awarded to Sara C. Pryor).

Table of Contents

LIST OF FIGURES

LIST OF TABLES

CHAPTER 1: INTRODUCTION

1.1 Atmospheric Aerosol Particles

Atmospheric aerosol particles are any solids or droplets suspended in the atmosphere. These particles can impact climate (Charlson et al., 1992) and are associated with detrimental health impacts (Dockery et al., 1992). Climate forcing by aerosol particles can be direct through scattering and absorption of shortwave solar radiation (Charlson et al., 1991; Menon et al., 2002) or indirect by altering cloud properties (Lohmann and Feichter, 2005). The smallest aerosol particles (i.e., those with diameters < 100 nm) are referred to as ultrafine particulate matter (UFP) and may be particularly toxic to humans (Li et al., 2003). Exposure to UFP has been associated with an array of cardiovascular ailments. Inhalation of UFP can lead to inflammation, changes in autonomic regulation of the heart, and disruption of the ion channel functions of myocardial cells (Schulz et al., 2005). Due to the small size of UFP, these particles can be captured and transported to many parts of the body, including the brain (Oberdörster et al., 2004). Recent evidence even points to a connection between UFP and dementia and Alzheimer's disease (Underwood, 2017).

Aerosol particle size distributions (PSDs, i.e. the relative abundance of aerosol particles of different sizes) vary greatly in the atmosphere and are subject to a range of aerosol dynamic processes (summarized in Fig. 1-1). Aerosol particles enter the atmosphere either by direct emission or by new particle formation (nucleation). Newly formed particles and those that enter the atmosphere from primary particle emissions can grow through condensation of vapors, or by coagulation with other particles (Fig. 1-1).

Condensation does not change the number of particles in the PSD, but shifts the PSD to larger diameters, whereas coagulation decreases the aerosol particle number concentration and shifts the PSD towards larger diameters. These particles may be removed from the atmosphere via wet (precipitation removal, see Appendix A) or dry deposition (see explanations of aerosol particle dynamics given in Seinfeld and Pandis, 2006).

UFP dominate total number concentrations of particles (Fig. 1-1). They can originate from either biogenic or anthropogenic sources (Mäkelä et al., 1997; Morawska et al., 2008) and can be formed through primary or secondary pathways. Primary UFP are formed from direct sources such as soot from combustion processes and cooking (Buonanno et al., 2009). Secondary UFP are formed during a phase change of critical clusters of semi-volatile gases to the particle phase (Pryor et al., 2011). In North America, the mobile sector dominates anthropogenic UFP emissions (Paasonen et al., 2016), with the bulk of vehicle particle emissions being UFP (Fig. 1-2). However, there are variations in the chemical composition, size, and number concentration among different parts of the on-road fleet. For instance, particles from diesel engines range from 20-130 nm, while particles emitted by gasoline vehicles range from 20-60 nm (Morawska et al., 2008).

Currently, the U.S. Clean Air Act (United States Code 42) regulates the mass concentration of fine particulate matter with diameters less than 2.5 μm ($PM_{2.5}$), but does not regulate UFP number concentrations. $PM_{2.5}$ concentrations can be highly variable in urban environments (Sullivan and Pryor, 2014), and so having one or a few monitoring stations within a city may not be adequate to represent the actual human exposure to atmospheric particles. In addition, $PM_{2.5}$ measurements are mass-based and thus are only

weakly influenced by the number of UFP present (see Chapter 3). The eastern United States includes areas of very high particulate emissions, and some of the highest UFP emissions in the world, third to only some found in China and Russia (Fig. 1-3). For these reasons, there is a need for further research to understand the sources and ambient concentrations of UFP within urban areas of the eastern United States.

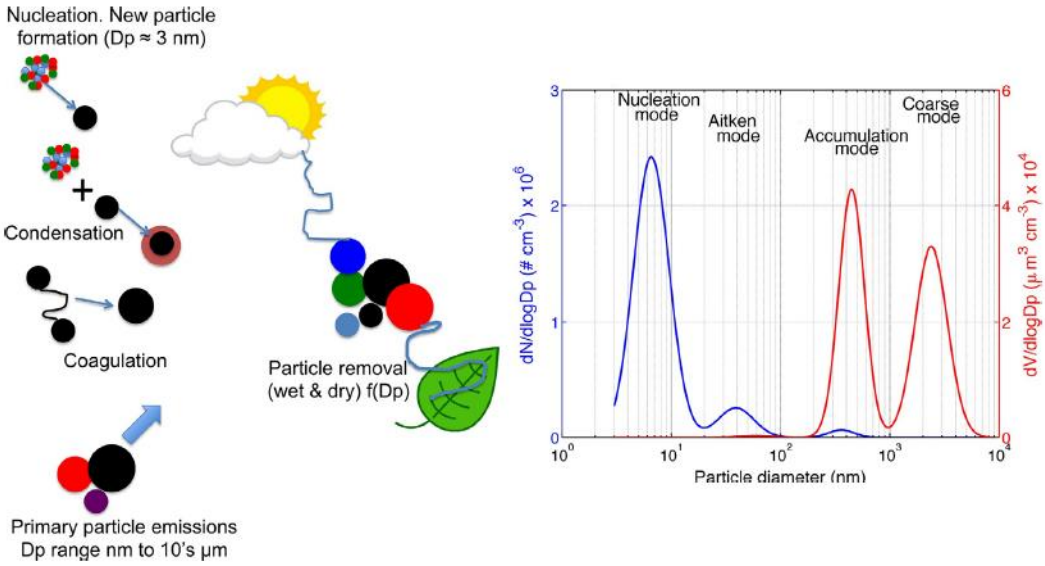

Figure 1-1. Illustration of aerosol dynamics (left) and an example of a particle size distribution expressed in terms of number concentration (blue) and volume concentration (red). Figure reproduced from Pryor et al. (2015).

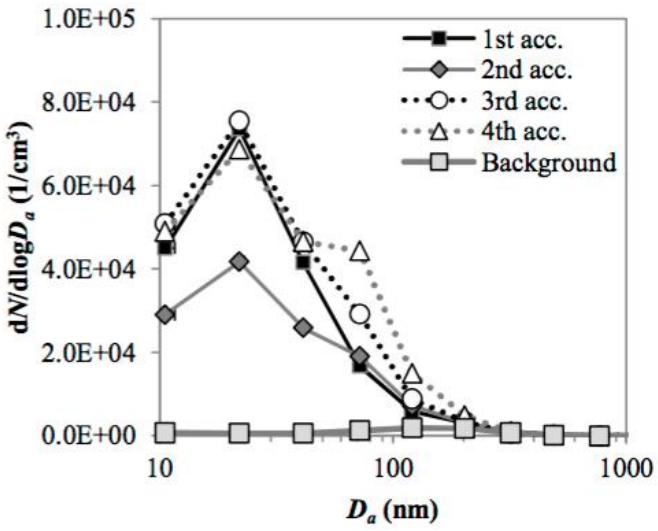

Figure 1-2. Particle size distributions from direct gasoline vehicle emissions under four acceleration scenarios. Figure reproduced from Karjalainen (2014).

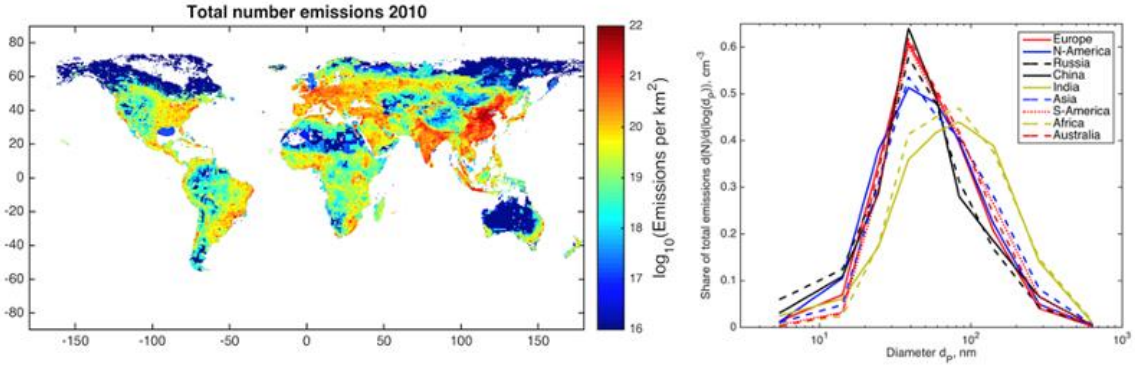

Figure 1-3. Total number emissions around the world for particles with diameters < 1000 nm (left), and particle size distributions for different regions (right). Figure reproduced from Paasonen et al. (2016).

1.2 Measuring UFP

The most commonly used instruments for measuring UFP concentrations are Scanning Mobility Particle Sizers (SMPS), Fast Mobility Particle Sizers (FMPS), and Electrical Low-Pressure Impactors (ELPI) that describe the size distribution of particle number concentrations, and standalone Condensation Particle Counters (CPC) which provide high-time resolution total number concentrations above some diameter threshold (Kulkarni et al., 2011). These instrumental approaches are briefly described and compared below.

Availability of size-resolved particle number concentrations is useful in understanding the likely atmospheric fate of particles, their possible source and also their potential human health or climate impact, but as described below, the disadvantage of using an SMPS is the comparatively slow time to fully characterize the PSD (typically ~1 minute or longer). Having PSDs can help in determining the source of the particles, since different sources contribute to different modes of a PSD. The disadvantage of using an SMPS is that it often takes 60 seconds or longer (depending on the number of diameters being sampled) to obtain a PSD, so for high-resolution data, an FMPS or standalone CPC that report total number concentration every second or at higher time resolution may be more appropriate.

- An SMPS has four main components (Fig. 1-4). The first is a cyclone inlet that, through inertial impaction, restricts the sizes of particles that may enter the instrument (Kang et al., 2012). The second component is an electrostatic classifier, which is responsible for charging the particles using ions (Adachi et al., 1992). Once charged, the particles are introduced to a differential mobility analyzer (DMA) that exposes the

particles to an electric field (Chen et al., 1998). The particles with high mobility are deposited upstream of the sample inlet, particles with low mobility are discharged with excess flow, and those with the mobility currently being sampled can reach the sampling hole and flow on to the CPC. In the CPC, particles are exposed to a vapor such as butanol, and are subsequently grown to a size that can be detected when passed through a light source (Fig. 1-5). The pulses detected by a photomultiplier are counted to obtain a particle count (i.e. number of particles). A P-Trak (TSI, Inc. Shorview, MN, USA) operates similarly to a CPC, yet is more portable, but best used in indoor applications (Zhu et al., 2006).

- An FMPS (TSI, Inc., Shoreview, MN, USA) differs from an SMPS in that it does not contain a CPC. Instead, the FMPS draws charged particles into a part of the instrument that is similar to a DMA, but has the ability to both size and count the particles due to the placement of electrometers around a high voltage electrode column (Tammet et al., 2002) (Fig. 1-6). Particles with high electrical mobility will strike electrodes near the top of the column, and particles with low electrical mobility will travel further down the column before striking an electrode. Because the FMPS can size and count particles of all diameters at one time, the time resolution of the data is higher than that for an SMPS.

- An ELPI is capable of measuring a wide range of particles, including UFP at high frequency (10 Hz) (Keskinen et al., 1992). An ELPI contains three main components. The first component is a unipolar corona charger that charges the particles. The second component is a cascade low pressure impactor. A vacuum pump creates low pressure that pulls the particles through the cascade impactor. Larger particles will

collect on the top impactor stages, and smaller particles will be collected on the last impactor stages. Each impactor stage is equipped with an electrometer that can detect each charged particle. The charge and location in the impactor can be related to the particle number concentration and size.

In this study, a smaller, more portable version of a SMPS, hereafter referred to as a Nanoscan (Fig.1-7) is used. The Nanoscan operates on a similar principle to full-sized SMPS systems but contains no radioactive source, and instead has a unipolar charger with a corona needle to generate charged ions (Stommel and Riebel, 2005). Like a standard SMPS, the charged particles next flow into a DMA that sizes the particles and releases one diameter at a time to the CPC. Unlike many CPCs that use butanol or water to grow particles to detectable sizes, the Nanoscan uses isopropyl alcohol. The Nanoscan discretizes the particle number size distribution from 10 to 420 nm into 13 logarithmically spaced diameters and operates in two modes: single and scan. In single mode, the charge of the DMA is fixed so that the instrument samples the concentration of particles with fixed diameter every second, while scan mode records a size distribution including all diameters every 60 seconds. Additional instrument specifications are given in Table. 1-1.

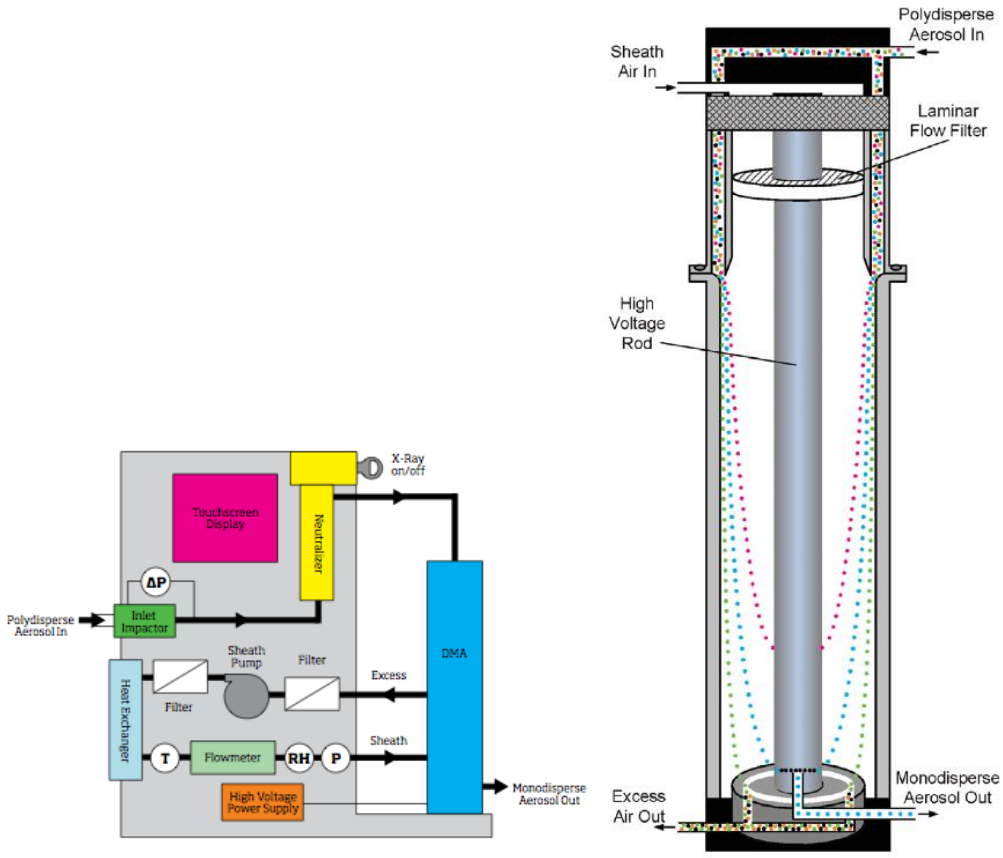

Figure 1-4. Schematic of the components of and flow in a scanning mobility particle sizer (left) and the differential mobility analyzer included therein (right). Figure reproduced from TSI, Inc. (2012a).

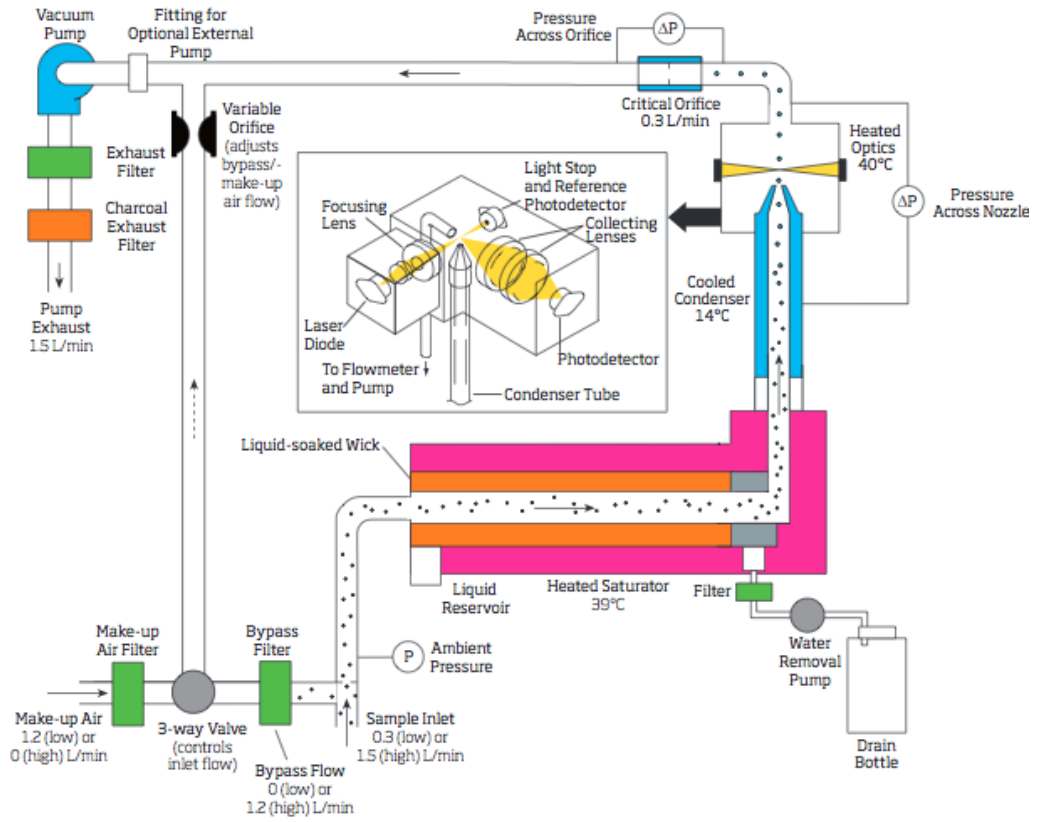

Figure 1-5. Schematic of the components of and flow in a condensation particle counter. When a condensation particle counter is employed as part of a scanning mobility particle sizer it is connected to the differential mobility analyzer (Fig. 1-4) at the monodisperse aerosol outlet. Figure reproduced from TSI, Inc. (2012b).

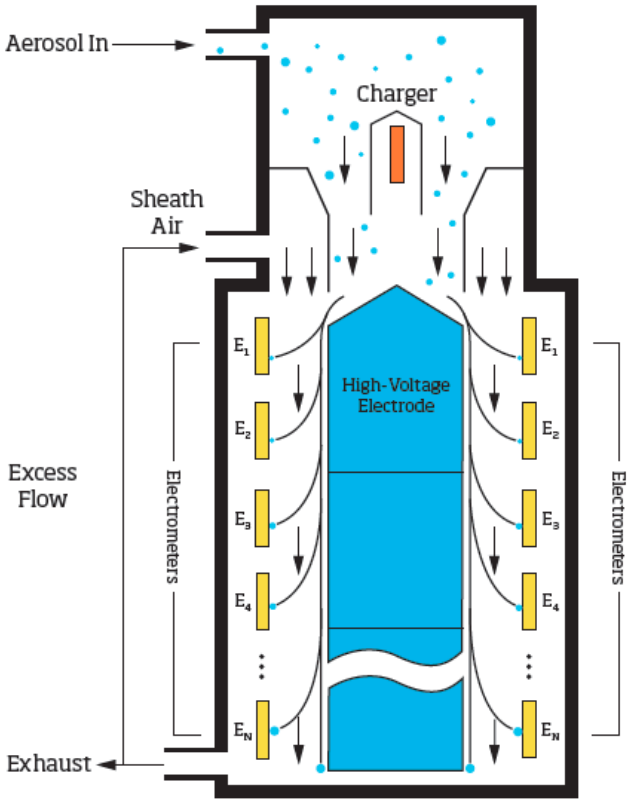

Figure 1-6. Schematic of flow of aerosols through a TSI Fast Mobility Particle Sizer.

Figure reproduced from TSI, Inc. (2015).

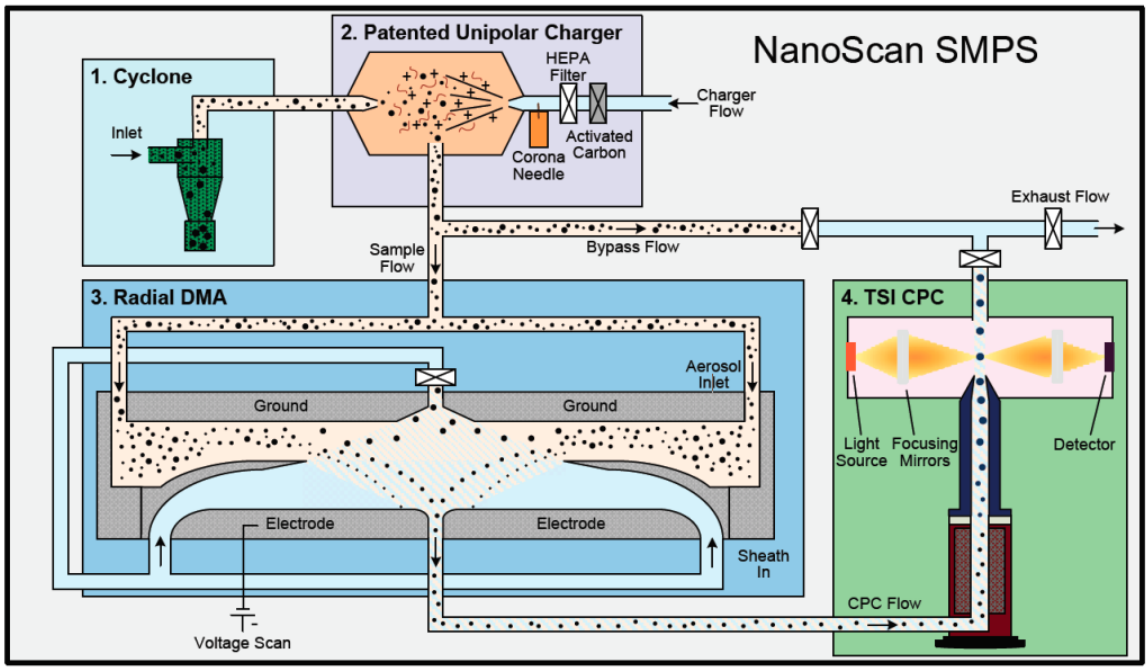

Figure 1-7. Schematic of aerosol flow through a TSI Nanoscan scanning mobility particle sizer. Figure reproduced from TSI, Inc. (2012c).

Table 1-1. TSI Nanoscan scanning mobility particle sizer specifications

Diameter Size Range	10-420 nm
Size Channels	13
Measurement Time Resolution	Scan mode: 60 s Single Mode: 1 s
Particle Concentration	100-1,000,000 cm^{-3}
Flow Rate	0.75 lpm ± 20% at inlet, 0.25 lpm ±10% at sample
Zero Count	≤0.1 cm^{-3}

1.3 Mobile sector UFP emissions

In urban areas, vehicular traffic can be a major contributor to local UFP emissions and concentrations (Janhäll et al., 2012). Accordingly, residents of homes near high-traffic roadways may be more likely to experience ailments, such as asthma (Juhn et al., 2010). This situation is particularly troubling given the majority of the United States' population resides in urban areas (2010 Urban and Rural Classification - Geography - U.S. Census Bureau), and many U.S. cities have high-traffic roadways running through, or near-to, their urban cores. Thus, UFP from the mobile sector may be an important source of increased urban mortality and morbidity (Stölzel et al., 2007).

Vehicular traffic contributes to atmospheric particle concentrations in several ways. The most obvious mechanism is through the combustion of fuels such as gasoline and diesel. UFP can be produced in this process either through primary or secondary formation. For instance, black carbon (BC) is released in the vehicle's exhaust (primary) (Dallmann et al., 2014) while sulfur dioxide (SO_2), when exhausted, can lead to sulfite (SO_3) formation, that when hydrolyzed, forms sulfuric acid (H_2SO_4) – an important precursor for new particle formation (secondary) (Vogt et al., 2003). Less obvious, but arguably a larger contributor to near-road UFP concentrations, is engine lubricating oil in both gasoline and diesel engines (Dallmann et al., 2014).

Non-exhaust emissions can also contribute to near-road particle number concentrations. Brake and tire wear can produce particles in the range of $PM_{2.5}$ and coarse particulate matter with diameters less than 10 μm (PM_{10}), and road wear and dust often contribute to PM_{10} or even larger sizes of particles (Thorpe and Harrison, 2008).

1.4 Summary of previous research on vehicular emissions of UFP and near-source variability of UFP

Table. 1-2 summarizes many of the previous studies that have sought to examine UFP emissions and concentrations within urban areas and near to major roadways. The common themes within these studies and the outstanding research questions are briefly summarized below.

1.4.1 Emission Factors

Emission factors are representative values that are used to characterize true particle emissions (size and concentration) from specific sources in terms of, for example, the operating conditions (e.g. vehicle acceleration). Emission factors for the mobile sector are typically obtained using dynamometer tests (Schauer et al., 1999; Zielinska et al.; 2004; Fujita et al., 2007).

The alternative to dynamometer tests (where a vehicle is operated on rollers connected to an electric motor) is to use on- or near-road measurements and traffic data to infer emission rates. The advantage of dynamometer tests is that an individual vehicle can be monitored in a controlled environment and emission rates observed over a range of conditions (e.g. engine temperature, engine speed, etc.). However, on-road/near-road measurements capture the true emissions from the operating fleet.

When direct measurements of the pollutant of interest are not available, the concentration of one pollutant and occasionally meteorological measurements can be used to estimate the quantity of the pollutant of interest (Gramotnev et al., 2003; Kittelson et al., 2004; Kristensson et al., 2004). Because vehicles emit several pollutants

that can be related to UFP, studies have utilized measurements of carbon monoxide (CO), BC, and nitrogen oxides (NO_x) in order to estimate the concentration of UFP emitted by a vehicle over some distance (Gramotnev et al., 2003; Kittelson et al., 2004; Kristensson et al., 2004).

Ambient estimates of emission factors vary from study to study and place-to-place because they depend on the fleet of vehicles and the method by which the emission rates were estimated. For instance, a study based in Gothenburg, Sweden estimated UFP emission factors for 3-900 nm particles between 1×10^{13} and 14×10^{13} particles km^{-1} (Kristensson et al., 2004), while in Minneapolis, Minnesota, another study estimated emission factors for particles > 3 nm as high as 1.1×10^{16} particles km^{-1} (Kittelson et al., 2004). These differences likely reflect differences in fleet composition and age as well as differences in fuel composition.

1.4.2 On-road UFP

Prior research has shown that UFP concentrations are systematically higher near high-traffic roadways (Hagler et al., 2010; Kittelson et al., 2004), but the PSD of UFP (and all particles) is impacted by vehicle speed (typically slower moving traffic produces larger particles and volumes compared with faster moving traffic (Giechaskiel et al., 2005; Kittelson et al., 2004)), and that ambient near-source PSD and UFP concentrations are dominated by very few high polluting vehicles (Park et al., 2011).

Some high-polluting vehicles may have underlying mechanical issues, but fuel type and composition, and vehicle mode of operation are also factors that can impact a vehicle's UFP emissions. Diesel-fueled vehicles tend to emit higher total particle

concentrations with PSDs concentrated in the accumulation mode, whereas gasoline-fueled vehicles tend to emit particles with PSDs dominated by UFP (Huang et al., 2013; Miguel et al., 1998). The sulphur content of diesel fuel is highly correlated with UFP emissions, and multiple studies have found that decreasing sulphur levels in diesel fuels significantly decreases emitted UFP concentrations (Andersson et al., 2001; Bagley et al., 1996). UFP emission factors increase with increasing vehicle flow rates (Zhai et al., 2016), and under heavy load or aggressive driving conditions (Huang et al., 2013). The increase in UFP emissions under these conditions is likely due to the formation of nucleation mode particles from incomplete combustion and smaller amounts of primary soot and metal particles from engine lubricating oil (Dallmann et al., 2014).

Several meteorological variables affect vehicle UFP emissions. Numerous studies have shown vehicle UFP emissions to be inversely related to temperature (Charron and Harrison, 2003; Janhäll et al., 2012; Olivares et al., 2007). Colder temperatures facilitate secondary particle formation through condensation because the vapor pressure of emitted gases is lower under these conditions (Takekawa et al., 2003). Relative humidity is also important for certain types of particle formation. In a study examining the effects of humidity on $PM_{2.5}$ concentrations, relative humidity was positively correlated with sulfate and nitrate concentrations, but negatively correlated with organic and elemental carbon (Tai et al., 2010). Precipitation acts to scavenge, or remove UFP from the atmosphere by colliding with particles. While scavenging coefficients (s^{-1}) reach a minimum around 100-200 nm, median UFP scavenging coefficients from a forested site in Indiana, USA ranged from ~1.6×10^{-5} s^{-1} to ~4.1×10^{-5} s^{-1}, thus contributing to the removal of UFP from the atmosphere (Appendix A, Pryor et al., 2016). Lastly, wind

speed is especially important in the on-road and near-road environment. Wind speed accelerates coagulation, dilution, and deposition rates, thus decreasing the concentration of UFP. In a study of UFP in near-road environments in Durham, NC, UFP concentrations were nearly double when wind speeds were low and meandering, compared with when wind speeds were higher and in a crosswind direction from the roadway (Hagler et al., 2010).

1.4.3 Near-road UFP

The decay of UFP concentrations from a line source, such as a highway, can be modeled using a simple exponential function (Neumann, 1978). The horizontal crosswind spread of particles can be approximated using,

$$\sigma_y^2 = 2v^2 L\left\{t - L(1 - e^{-\frac{t}{L}})\right\} \qquad (1\text{-}1)$$

where σ_y is the horizontal crosswind spread of particles, *v* is the horizontal crosswind component of turbulent velocity, t is the travel time, and L is the Lagrangian integral time scale,

$$L = \int_0^\infty R(t)dt \qquad (1\text{-}2)$$

where R(t) is the correlation function of the crosswind component *v* of turbulent velocity, and,

$$\mathrm{R(t)} = \mathrm{e}^{-t/L} \qquad (1\text{-}3)$$

In general, field studies confirm the *a priori* expectation that UFP concentrations decrease exponentially with distance from a highway (Hagler et al., 2009; Zhu et al., 2002b, 2002a). The exponential decay of UFP concentrations is especially apparent

when the wind direction is such that measurements are made downwind of the highway (Zhu et al., 2002b). Because UFP are subject to rapid near-source changes in number concentration due to dilution, deposition, coagulation, and condensation, exponential decay may not always be observed.

The particle dynamics responsible for exponential decay are still debated and may vary by location. Near a Texas roadway, UFP were removed readily through coagulation with fine particles near the highway, but farther from the highway, reduction of UFP was dominated by dilution (Choi and Paulson, 2016). In contrast, a study that utilized data from highways in Los Angeles, California suggested that coagulation and deposition played minor roles, whereas dilution and condensation were the major mechanisms responsible for changes in downwind PSDs because the "tailpipe-to-road" and "road-to-ambient" timescales favored dilution over coagulation (Zhang and Wexler, 2004).

Studies investigating the evolution of UFP concentrations away from roadways often employ multiple sampling locations at different distances from the highway (Hagler et al., 2009; Reponen et al., 2003; Zhu et al., 2002a, 2002b). These studies report differing distances away from the highway that must be reached in order for UFP concentrations to decay to background levels. In one study, UFP concentrations at 300 m downwind of a freeway were comparable to those at 300 m upwind (Zhu et al., 2002b); however, in another study, the authors postulated that the region of impact beyond a major Raleigh, North Carolina roadway could exceed 300 m during high volume traffic conditions (Hagler et al., 2009).

The variation in distance needed for UFP concentrations to decay to background is expected as wind direction, wind speed, and landscape and topography can all play

roles in how far UFP travel before depositing, coagulating, growing by condensation, or diluting (Choi et al., 2016). Decay rates may be much higher when the wind direction is perpendicular to the highway as opposed to parallel (Reponen et al., 2003).

The type of vehicles travelling on the highway can also impact downwind UFP concentrations. Average total particle number concentrations have been reported to be higher on roadways with a large proportion of heavy duty diesel vehicle (HDDV) traffic (Zhu et al., 2002a).

As implied by the above, despite numerous studies on this topic, many inferences relating to near-road UFP concentrations remain applicable only to the site at which they were developed (Gidhagen et al., 2004; Hagler et al., 2009; Reponen et al., 2003; Zhu et al., 2002b, 2002a).

1.4.4 Modeled near-road UFP

Since near-road UFP studies can be resource-intensive and site-specific, there is a need for UFP-specific dispersion models that can be applied to a variety of roadways. Currently, the most widely used near-road air pollutant dispersion models are CALINE4 (Benson, 1984), AERMOD (Cimorelli et al., 2005; Perry et al., 2005), ADMS (Carruthers et al., 1994), and RLINE (Snyder et al., 2013). These dispersion models are designed for line sources, like roadways, and are based on the steady-state Gaussian diffusion equation (Eq. 1-4),

$$c(x,y,z) = \frac{Q}{2\pi\sigma_y\sigma_z u} e^{\frac{-y^2}{2\sigma_y^2}} \left(e^{\frac{-(z-h)^2}{2\sigma_z^2}} + e^{\frac{-(z+h)^2}{2\sigma_z^2}}\right) \qquad (1\text{-}4)$$

where *c* is the concentration at a given position, *x*, *y*, and *z* are the downwind, crosswind, and vertical directions, *Q* is the source term, σ_y and σ_z describe the crosswind and vertical mixing of the pollutant, *u* is wind speed, and *h* is the height of the plume where pollutants are released. While these models are generally adequate for modeling the dispersion of gaseous pollutants, as has been validated through comparison with tracer studies (Heist et al., 2013), these models do not include particle dynamics, and thus are not ideal for modeling near-road UFP concentrations.

To better understand particle dynamics near vehicle sources, wind tunnel experiments may be used. A scaled-down model of vehicles on a roadway can be placed in the wind tunnel and when emitting known concentrations of UFP near the tailpipe of modeled vehicles, vehicle- and road-induced turbulences can be studied. A wind tunnel study examining UFP dispersion from a model truck determined that vortices that formed in the wake of the truck acted to disperse the particles and that the dispersion was influenced by vehicle speed, with higher vehicle speeds leading to greater UFP dispersion (Mehel and Murzyn, 2015).

Findings from wind tunnel experiments can then be used to inform larger-scale near-road UFP dispersion models, such as the Comprehensive Turbulent Aerosol Dynamics and Gas Chemistry (CTAG) model (Wang and Zhang, 2012). CTAG encompasses three scales that allow for modeling of particle dynamics from the tailpipe all the way to the regional domain. CTAG has been validated with near-road UFP measurements and performs adequately, but is much more computationally intensive than other near-road pollutant dispersion models such as AERMOD (Wang et al., 2013). A recent study has attempted to reduce the computational demand of near-road UFP

dynamics modeling by applying periodic boundary conditions (Huang et al., 2014). These authors compared modeled results with results from a near-road sampling study and using sensitivity analyses, determined that modeled UFP concentrations are sensitive to H_2SO_4-H_2O binary homogeneous nucleation, condensation and evaporation of semi-volatile organic compounds, and dry deposition, but were not sensitive to coagulation. Additionally, the authors found that UFP concentrations are sensitive to atmospheric boundary layer conditions, and it was suggested that future models should include these conditions to improve model performance. Further, there is a need for additional observational data to evaluate and validate these models.

1.4.5 Mitigation

The most aggressive strategy for reducing UFP concentrations near roadways is decreasing the number of vehicles. In urban areas, where existing public transportation could be bolstered, this reduction could be possible. But some high-traffic urban roadways are interstates with a large portion of traffic being through and not commuter. In these cases, vehicle reduction may be more difficult, but other options remain.

A recent trend that is likely to have an impact on urban UFP concentrations is the removal of urban freeways from city centers (Napolitan and Zegras, 2008). While once seen as a great convenience, having a large freeway running through an urban area is more often seen as a nuisance to air quality, businesses, and housing (Kang and Cervero, 2009). Cities such as San Francisco, California and Milwaukee, Wisconsin have replaced urban freeways with park space, pedestrian and bike paths, and public transit routes, and others are following suit (Napolitan and Zegras, 2008).

Syracuse, New York is the focus of the current study and is proposing to reroute through traffic on interstate 81 (I-81) to a neighboring freeway outside of the city, and replace the aging elevated highway with a street-level boulevard. The conversion of highway to boulevard is aimed at enabling better access to local business through street parking, as well as improving pedestrian and bike safety through additions of sidewalks and bike paths (I-81opportunities).

Another option for reducing near-road UFP concentrations is the use of trees and barriers between highways and residential or other populated areas. Hagler et al. (2010) found that a solid, 6-m structural barrier lowered UFP concentrations away from the highway by approximately half, but that a vegetative barrier had much more variable results likely due to its thin, non-continuous structure (Hagler et al., 2012). Variability of particle concentrations behind tree barriers has also been observed for $PM_{2.5}$ and linked to decreased Turbulent Kinetic Energy downwind of trees (Tong et al., 2015)

1.5 Research Objectives and Hypotheses

High-traffic roadways have been shown to be sources of UFP; however, measured concentrations and the spatial variability of concentrations around the highway sources differ substantially between studies. Further, there is a need for studies on the contribution of elevated urban freeways to near-road UFP concentrations to better understand how UFP from urban high-traffic roadways evolve and vary in an urban environment.

The purpose of this study was to undertake measurements of UFP along a transect oriented perpendicular to I-81 in Syracuse, New York in order to:

1) Demonstrate the feasibility of using a bicycle-mounted Nanoscan SMPS (described in Chapter 2). Initial testing suggested the TSI Nano-SMPS systems are comparatively insensitive to vibration and have sufficient internal logging capabilities. I hypothesize that the Nanoscan measurements will be unaffected (i.e., show no response) to vibrations encountered during testing and will be on the same order as studies that have utilized full-size SMPS systems in moving vehicles in previous near-road studies.

2) Quantify how concentrations of UFP decay with lateral distance during rush hour and non- rush hour. Traffic counts from I-81 and along the sampling transect are used to evaluate whether differences in rush hour and non-rush hour UFP concentrations may be associated with changes in vehicle counts or other influences. I hypothesize that UFP concentrations will be greatest during rush hour sampling periods.

3) Relate the day-to-day variations in UFP concentration decrease with increasing distance from the highway to factors such as wind speed, temperature, and transect vehicle traffic. Meteorological data from a nearby tower and transect vehicle count data from a bicycle-mounted camera are employed to assess the impacts on near-road UFP concentrations. Consistent with empirical studies (Hagler et al., 2009; Zhu et al., 2002b, 2002a), a highway when modeled as a line source, will emit UFP concentrations that will decay exponentially with lateral distance. I hypothesize that UFP concentrations will decrease exponentially from I-81, but the rate of decay is modified by whether it is rush hour or not on I-81 due to decreased highway vehicle traffic and, and will show a significant

dependence on wind speed and temperature. Local vehicle sources may also influence sampled UFP concentrations on the cross-street below the highway and thus confound interpretation of my transect sampling relative to highway traffic. While some vehicles may be more polluting than others, the general trend will be the more local traffic, the higher UFP concentrations and larger spread above the mean. Based on previous research that 10% of vehicles contribute 50% of gaseous pollutant emissions (Stedman et al., 1997), I postulate that cases where my measurements with distance from the highway do not exhibit exponential form may be associated with individual vehicles on the local road on which I was sampling.

Table 1-2. Summary table of previous related research

Author, Year	Geographic Area	Particle Size Range	Instrumentation	Highway Structure	Sampling strategy	Relevant Results
Janhäll et al., 2012	Gothenburg, Sweden	20-100 nm	SMPS	Ground-level city streets	Stationary rooftop sampling from 30 m above city center. Duration: 4 weeks	Total particle number concentration range: 2000 – 11000 cm^{-3}. UFP emissions increase with decreasing CO and emission factors increase with decreasing temperature.
Zhu et al., 2002b	Los Angeles, CA, USA	6-220 nm	CPC and SMPS	North south oriented, 9 lane highway that is elevated ~4.5 m above sampling locations	UFP measurements at 30, 60, 90, 150, and 300 m downwind from the center of the highway, and 300 m upwind. Duration: 9 days, 4.5-5.5 hours/day	Total particle number concentration range: $5x10^4 – 2x10^5$ cm^{-3} UFP concentrations decreased dramatically with increasing distance from the highway. Concentrations at 300 m downwind were comparable to 300 m upwind. Larger particles were less affected by distance, but wind speed affected all particle number concentrations.
Zhu et al., 2002a	Los Angeles, CA, USA	6-220 nm	CPC and SMPS	North south oriented, 8 lane, ground-level	UFP measurements taken at 17, 20, 30,	Total particle number concentration range:

				highway dominated by HDDV traffic	90, 150, and 300 m downwind, and 200 m up wind. Duration: 7 days, 5.5 hours/day	$0.1x10^5 – 3x10^5$ cm^{-3} UFP concentrations decreased dramatically with distance from the highway
Park et al., 2011	Los Angeles, CA, USA	$PM_{2.5}$ and UFP	CPC, FMPS, and DustTrak ($PM_{2.5}$)	Two routes: 1) port/freeway/truck 2) residential	On-road sampling from electric vehicle. Duration: 30 miles driven twice a day, 2-3 times/week during winter and summer	Total particle number concentration range: $100x10^3 – 2x10^6$ cm^{-3} 5% of vehicles sampled were identified as "high-emitters" and emitted 5-25 times higher particle concentrations than the fleet mean.
Kittelson et al., 2003	Minneapolis, MN, USA	3-1000 nm	SMPS and CPC	Several routes	On-road measurements, with stationary measurements for background concentrations. Duration: 800 km in 5 days	Total particle number concentration range: $4x10^3 – 1x10^7$ cm^{-3} Particle concentrations increased dramatically as sampling vehicle approached a highway. Particle size decreased with increasing speed.
Reponen et al, 2003	Cincinnati, OH, USA	0.02-20 µm and $PM_{2.5}$	CPC, optical particle counter (OPC), and Harvard Impactor	North south oriented, ground-level highway	Sampled on eastern side of highway at distances ranging from 50 to 1600 m.	Total particle number concentration range: 13000 – 38000 cm^{-3} UFP concentrations decayed to half, under west winds, between 50 and 150 m east of the highway, and to 30%

						between 400 and 1600 m. Under parallel wind conditions, UFP concentrations decreased to 75-85% at 400 m. Duration: 3 sampling periods lasting 2-5 days each
Hagler et al., 2010	Durham, NC, USA	<100 nm	Engine exhaust particle sizer (EEPS) and SMPS	Ground-level roadways including a highway, arterial streets, residential and business streets	Measurements made from an electric vehicle driving a sampling route. Background measurements taken from a stationary vehicle. Duration: 6 days during 1 week, 1.5-3 hours/day	Total particle number concentration range: $1x10^4 – 4x10^4$ cm^{-3} The lowest UFP concentrations were observed in a neighborhood with trees and buildings obstructing the highway. The median highway UFP concentrations are a factor of 2.9 higher than median arterial road UFP concentrations. During downwind conditions, the median near-road UFP concentrations are a factor of 1.8 and higher than urban background. During calm wind conditions, UFP concentrations are regionally elevated

						relative to the crosswind levels and near-road UFP concentrations are still higher than nearby urban background areas by a factor of 1.2.
Wåhlin et al., 2001	Copenhagen, Denmark	6-700 nm	DMA and CPC	3 measurement locations: 1) busy road with 5-6 story row homes on either side, 2) urban background, 3) busy road with 1-2 story homes along road	Stationary measurements at each of the three locations	Total particle number concentration range: 10000 -200000 cm^{-3} Diurnal variation of particle concentration observed with a peak at rush hour during weekdays. The average particle size emitted by diesel vehicles was smaller than those emitted by gasoline. Urban background concentrations were significantly lower than at street locations.
Hagler et al., 2009	Raleigh, NC, USA	20-1000 nm	TSI P-Trak and Grimm model 107	Ground-level, high traffic roadway	4 sampling sites located 20-300 m NE of the roadway and an upwind site located about 50 m to the SW. Duration: continuous from August 3-10	Total particle number concentration range: $0.5x10^4 – 6x10^4$ cm^{-3} During morning rush hour, a five-fold increase is seen downwind of the highway as compared to upwind. UFP number counts poorly relate to

						$PM_{2.5}$
Gidhagen et al., 2004	Stockholm, Sweden	> 3nm	CPC	Ground-level highway	Two stationary measurement sites located 38 and 91 m downwind of the highway. Duration: 6 weeks	Total particle number concentration range: 100 – 5000 cm^{-3} Coagulation of UFP was of little importance over the first 100 m downwind of the highway. Instead, losses due to deposition were greater due to vehicle turbulence. More than half of the total concentrations of particles 63 m from the highway are < 18 nm.
Cheng et al., 2009	Northern Taiwan	6-560 nm	FMPS	Tunnel	Electric vehicle driven through tunnel. Duration: August 12-19	Total particle number concentration range: 10 – $4.5x10^4$ cm^{-3} Traffic volume affects UFP levels inside the tunnel. UFP levels increase with increasing distance from tunnel entrance. UFP concentrations are higher when traffic is travelling uphill.
Hagler et al., 2011	Central NC, USA	< 100 nm	FMPS, EEPS, and CPC	Ground-level roadways with vegetative or noise barriers	Mobile measurements using electric vehicle and stationary	Total particle number concentration range: 1000 – 130000 cm^{-3} Solid, 6 m structural

					measurements at different distances from highway barriers	barrier lowers UFP concentrations away from highway, but vegetative barrier results were much more variable.
Baldauf et al., 2008	Raleigh, NC, USA	$PM_{2.5}$ and UFP	EEPS and SMPS	Ground-level highway	Several stationary monitoring sites located at various distances from highway and mobile sampling routes driven near highway.	Total particle number concentration (20 nm) range: 200 - 1200 cm^{-3} Elevated concentrations of UFP occurred under many different wind directions – possibly due to vehicle turbulence.
Pirjola et al., 2005	Helsinki, Finland	3nm – 10µm	Electrical Low Pressure Impactor (ELPI) and SMPS	Six lane, ground-level, urban highway with grass median	Mobile laboratory driven on highway and parked at different distances away from highway for stationary measurements.	Total particle number concentration range: 0.8 x 10^{-4} – 1.8 x 10^{-5} cm^{-3} Positive correlation between traffic flow rate and particle number concentration. Higher wind speeds were associated with lower particle concentrations.
Hitchins et al., 2000	Tingalpa and Murrarie, Queensland, Australia	0.015 – 20 µm	SMPS	Two similar, ground-level roadways with average hourly traffic densities of 2550 and 3400 vehicles	Mobile laboratory parked at different locations away from the roadways	Total particle number concentration range: 400 - 850,000 cm^{-3} When the wind direction passed over the highway, toward sampling sites, particle concentrations

						decayed to around 50% at 150 m.
Beckerman et al., 2007	Toronto, Canada	10 nm-2.5 µm	P-Trak and CPC	Ground-level highway with AADT of 349,100 and 395,400	Hand-held instrumentation and mobile lab instrumentation sampling at different distances on two transects near highway	Total particle number concentration range: 4153-95,549 cm^{-3} UFP associated with NO_2, VOCs, and black carbon

CHAPTER 2:METHODS

2.1 Experimental methods

2.1.1 Site Description

As discussed in Chapter 1, many cities in the northeastern United States exhibit relatively high UFP emissions and concentrations, and there is evidence that the mobile sector is a major source of these emissions. I selected Syracuse in north-central New York for this study because it is transected by two interstate high-traffic roadways including I-81, and afforded an opportunity to examine what to date have been under-studied facets of understanding the UFP burden around highways – to what degree are near-source concentrations at ground level near elevated freeway portions different from previous studies that have taken measurements at the height of the freeway, and how the freeway's location in an urban area affect the decay of UFP concentrations away from the freeway.

The city of Syracuse has an estimated population of 144,142 (U.S. Census Bureau, 2010) and is transected by an elevated portion (~5 m above the ground) of I-81 that runs roughly north south. This portion of I-81 can experience Annual Average Daily Traffic (AADT) counts > 100,000, while most surrounding ground-level streets have AADTs < 10,000 (New York State Department of Transportation, (Fig. 2-1)). Samples of UFP number and size distributions were collected along a transect (Fayette Street) perpendicular to I-81 (Fig. 2-1). Fayette Street was chosen because it runs perpendicular to I-81 and has considerably lower AADT than other similar streets. This experimental design was selected to minimize contamination from local sources. There are few local

$PM_{2.5}$ point sources, and the dominant wind direction is from the WNW (Figs. 2-2, 2-3, Climate Syracuse), making this location and highway ideal for studying downwind UFP concentrations and size distributions.

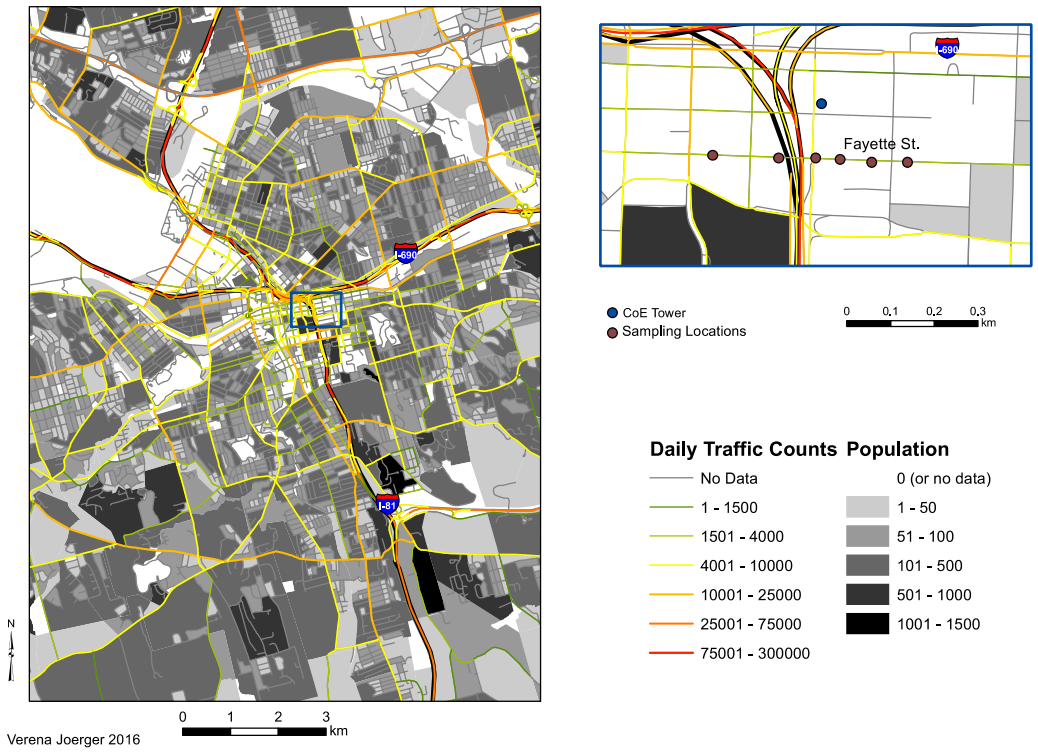

Figure 2-1. Traffic and 2010 census data for Syracuse, New York. Population is per census tract. Map inset shows approximate sampling locations at 30, 40, 130, 180, 300, and 520 m from the center of I-81 along Fayette Street and Syracuse Center of Excellence (CoE) tower where meteorological data were obtained.

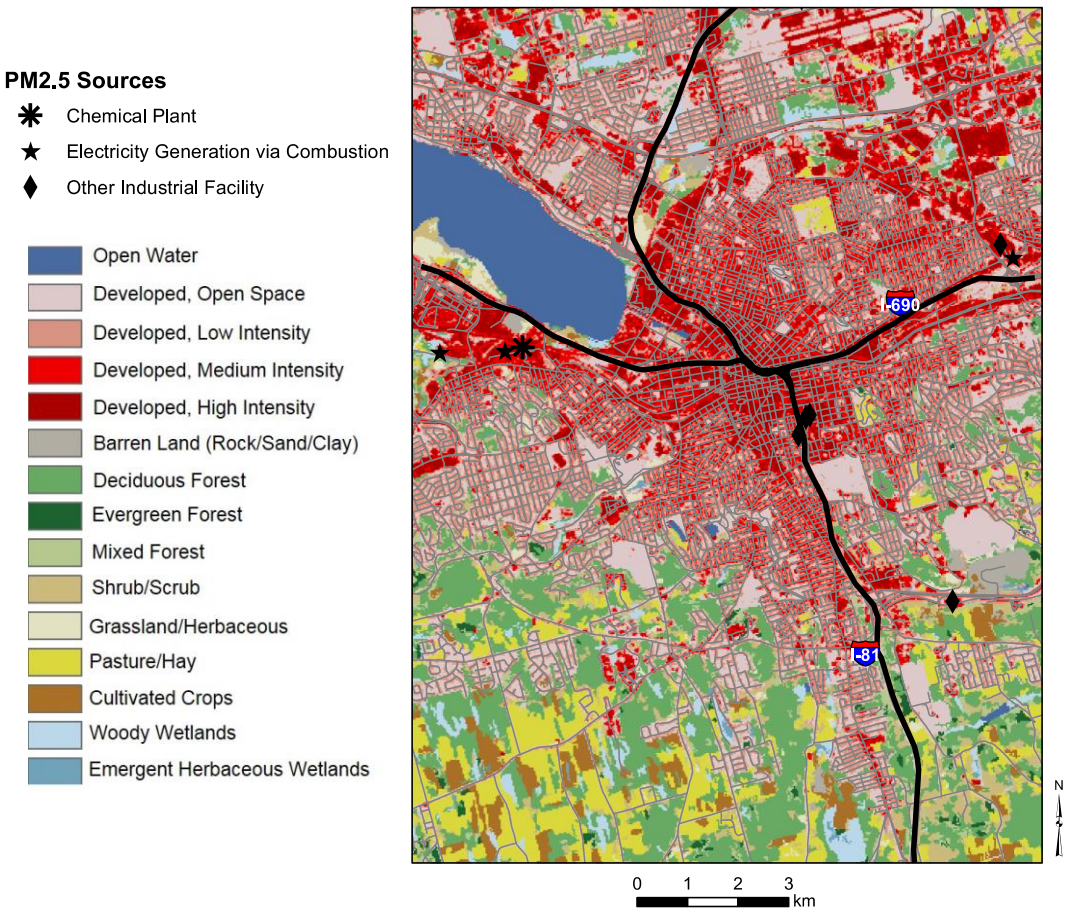

Figure 2-2. Map of Syracuse, NY showing land cover from the 2011 National Land Cover Database and known, local $PM_{2.5}$ point sources as identified by the EPA NY $PM_{2.5}$ Emission Summary (available at https://www.epa.gov/air-emissions-inventories). Total, annual $PM_{2.5}$ emissions from nearby chemical plants, electric generation facilities, and other industrial facilities are 6, 8.97, and 5.41 tons, respectively.

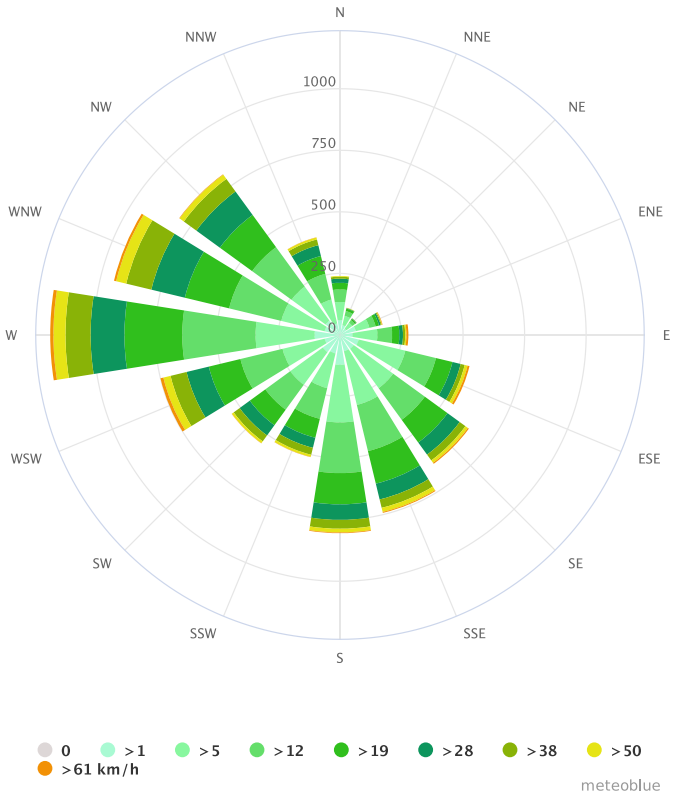

Figure 2-3 Wind rose of hourly wind data from (1981-2010) for Syracuse, New York, data compiled by, and figure reproduced from www.meteoblue.com.

2.1.2 Instrumentation

UFP concentrations and size distributions were sampled using a TSI Nanoscan SMPS (TSI, Inc., Shoreview, Minnesota, USA (Tritscher et al., 2013)) mounted on a bicycle (Fig. 2-4).

To my knowledge, only one other study has used a Nanoscan in a similar mobile application (Ruths et al., 2014), so a brief test was performed to evaluate its sensitivity to vibrations during the mobile sampling. A Nanoscan was placed on a rolling cart and wheeled along a sidewalk adjacent to Tower Road on the Cornell University campus for

two minutes then stopped for two minutes. This test was repeated for ~50 minutes. The resulting data did not indicate any differences between measurements made while in motion, and those made while stationary (Fig. 2-5). However, this test is illustrative of the impact a single vehicle can have on UFP concentrations. As shown in Figure 2-5 at a time stamp of 44 minutes a HDDV passed the Nanoscan on Tower Road leading to an almost 10-fold increase in particle number concentrations. To maintain the Nanoscan during the experiment, the cyclone inlet was cleaned before each sampling day and the wick was replenished with fresh isopropyl alcohol twice daily during sampling.

A GoPro action video camera was mounted on the bicycle to observe local, street-level traffic. The resulting camera footage was manually inspected for each transect to identify the presence of vehicles on the street and to characterize them as either cars or HDDV.

The GPS application, *Trails* (iosphere GmbH), was used on a bicycle-mounted iPhone to quantify the speed of the bicycle during mobile sampling and verify the stationary sampling locations between individual transects.

Figure 2-4. Sampling bike set-up with Nanoscan in secured, cushioned rear basket, and GoPro camera mounted to handlebars.

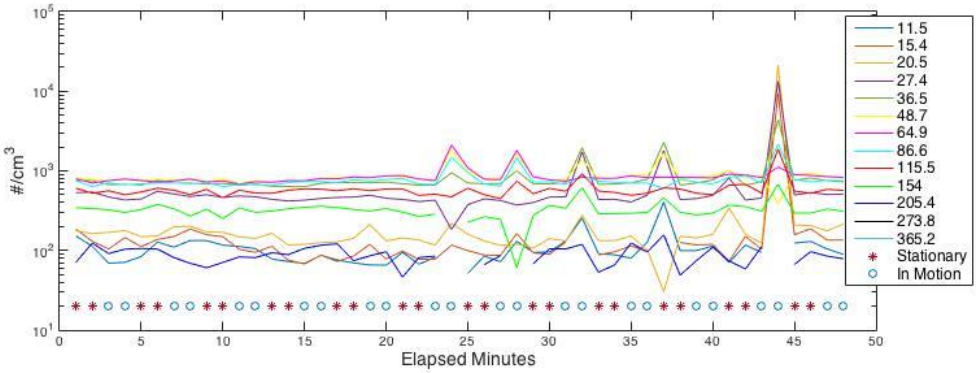

Figure 2-5. A time series of particle concentrations in each size bin collected by a Nanoscan SMPS during a test for motion sensitivity where the instrument was in motion on a rolling cart for 2 minutes, then stationary for 2 minutes, and repeated for 48 minutes.

Fifteen-minute mean meteorological data (wind speed, wind direction, and temperature) were obtained from 43 m and 1.8 m above ground level on the Syracuse Center of Excellence (CoE) tower located one block north of the sampling transect (Fig. 2-1) (Buckley et al., 2016). Wind speeds and direction were measured by a cup anemometer and vane (Climatronics F460 Wind Sensor) and temperature data were

measured using a model Climatronics 102090 dual element thermistor (Climatronics Corporation, Bohemia, NY, USA).

Hemispherical photos were taken along the sampling transect at 180 and 30 m west and 40, 130, 300, and 520 m east of the center of I-81. The hemispherical photos were used to compute sky view factors (SVF) using SkyViewFactorCalculator (Lindberg and Holmer, 2012). SVF were calculated using the methods developed by Holmer et al. (2000), which involve converting a color hemispherical photo into a black and white scale image and relating pixel values to sky and non-sky elements to obtain a ratio of sky pixels to non-sky pixels. SVF are used herein to evaluate the degree to which each of the stationary sampling locations had a clear sky-view (unimpeded by buildings) and thus the degree to which emissions from the elevated highway could be entrained into the street and the degree to which local emissions can be ventilated from the street (Allwine et al., 2002).

2.1.3 Sampling Procedure

Sampling was conducted on 20 weekdays without precipitation between July 13th and October 17th, 2016. A rush hour (RH) sample was collected between the hours of 07:30 and 09:00, and a non-rush hour (NRH) sample was collected between 10:30 and 12:00. Each sample consists of UFP size distributions from six stationary locations at 180 and 30 m west and 40, 130, 300, and 520 m east of the center of I-81. Additionally, mobile transects of UFP concentrations with diameters of 15 and 50 nm were taken between stops (Fig. 2-1). These diameters were chosen to represent the two modes of PSDs associated with vehicle emissions (Fig. 1-2).

To estimate the difference in traffic on I-81 between RH and NRH, car and HDDV traffic on I-81 was counted on nine days during the sampling period. Because counts were performed manually by watching live traffic footage of a traffic camera located ~1.2 km north of the sampling locations on I-81 (http://cnycentral.com/weather/cameras/route-81-04-28-2016), the counts were not made on days when UFP sampling occurred, but were made during RH and NRH, and under the criteria of weekdays with no precipitation.

2.2 Statistical Methods

Since UFP number concentrations are not normally distributed, I employ non-parametric tests, and use the median and interquartile range to characterize the central tendency and variability.

Previous studies have observed diurnal variations in UFP concentrations associated with morning and evening commuter traffic (Hagler et al., 2009; Wåhlin et al., 2001). To test the hypothesis that UFP number concentrations adjacent to the I-81 highway would be higher during rush hour, the differences in RH and NRH samples are established by conducting a Wilcoxon Rank Sum test (Gibbons and Chakraborti, 2010; Hollander et al., 2013) of the difference in median values of total UFP number concentrations and PSDs of UFP at the six stationary sampling locations for NRH and RH.

PSD are analyzed by comparing concentrations during RH and NRH and examining the variability within the PSD during the two sampling times. To assess the influence of wind direction on PSDs, PSD data are grouped according to wind direction.

Perpendicular wind samples include PSD data collected during flow between 240˚ and 300˚. Parallel wind samples include PSD data collected during wind directions from 330˚ to 30˚ and 150˚ to 210˚ (i.e. aligned with I-81).

While most empirical studies of UFP near roadways tend to indicate that concentrations decrease exponentially (Eq. 2-1) with distance from the roadway, two other types of fits were also made to median total number concentrations (normalized to the 30 m concentration) at the six stationary sampling locations of this study (Eqs. 2-2 and 2-3) – one in which concentration was assumed to decrease with the reciprocal of lateral displacement from the highway and one in which the concentration decreased with the reciprocal of the square of the lateral displacement:

$$y = a \times e^{bx} \qquad (2\text{-}1)$$

$$y = a \times \frac{1}{x} \qquad (2\text{-}2)$$

$$y = a \times \frac{1}{x^2} \qquad (2\text{-}3)$$

where y is the UFP concentration (number cm^{-3}), a and b are multipliers and x is the distance from the center of I-81 (m).

The precise form of the distance decay relationship is important not only to generating insights into the physical causes of reduced UFP concentrations with displacement from the source (I-81) but also in considering urban design to minimize human exposure.

All of model forms considered here are inverse distance. Model 2-2 assumes concentrations are reduced linearly with increasing distance from the source. Model 2-3 assumes concentrations are reduced by one over the square of distance, while model 2-1 assumes concentrations exhibit negative exponential dependence on distance.

The quality of fits is evaluated through calculation of the root mean square error (RMSE), which quantifies the difference between observed and predicted values. RMSE is used in this analysis to determine how well UFP concentrations at the six stationary sampling locations fit the modeled decay function.

While local traffic on the sampling route is less than a third of that on I-81, individual vehicles can be disproportionally polluting (Park et al., 2011), I examine the influence of local traffic and SVF on sampled number concentrations by relating the anomalies from the theorized exponential decrease in UFP number concentrations with distance from the highway during RH and NRH sampling to the number and type of vehicles on the local street where sampling took place. The influence of local traffic is also examined by plotting the minimum and maximum UFP concentrations around the mean with local car and HDDV counts and evaluating the variability in minimum and maximum concentrations in relation to vehicle counts.

Past studies have also suggested that temperature, wind speed, and wind direction can modify UFP concentrations away from a roadway source (Hagler et al., 2010; Janhäll et al., 2012; Reponen et al., 2003; Zhu et al., 2002b). To test which of the recorded independent variables could be influential in this dataset, a linear mixed-effects model (LME) is developed. LME is an extension of a linear regression model that is ideal for grouped data (Carey and Wang, 2001). LME can be used to describe the relationship

between a response variable and independent variables, and includes coefficients that vary based on the grouping variables. LME takes the form of Equation 2-4:

$$y = X\beta + Zb + \varepsilon \qquad (2\text{-}4)$$

where the first term is a fixed-effects term that is part of conventional linear regression, the second term is the random effects term which is associated with individual data points drawn at random from the population, and the third term is an error term. The data from Syracuse fit the criteria for LME because the data are grouped by six stationary stops where UFP concentrations and independent variables were recorded.

The independent variables included in the LME were local traffic counts, wind speed, wind direction, temperature, and distance from the center of I-81. Wind direction was transformed from 0-360˚ to values between 0 and 1. A value of 1 corresponds to a wind direction directly perpendicular with I-81 (east or west), and a value of zero corresponds to parallel winds (north or south). To allow for inter-variable comparison, all independent variables were standardized to z-scores (i.e. an estimate of the number of standard deviations from the mean) using Equation 2-5:

$$x' = \frac{x-\mu}{\sigma} \qquad (2\text{-}5)$$

where x' is the transformed data, x is the original data, μ is the mean, and σ is the standard deviation.

CHAPTER 3: RESULTS AND DISCUSSION

3.1 Observed Conditions

3.1.1 Meteorology

During the sampling period, mean temperatures at a height of 1.8 m on the Syracuse CoE tower during rush hour (RH) ranged from 6.4 to 29.3 °C, while non-rush hour (NRH) sampling mean temperatures were higher and ranged from 12.2 to 32.9 °C (Fig. 3-1). This is an inevitable consequence of the sampling time differences; RH (07:30 – 09:00), NRH (10:30 – 12:00) and has some implications for measured UFP concentrations. Since colder temperatures are usually associated with a lower boundary layer and less vertical mixing than higher temperatures, UFP may not dilute as rapidly in a colder environment. In addition, colder temperatures promote secondary particle formation from vehicle exhaust. Less dilution and better formation conditions are two factors that may lead to higher UFP concentrations during RH, even if traffic volume on I-81 was the same during RH as NRH.

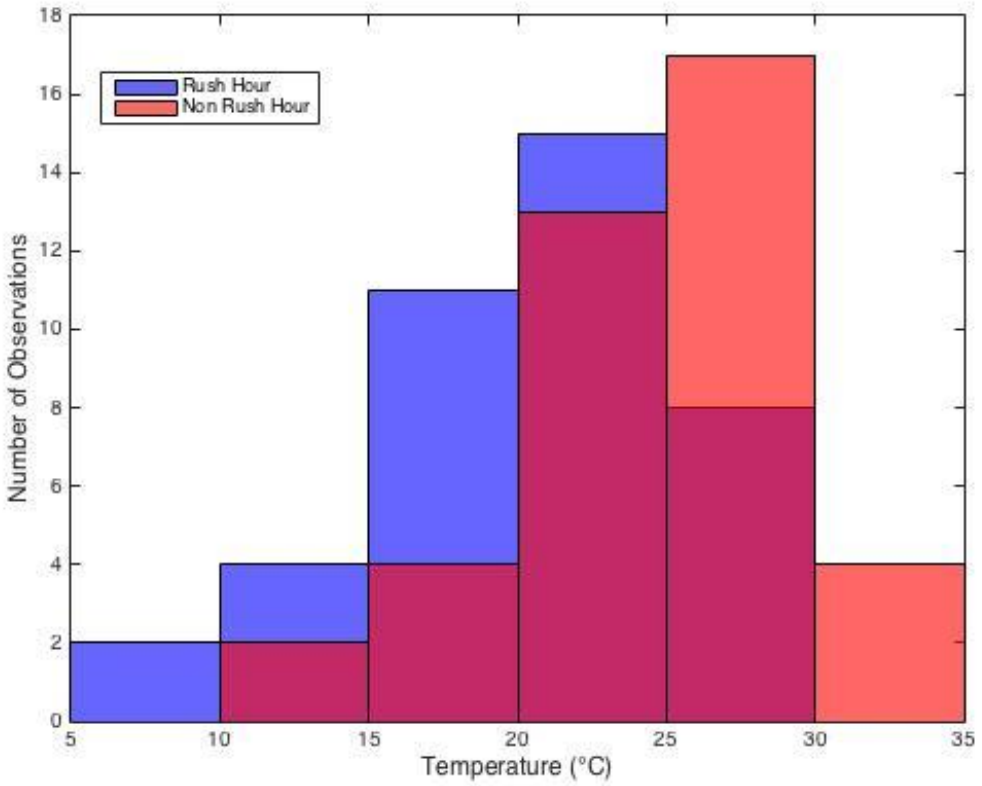

Figure 3-1. Histogram of mean air temperatures recorded at a height of 1.8 m at the Syracuse Center of Excellence tower during rush hour (07:30-09:00) and non-rush hour (10:30 – 12:00) sampling periods.

Wind speed and direction can affect UFP concentrations near roadways. UFP concentrations are highest near roadways when wind speeds are low, and UFP measurements are made downwind of the roadway (Durant et al., 2010; Hagler et al., 2009, 2010; Reponen et al., 2003; Zhu et al., 2002b, 2002a). Observed wind speeds during the sampling period remained fairly low at < 6 m s^{-1} and were only slightly faster during NRH (Fig. 3-2). The similarity in wind speeds during RH and NRH, indicate that both may have similar dilution rates and any differences between RH and NRH UFP concentrations are not likely to be attributed to differences in wind speed.

However, the observed wind directions did vary between RH and NRH, but still resemble the 30-year climatology displayed in Fig. 2-3. The dominant wind directions in both RH and NRH are from the west and south; however, a fairly strong component from the north is present during ~8% of the RH data, and southern wind directions are skewed further to the southeast during NRH (Fig 3-2). Dominant wind directions were both parallel and perpendicular to I-81, with the parallel winds originating from the north and south, and perpendicular winds from the west. Under perpendicular, northerly wind conditions, one could expect to observe the decay of UFP concentrations along the eastern sampling locations. However, under parallel wind conditions, UFP concentrations will likely decay much faster with lateral distance from the highway and reach ambient concentration closer to I-81. In the case of NRH, where southeasterly winds were prevalent, the study design may not be ideal as no sampling locations are located downwind; however, UFP concentration decay may be observed between the two western sampling sites.

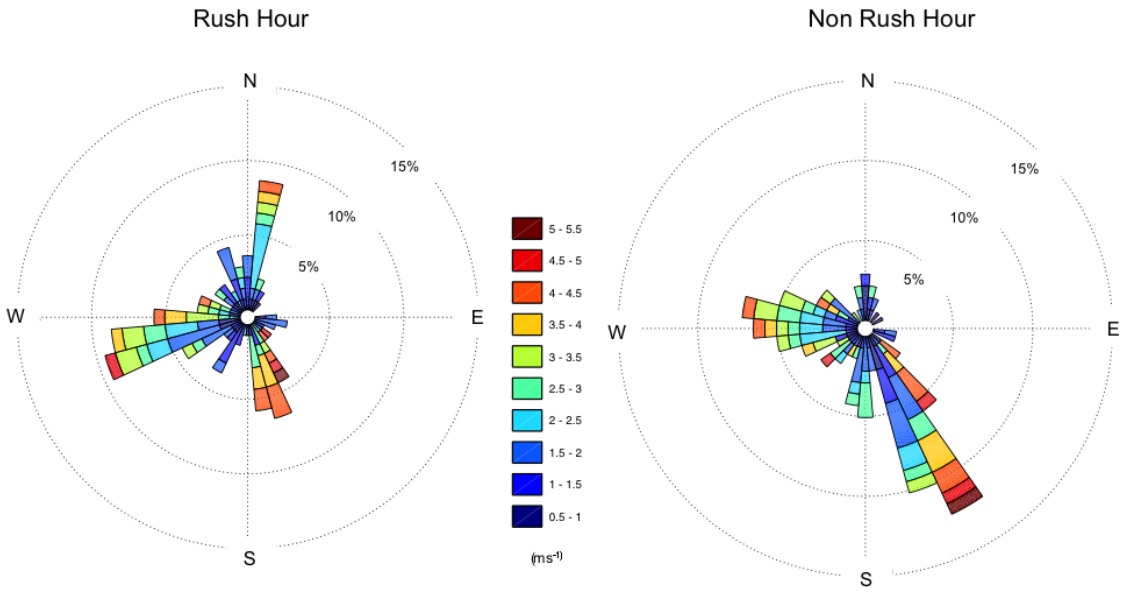

Figure 3-2 Wind roses of 15-minute mean wind data observed during rush hour (07:30 – 09:00) (left) and non-rush hour (10:30 – 12:00) (right) sampling periods at a height of 43 m on the Syracuse Center of Excellence tower.

3.1.2 Sky View Factors

Buildings, walls, and vegetation can decrease the ventilation of an area, trap pollutants, and create canyon effects (Hagler et al., 2012, 2010; Wåhlin et al., 2001). SVF can be used to approximate how well ventilated an area is. An SVF of 0 corresponds to no sky visible in the hemispherical photo (not well ventilated), and a value of 1 corresponds to 100% sky (well ventilated). SVF estimated at the six stationary sampling locations range from 0.515 to 0.926 (Table 3-1.). The most obstructed sites are at 180 m west (0.515) and 40 m east of I-81 (0.609), and the most open sites are at 130 and 300 m east of I-81. A multi story church to the south as well as several trees to the north obstructs the site located 180 m west of I-81. At the 40 m site, the main obstruction is a multi-story parking garage to the south.

Table 3-1. Sky view factors estimated for each of the six stationary sampling locations.

Site, direction, and distance from I-81	Sky View Factor
1) 180 m (west)	0.515
2) 30 m (west)	0.717
3) 40 m (east)	0.609
4) 130 m (east)	0.917
5) 300 m (east)	0.926
6) 520 m (east)	0.893

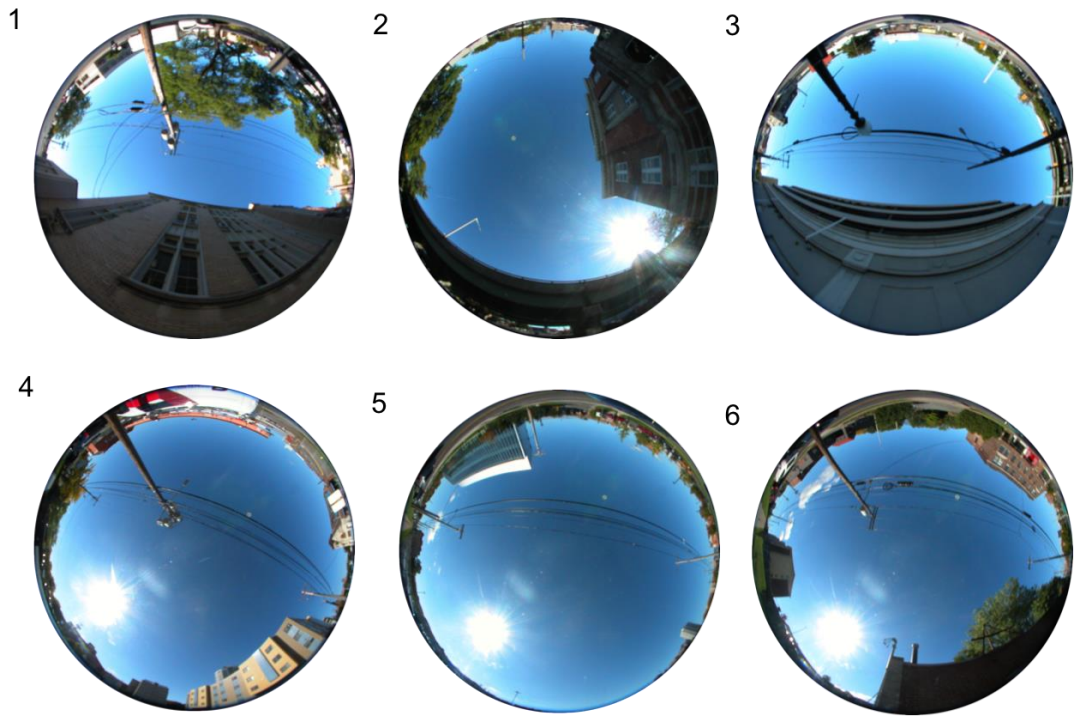

Figure 3-3. Hemispherical photos taken at the six stationary sampling locations: 1) 180 m W, 2) 30 m W, 3) 40 m E, 4) 130 m E, 5) 300 m E, and 6) 520 m E and used to calculate Sky View Factors.

3.1.3 I-81 Traffic

Consistent with *a priori* expectations, roadway traffic on I-81 is higher during RH than NRH, with the number of cars per minute averaging 134 and 87, respectively (Fig. 3-4). The difference in traffic volume is likely due to commuter traffic entering Syracuse during RH. The same difference is not seen in HDDV traffic on I-81. HDDV traffic counts during NRH are 95% of RH counts, and in total, account for 4-5% of traffic on I-81 (Fig. 3-4) which is in line with the national highway average of ~4% (U.S. Department of Transportation, 2013).

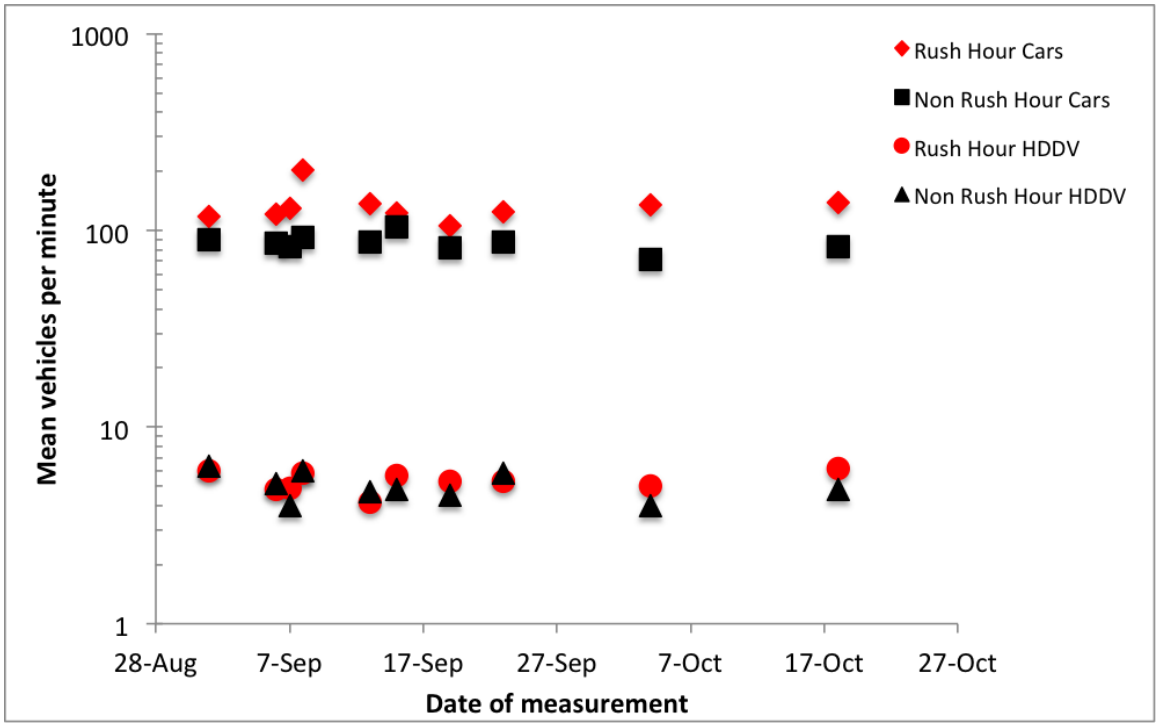

Figure 3-4. Mean vehicles (cars and heavy duty diesel vehicles (HDDV)) per minute on I-81 in Syracuse, NY during rush hour (0730 – 0900) and non-rush hour (1030 – 1200) for 10 days between September 1st, and October 18th, 2016.

3.2 Ultrafine particle concentrations

3.2.1 $PM_{2.5}$ vs. UFP

Consistent with previous literature that has shown only a weak relationship between UFP and fine particle mass concentrations in urban areas (Hagler et al., 2009), UFP concentrations at 300 m east of I-81as measured in this study are not correlated with daily mean $PM_{2.5}$ concentration data for East Syracuse (~6 km east of my sampling location) as measured by the New York Department of Environmental Conservation (Fig 3-5) and accessed via the EPA's Air Data database (https://www.epa.gov/outdoor-air-

quality-data). Indeed, there is a weak negative correlation between UFP concentration and $PM_{2.5}$, reemphasizing the need for, and the importance of, PSD measurements.

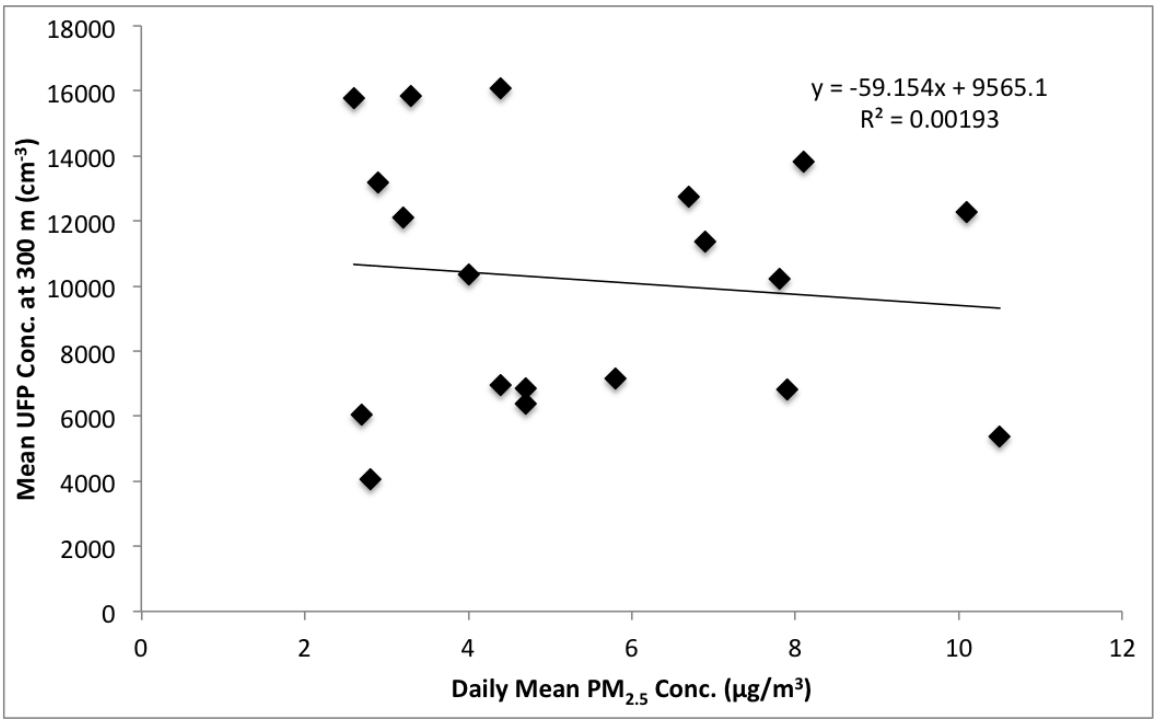

Figure 3-5. Mean UFP concentrations at 300 m east of I-81 during the 20 study days related to daily mean $PM_{2.5}$ reported by New York Department for Environmental Conservation for East Syracuse and accessed via https://www.epa.gov/outdoor-air-quality-data.

3.2.2 Rush hour vs. non-rush hour UFP concentrations

There are distinct differences between UFP concentrations during RH and NRH sampling. Median UFP concentrations of all diameters are highest during RH. Close to I-81, concentrations of 15 and 50 nm particles are elevated, whereas relatively low concentrations of 20 nm particles are detected during RH and NRH at all of the six stationary sampling locations (Fig. 3-6). While, differences in the meteorology between

RH and NRH sampling times cannot be ignored, higher traffic volumes on I-81 may be partially responsible for elevated RH UFP concentrations, as has been observed near other roadways with commuter traffic (Hagler et al., 2009; Hofman et al., 2016; Wåhlin et al., 2001). Median total UFP concentrations measured at all of the six sampling locations during RH are 1.33 times higher than those measured during NRH, while the ratio of traffic counts is ~ 1.5.

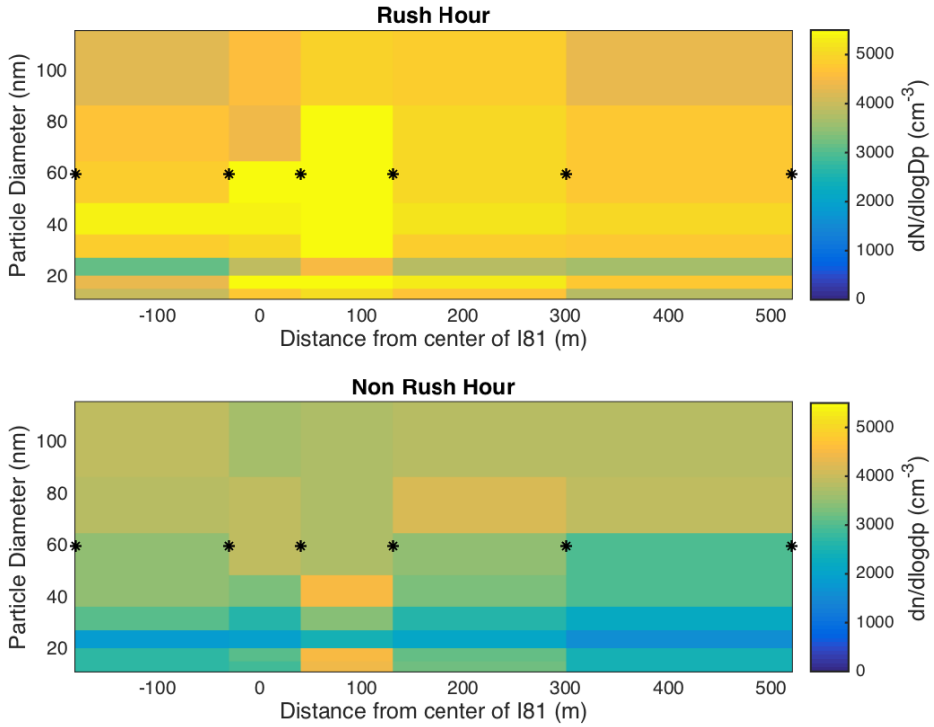

Figure 3-6. Median particle size distribution and number concentrations at the six stationary sampling locations (30, 40, 130, 180, 300, and 520 m from the center of I-81) during rush hour (07:30-09:00) and non-rush hour (10:30-12:00). Negative distance values correspond to sites west of the center of I-81.

With increasing distance from a source, one expects to see changes in PSDs due to dilution, coagulation, condensation, deposition, and evaporation. While several of

these processes are difficult to detect by solely examining PSDs, a couple of observations can be made. During RH and NRH, median PSDs at the six sampling locations are very similar, and for the most part, total particle number decreases with increasing distance from the center of I-81 (Fig. 3-7). This trend is characteristic of atmospheric dilution. A possible reason for this observation that particle concentrations are higher at 40 m, rather than 30 m are the effects of wind direction and local traffic contamination from Almond Street, which runs perpendicular to the east side of I-81, or it may reflect the complexity of flow around the elevated highway.

There are two modes in the RH and NRH PSDs. The first is centered at particle diameter (D_p)~ 15 nm, and the second is noted for D_p 30 - 50 nm. The relative magnitude of these two peaks is a function of the sampling location. The dominance of these two modes is consistent with PSDs from vehicle emissions (Morawska et al., 2008), and is similar to UFP PSDs observed near two major Los Angeles, California roadways (Zhu et al., 2002b, 2002a). While some studies have observed shifting and/or new modes in PSDs at different distances away from highways, suggesting coagulation as the main mechanism in altering the PSD (Zhu et al., 2002b, 2002a), new or shifting modes are less apparent in this dataset. It is possible that with higher diameter resolution (increased number of sampled diameters), that subtle changes of the PSD may have been more evident.

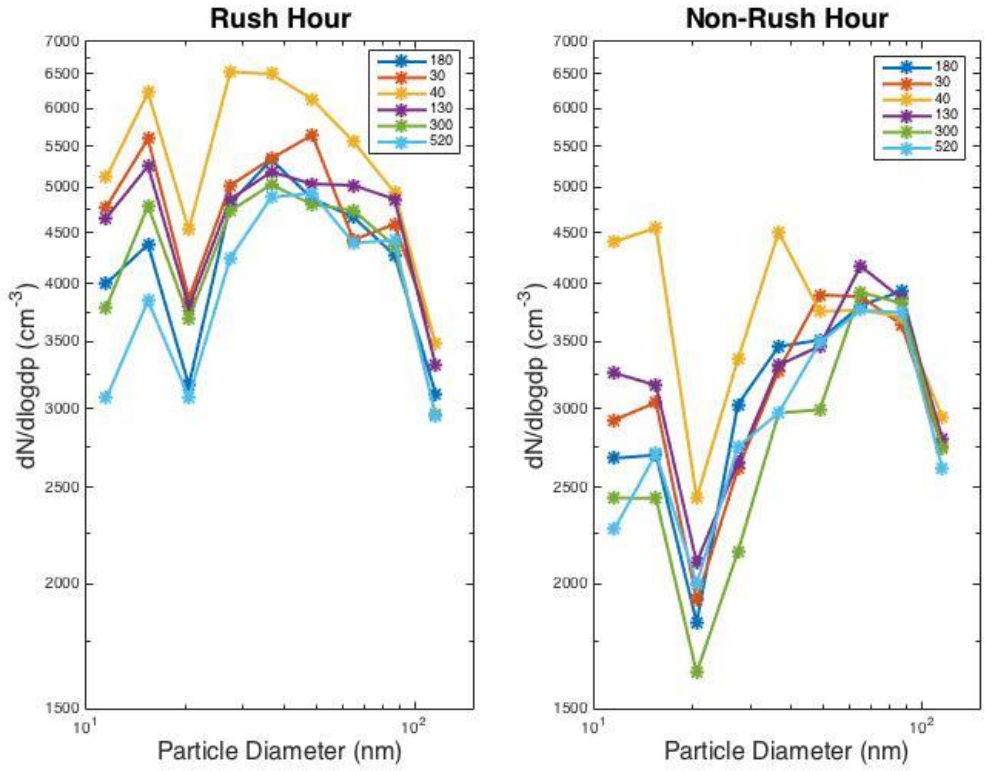

Figure 3-7. Median particle size distributions of UFP at the six stationary sampling locations (30, 40, 130, 180, 300, and 520 m from the center of I-81) during rush hour (RH) (07:30-09:00) and non rush hour (NRH) (10:30-12:00) sampling periods.

Figure 3-8 shows the change in median number concentrations between 30 m and 520 m from the center of I-81 during RH and NRH for all sampled UFP diameters. A decrease in number concentration is seen in most diameters in both RH and NRH, with the greatest decrease in 10-nm particles for both RH (23%) and NRH (15%). Some diameters (~15 nm (NRH), ~20 nm (NRH), ~50 nm (RH), and ~90nm (RH)) show small increases (under 10%) in number concentration. These results indicate that for most sizes of UFP, concentrations are lower further from I-81. For particles with D_p > 10 nm, smaller decreases and even increases may occur due to the combined effects of dilution,

coagulation, and condensation, as well as contamination from local, non-I-81 sources, such as local vehicle traffic.

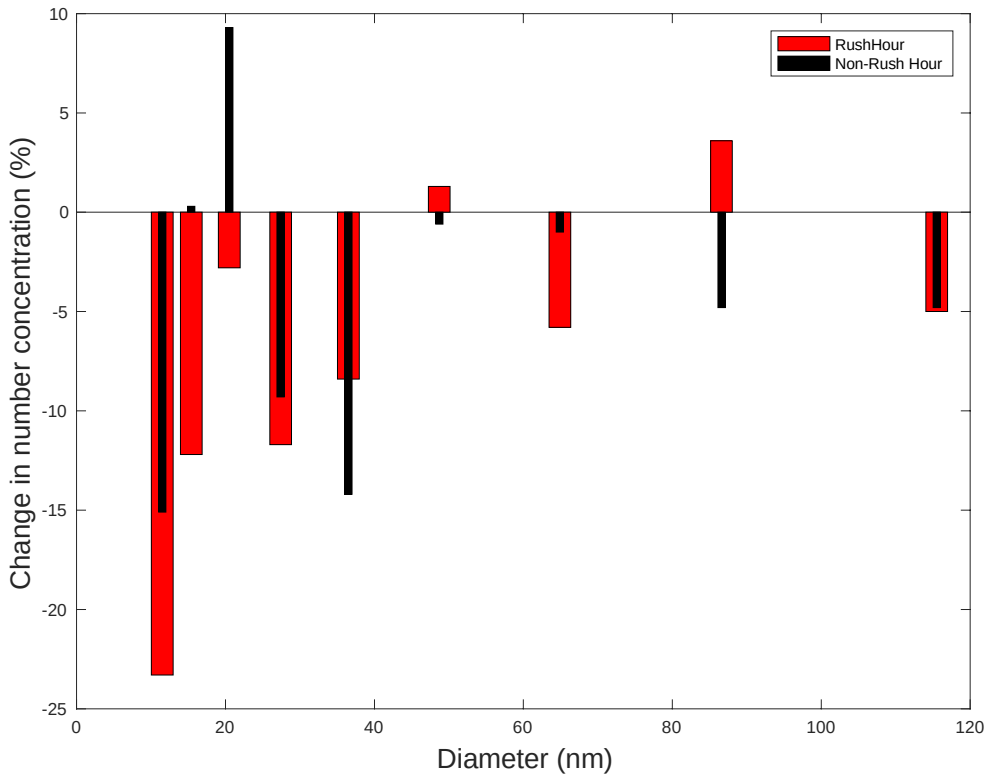

Figure 3-8. Change in median number concentration of UFP from 30 m west to 520 m east of the center of I-81 during rush hour (07:30 – 09:00) and non-rush hour (10:30 – 12:00).

The ratio of nucleation mode (<50 nm) to accumulation mode (50 - 420 nm) particle concentrations at all sampling locations is greatest during RH (Fig. 3-9). These mode classifications are unconventional, but were adopted for this analysis in order to compare the results with Pirjola et al. (2006). The ratio is highest close to I-81, with an overall decreasing trend with distance from I-81. Pirjola et al. (2006) observed a similar trend during winter near an urban highway in Finland and concluded that nucleation

mode particles are more effectively diluted than accumulation mode particles due to urban background sources of accumulation mode particles.

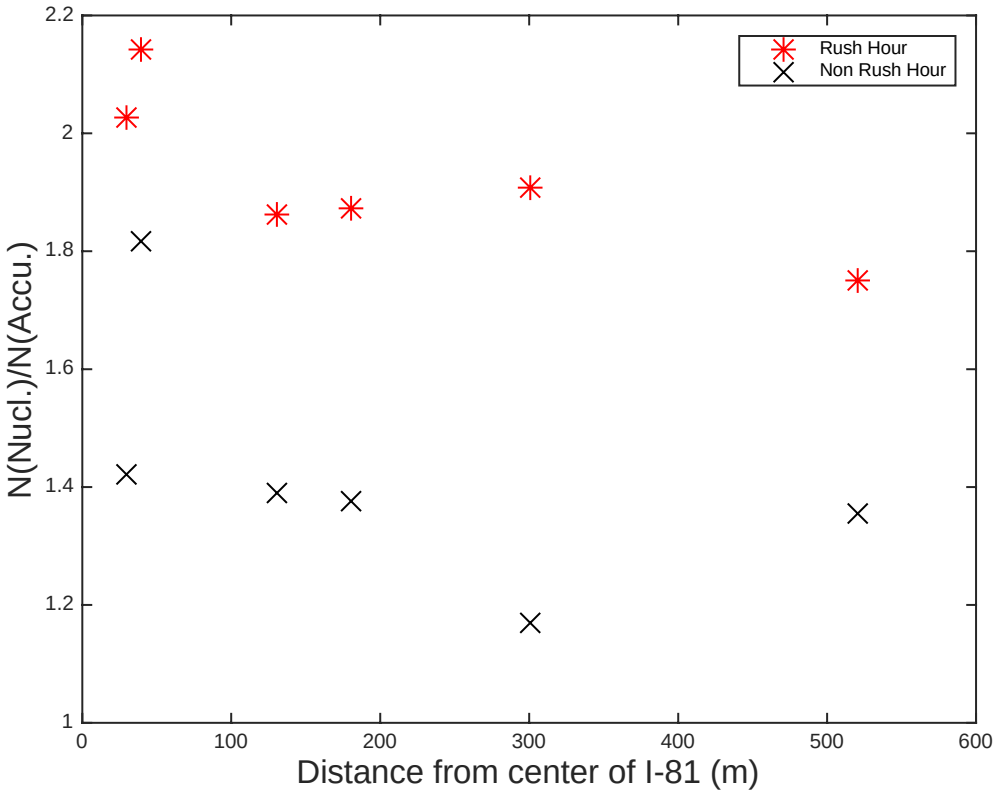

Figure 3-9. Ratio of median nucleation mode (<50 nm) particle concentrations to median accumulation mode (50-420 nm) particle concentrations at the six stationary sampling locations (30, 40, 130, 180, 300, and 520 m from the center of I-81) during rush hour (07:30 – 09:00) and rush hour (10:30 – 12:00) sampling.

Sample to sample variability in the median PSDs is less during RH (Fig. 3-10). The 75th and 25th percentile is smaller than that during NRH. Also, the interquartile range of the individual datasets is lower during RH, and particularly the 25th percentile values are highly variable in the NRH samples. Possible explanations for the greater variability in NRH samples include:

- Greater dilution rates during NRH due to slightly higher wind speeds
- Higher variability of the wind direction during NRH (southeastern winds were more common during NRH and which are associated with neither parallel or perpendicular flow relative to I-81)
- Lower traffic volume on I-81, allowing other possibly more time varying sources to play a greater role in dictating UFP concentrations.

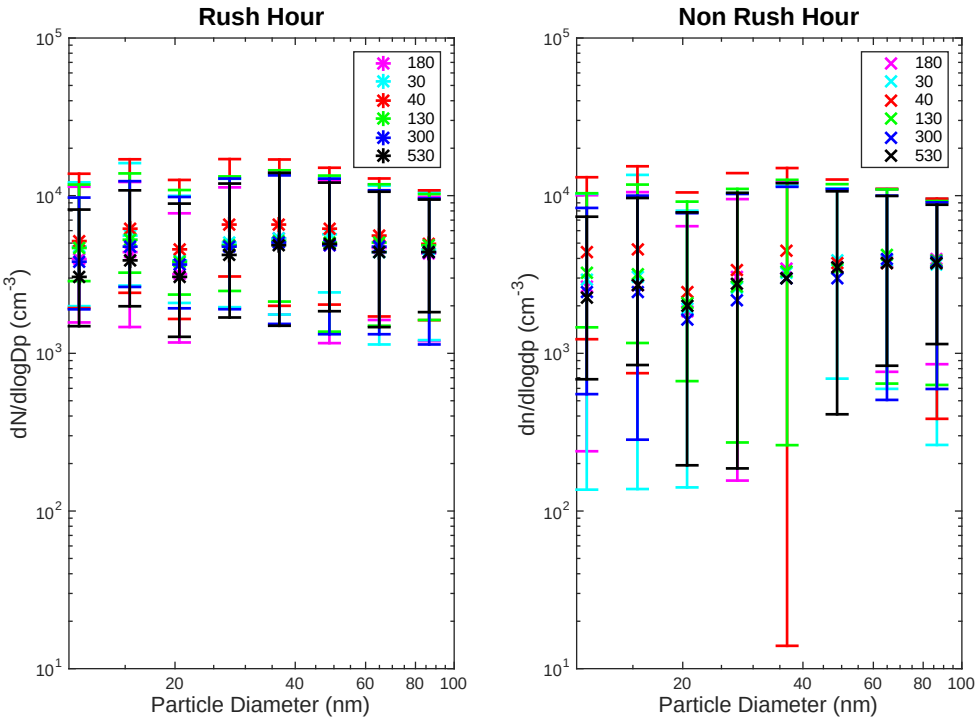

Figure 3-10. Median and interquartile range of particle size distributions at the six stationary sampling locations (30, 40, 130, 180, 300 and 520 m from the center of I-81) during rush hour (07:30-09:00) and non-rush hour (10:30-12:00) sampling. The asterisks denote the median value for each diameter, while the vertical line extends from the 25th to the 75th percentile. The different colors indicate different sampling locations (see legend) from I-81 in m.

Consistent with expectations, when median particle concentrations at the six stationary locations during RH and NRH samples were subject to a Bootstrapped Wilcoxon Rank Sum Test, all p-values were < 0.05, suggesting significant differences in median particle concentrations during RH and NRH (Fig. 3-11).

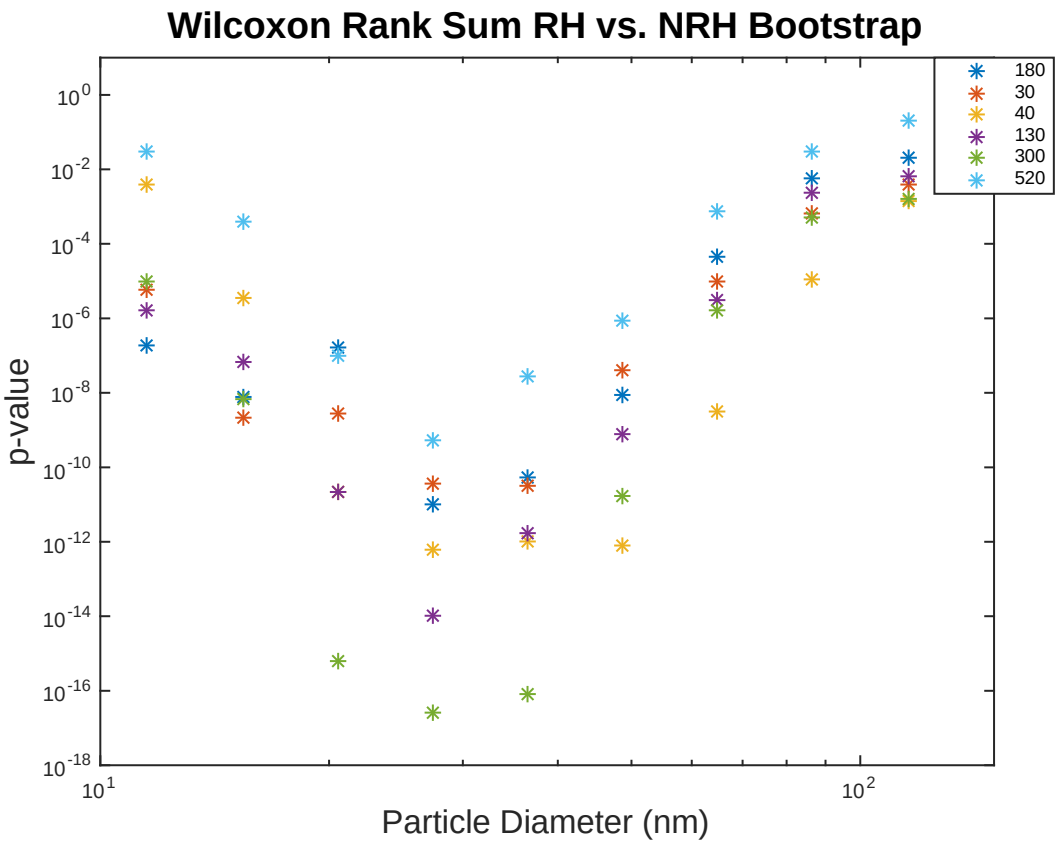

Figure 3-11. Median p-values for ultrafine particle diameters from a bootstrapped Wilcoxon rank sum test comparing median particle concentrations at the six stationary sampling locations (30, 40, 130, 180, 300, and 520 m from the center of I-81) during rush hour (07:30-09:00) and non-rush hour (10:30-12:00).

Differences in PSDs sampled under different wind direction conditions are also evident. During RH, the median total UFP concentrations at 520 m from I-81 are 17% lower than those at 40 m under parallel winds, compared with perpendicular winds.

During NRH, the difference is -24% during parallel winds (Fig. 3-12). The difference (concentration (40 m) – concentration (520 m)) is greatest during parallel winds because UFP from I-81 decayed faster with distance from the highway, as the sampling locations are not downwind from the highway source. Similar results were found in Cincinnati, Ohio. UFP concentrations decayed by up to 80% at a distance of 400 m from the roadway under parallel wind conditions, but as little as 10% under perpendicular winds (Reponen et al., 2003).

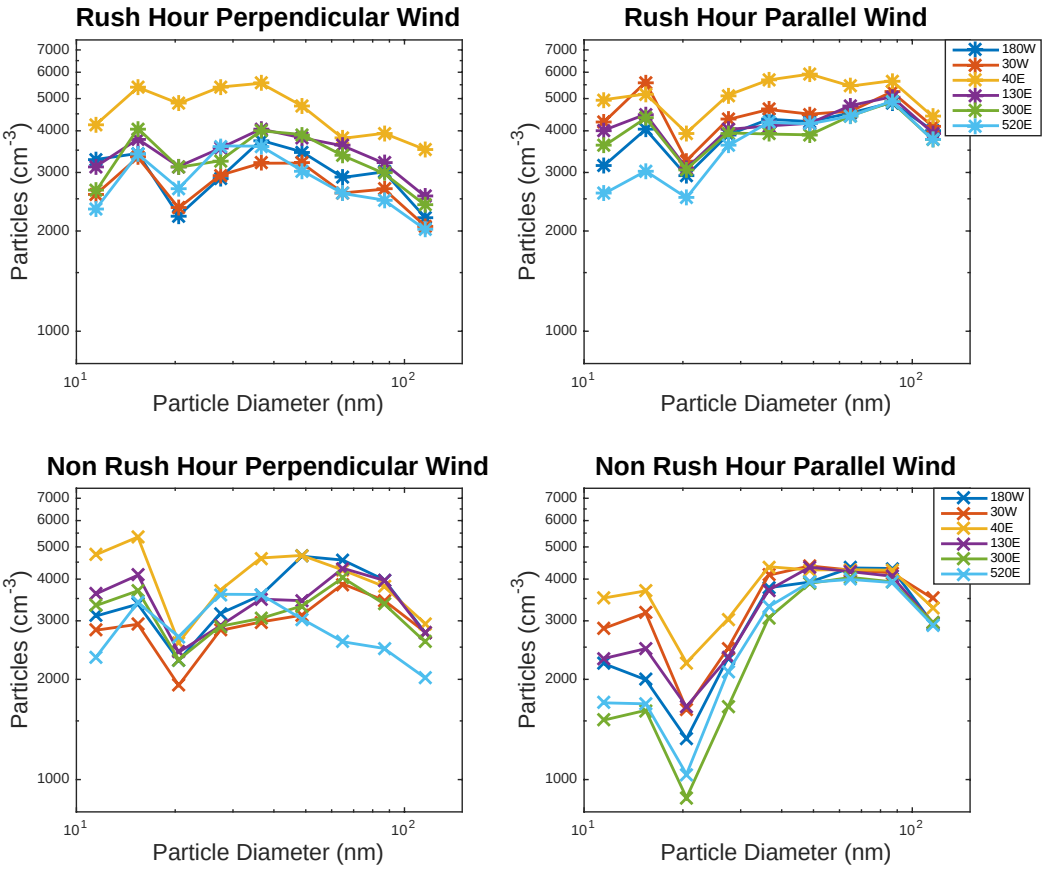

Figure 3-12. Median number ultrafine particle size distributions during rush hour (07:30-09:00) and non-rush hour (10:30-12:00) at the six sampling locations (30, 40, 130, 180, 300, and 520 m from the center of I-81) under parallel (330˚ to 30˚, and 150˚-210˚) and perpendicular (240˚ to 300˚) wind directions.

Mobile measurements taken along the transects of 15- and 50-nm diameter particles along Fayette Street indicate consistently higher concentrations of 50 nm particles during both rush hour and non-rush hour periods (Fig, 3-13), but the median values computed across all 20 sampling days do not indicate a clear tendency towards decreased concentrations with lateral displacement from I-81. This is examined further below.

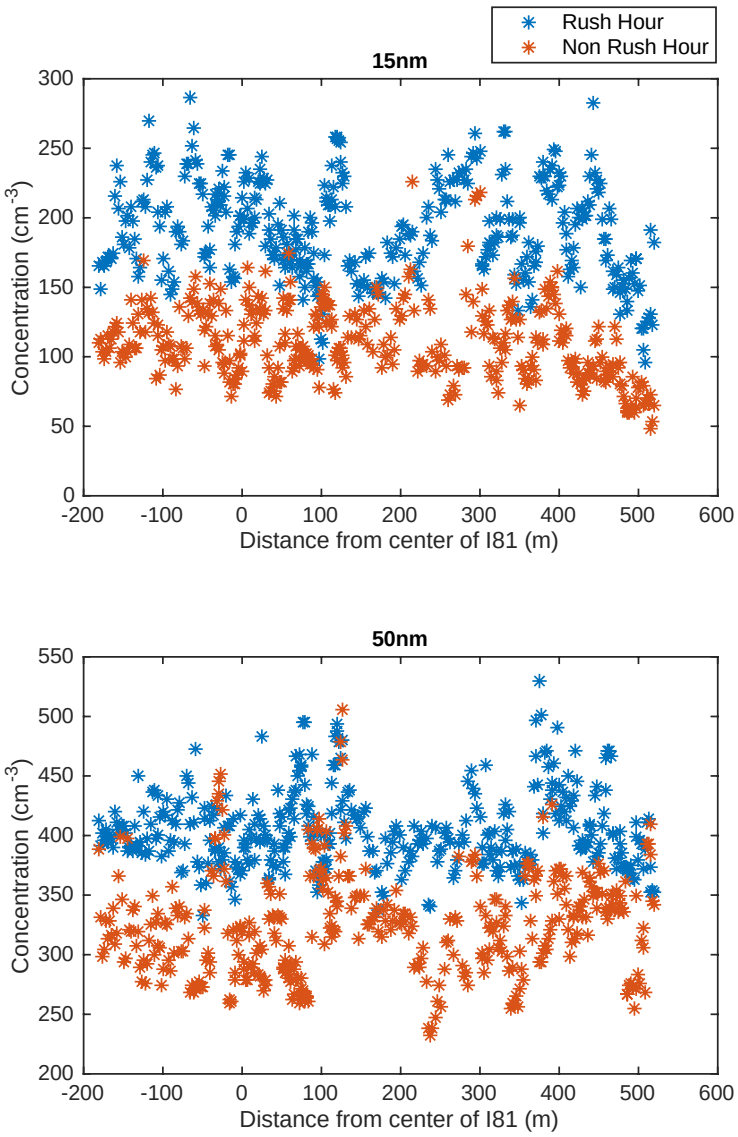

Figure 3-13. Median 1-second number concentrations of 15 and 50 nm particles from mobile sampling during rush hour (07:30-09:00) and non-rush hour (10:30-12:00).

3.2.3 Variation of UFP concentrations with lateral distance from I-81

Out of the three fits attempted, the exponential form $y = a \times e^{bx}$ best describes the decay of UFP from I-81 during RH and NRH (Table 3-2, Fig. 3-14). This finding is

in agreement with those from similar empirical studies (Hagler et al., 2009; Zhu et al., 2002b, 2002a); however, RMSE values only indicate a moderate relationship for RH and a weak relationship for NRH.

Table 3-2. Root mean square error (RMSE) for the three attempted fits of normalized, median ultrafine particle concentrations at the six stationary sampling locations (30, 40, 130, 180, 300, and 520 m from the center of I-81), and distance from the center of I-81.

Equation	Rush Hour RMSE	Non Rush Hour RMSE
$y = a\frac{1}{x}$	0.69	0.75
$y = a\frac{1}{x^2}$	0.83	0.92
$y = ae^{bx}$	0.06	0.15

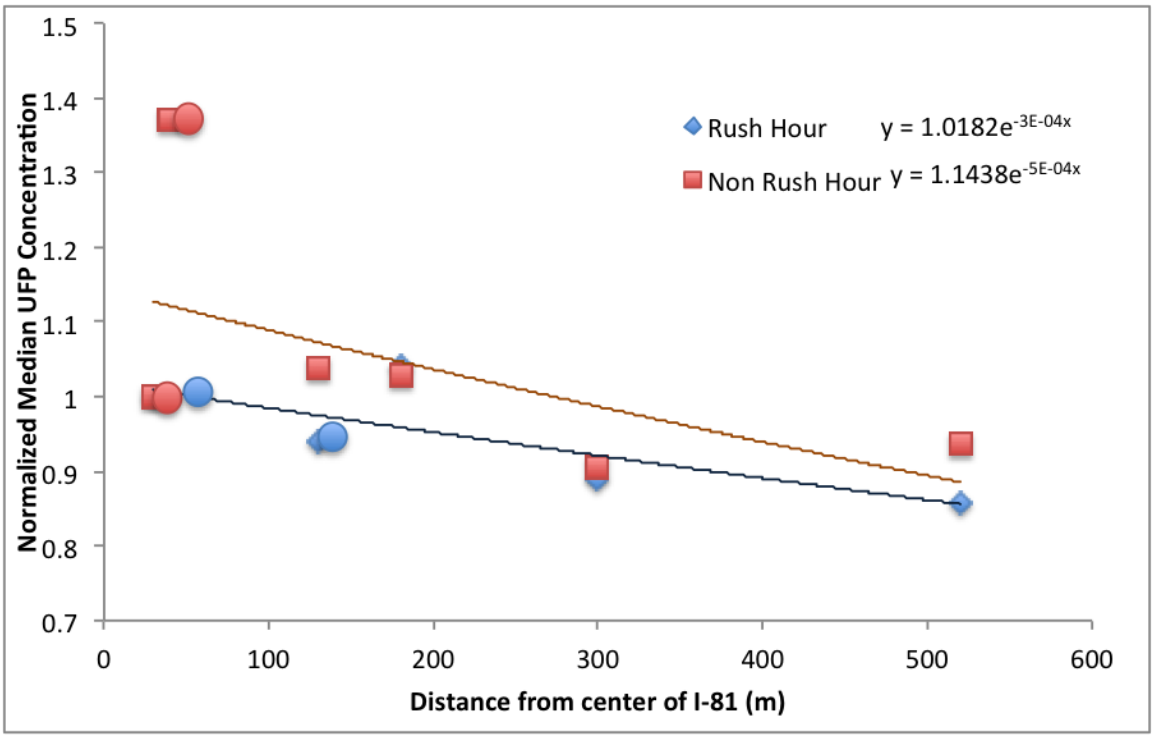

Figure 3-14. Exponential fits to normalized median ultrafine particle concentrations during rush hour (0730-0900) and non-rush hour (1030-1200) with distance from the center of I-81 (m) at the six stationary sampling locations (30, 40, 130, 180, 300, and 520 m). Due to the large sample-to-sample variability in UFP concentrations, the UFP are normalized for each sample to the value at 30 m displacement and then an average of those normalized values is computed. Circular points indicate sampling locations west of I-81; all other points correspond to sampling locations east of I-81.

To compare UFP concentrations near I-81 measured in this study with previous near-roadway studies, data from five other studies are plotted with data from this study (Fig. 3-15). UFP concentrations at all sampling locations are at least three times greater in the two Los Angeles, California-based studies (Zhu et al., 2002b, 2002a). While the two Los Angeles studies measured a greater range of particle diameters (6-220 nm) than this study, the most likely reasons for the higher concentrations are consistent wind direction

that crossed over the highways and directly toward the sampling locations, and both highways included in these studies have 8-9 lanes and experience greater traffic volumes than the studied portion of I-81 in Syracuse. The study with a UFP decay profile most like the one observed in this study is from a roadway in Raleigh, North Carolina (Hagler et al., 2009). The Raleigh study took place near a roadway with traffic volumes only slightly greater (~125,000 day^{-1}) than the AADT of the studied portion of I-81, but differs in that the near-roadway environment is much more open and free from buildings and obstructions than that in this study. While one of the comparison highways (405 in Los Angeles) is elevated to a similar height above the ground as I-81 (Zhu et al., 2002b), it is not open underneath like I-81, and therefore is not suitable as comparison. The structure of I-81 likely allows for greater UFP dispersion as UFP can be circulated down to the street below and through the median and sides of I-81. Without a suitable comparison stretch of I-81, it is impossible to test this hypothesis; however, the structure of I-81 is likely influential in dispersing UFP. It is also important to note that in this study, it was determined that the UFP data were not normally distributed, and thus I present the median data; however, the studies included in the comparison figure (Fig. 3-15) presented mean UFP concentrations.

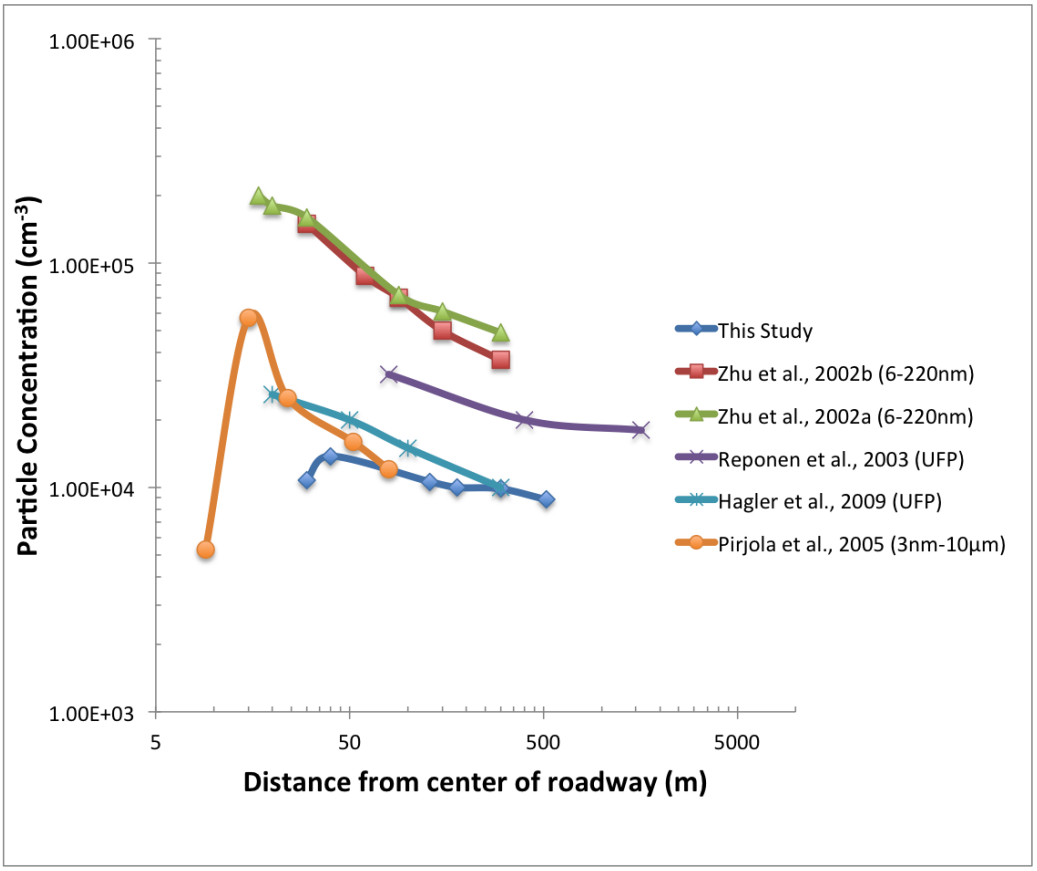

Figure 3-15. Comparison between median ultrafine particle concentrations (diameters < 100 nm) measured in this study, with reported particle concentrations from similar, near-roadway studies.

In contrast to the overall ensemble, very few individual RH and NRH transects of median UFP concentrations conform to exponential decay. Of the RH sample, 11 of the 40 transect fits have RMSE values less than 0.15, and during NRH that number is only 7 out of 40. While unanticipated, these results serve as an important reminder and example of how variable (in both space and time) UFP are in an urban environment as previously noted by Costabile et al.(2009).

To investigate a possible explanation for the large portion of individual transects that do not conform to exponential decay, anomalous data points (i.e., data points from

individual transects that fall above the line of best fit) were plotted against the SVF, local car counts, and local HDDV counts from respective sampling locations (Fig. 3-16). Spearman's Rank Correlation (Gibbons and Chakraborti, 2010) was performed and results are displayed in Table 3-3. NRH anomalous normalized UFP concentrations are significantly correlated with SVF, but not as expected. It was expected to see a decreasing trend of anomalous normalized UFP concentrations with increasing SVF, as a SVF close to one suggests an open, well-ventilated area. However, many of the highest anomalously high normalized UFP concentrations occurred at sampling locations with SVF of ~0.9. Likely, there is another source of contamination related to the sampling location (520 m) that is responsible for the anomalous UFP concentrations. Occasionally, lawn mowers and leaf blowers were present at the sampling locations during RH. The presence of these UFP sources may have influenced some of the anomalous data as previously suggested by Drewnick et al. (2008).

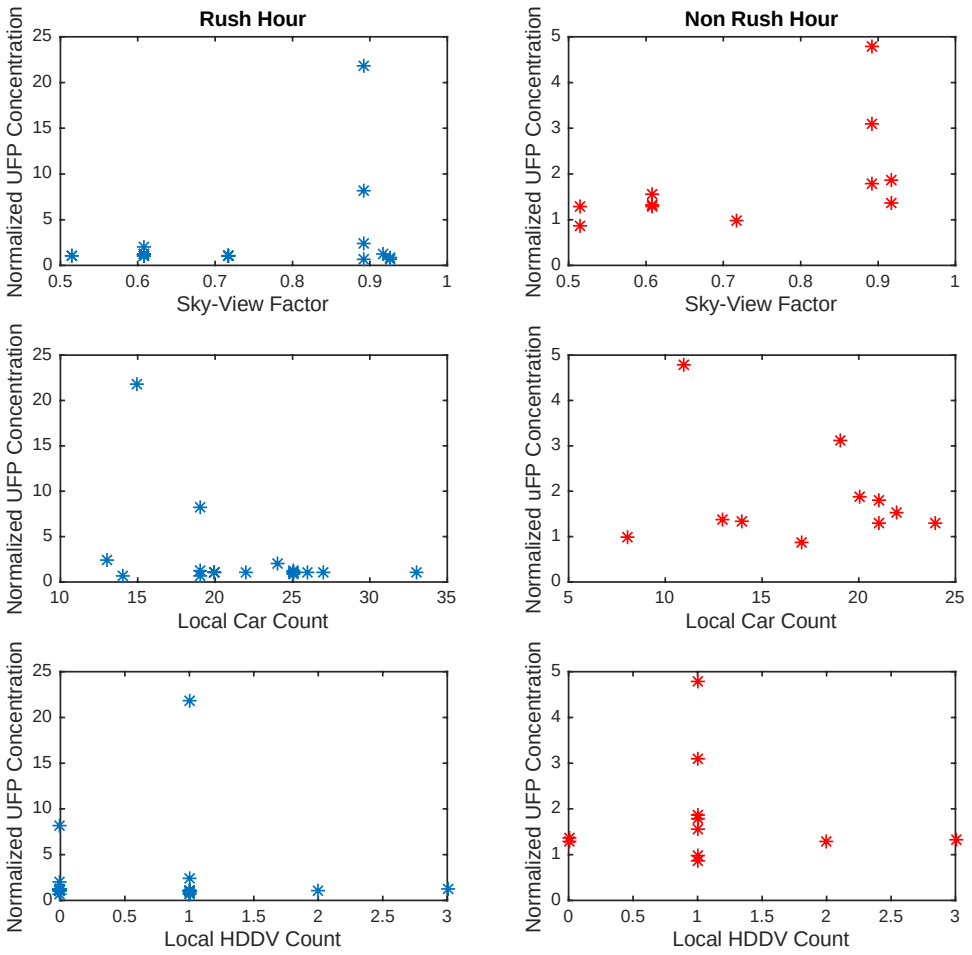

Figure 3-16. Anomalous normalized ultrafine particle concentrations from rush hour (07:30 -09:00) and non-rush hour (10:30 – 12:00) plotted against respective sky-view factors, local car counts (5 min^{-1}) and local HDDV counts (5 min^{-1}).

Table 3-3. Results from Spearman's Rank Correlation of anomalous normalized ultrafine particle concentrations from rush hour (0730 -0900) and non-rush hour (1030 – 1200) with respective sky-view factors, local car counts (5 min^{-1}) and local HDDV counts (5 min^{-1}).

	Rush Hour		**Non Rush Hour**	
	Spearman's Rank Coefficient	P-Value	Spearman's Rank Coefficient	P-value
Sky-View Factor	-0.16	0.54	0.69	0.02
Local Car Count	-0.24	0.35	0.0023	0.99
Local HDDV Count	-0.02	0.95	-0.04	0.91

To fit an exponential to 15 and 50 nm particle concentrations from mobile data, a moving average was applied to median concentration data and the sample size was reduced to 15 to smooth the data. The data were then normalized to the particle concentration closest to the center of I-81 (~9 m). The RMSE values for the exponential fits indicate that 15- and 50-nm particles may not follow the overall trend of total particle concentrations, or may be slow to decay (Fig. 3-17,18). Fifteen- and 50-nm particles may be slower to decrease in this environment, perhaps because of sources outside of I-81 such as local traffic.

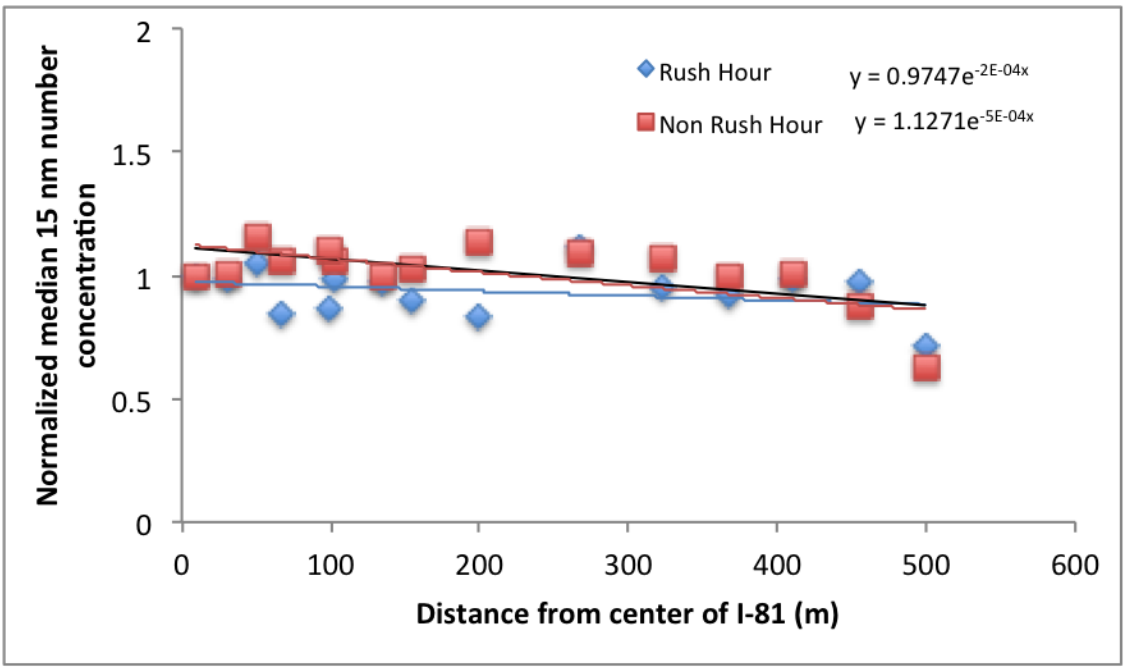

Figure 3-17. Exponential fits of the median number concentration of particles with a diameter of 15 nm with lateral distance (m) from I-81 as measured during the mobile sampling conducted during rush hour (07:30-09:00) (RMSE = 0.10) and non-rush hour (10:30 – 12:00) (RMSE = 0.11).

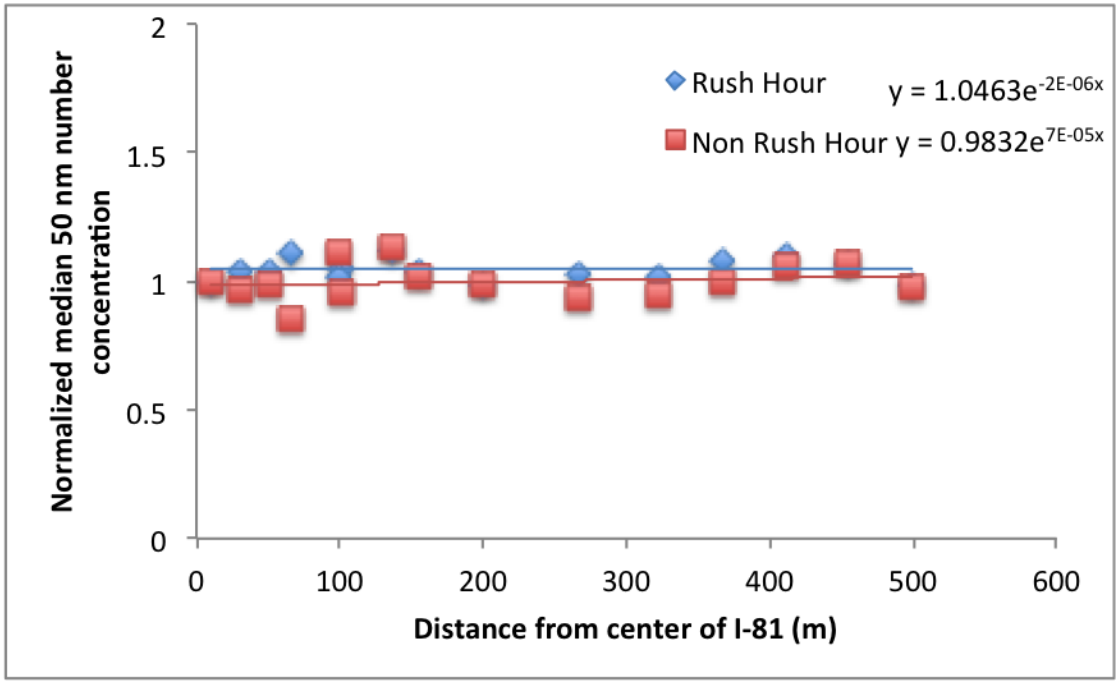

Figure 3-18. Exponential fits of the median number concentration of particles with a diameter of 50 nm with lateral distance (m) from I-81 as measured during the mobile sampling conducted during rush hour (07:30-09:00) (RMSE = 0.04) and non-rush hour (10:30 – 12:00) (RMSE = 0.07).

3.2.4 Evaluation of the influence of local traffic on Fayette Street

While some vehicles may be more polluting than others, it was hypothesized that more local traffic on Fayette Street would lead to increased UFP concentrations and greater variance around the transect mean and median.

For total UFP number concentrations during RH and NRH, there are no clear, observable differences in mean concentration or variance around the mean when few cars passed by the sampling location versus many cars (Fig. 3-19, 3-20). When 15- and 50-nm

number concentrations are analyzed separately, the results are similar despite the connection between particles of those sizes and vehicle emissions (Figs. 3-21, 3-22).

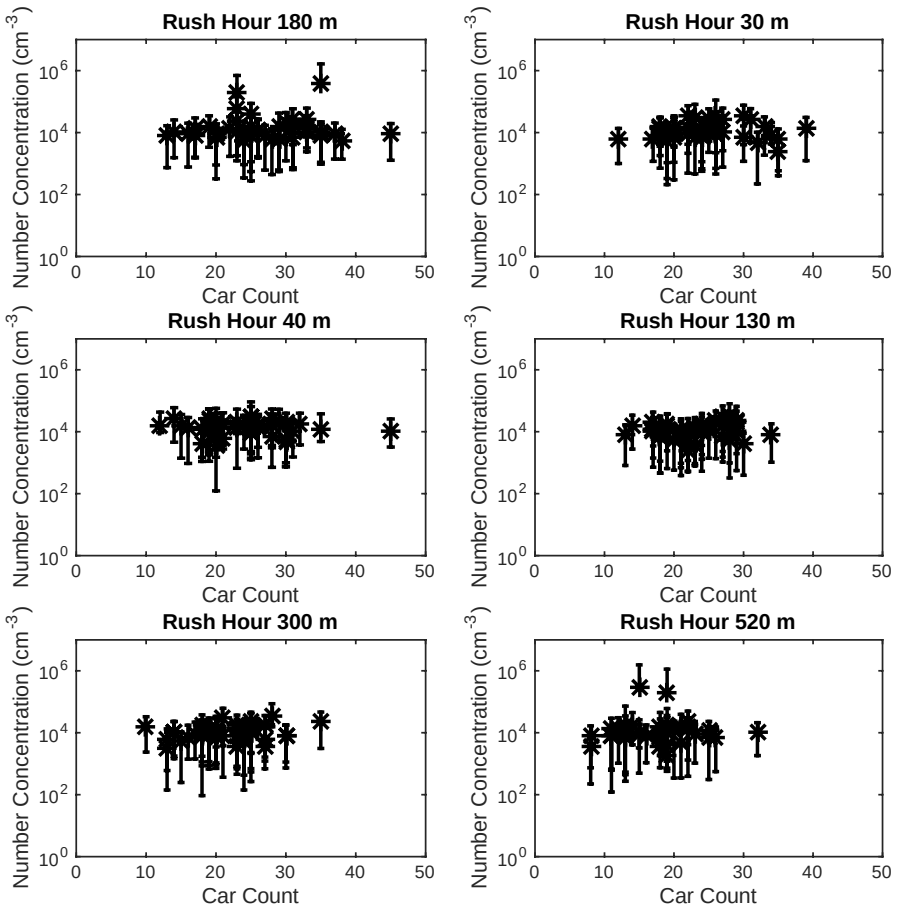

Figure 3-19. Mean total ultrafine particle number concentration versus car counts during rush hour (07:30-09:00) at the six stationary locations (30, 40, 130, 180, 300, and 520 m from the center of I-81). Top and bottom bars correspond to maximum and minimum concentrations, respectively.

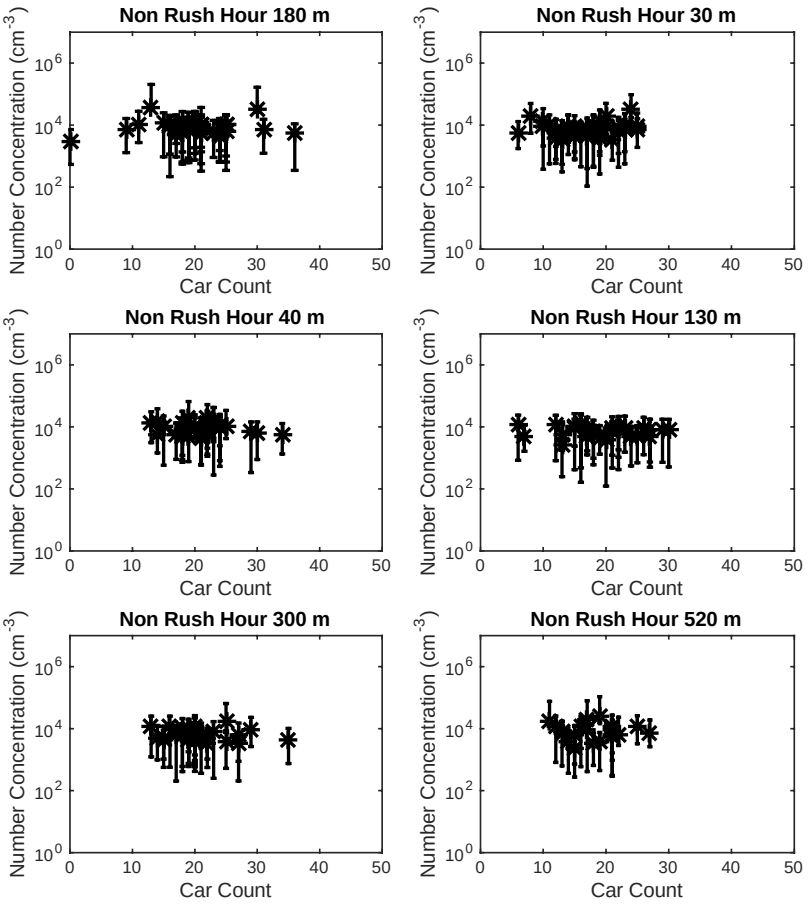

Figure 3-20. Mean total ultrafine particle number concentration versus car counts during non-rush hour (10:30-12:00) at the six stationary locations (30, 40, 130, 180, 300, and 520 m from the center of I-81). Top and bottom bars correspond to maximum and minimum concentrations, respectively.

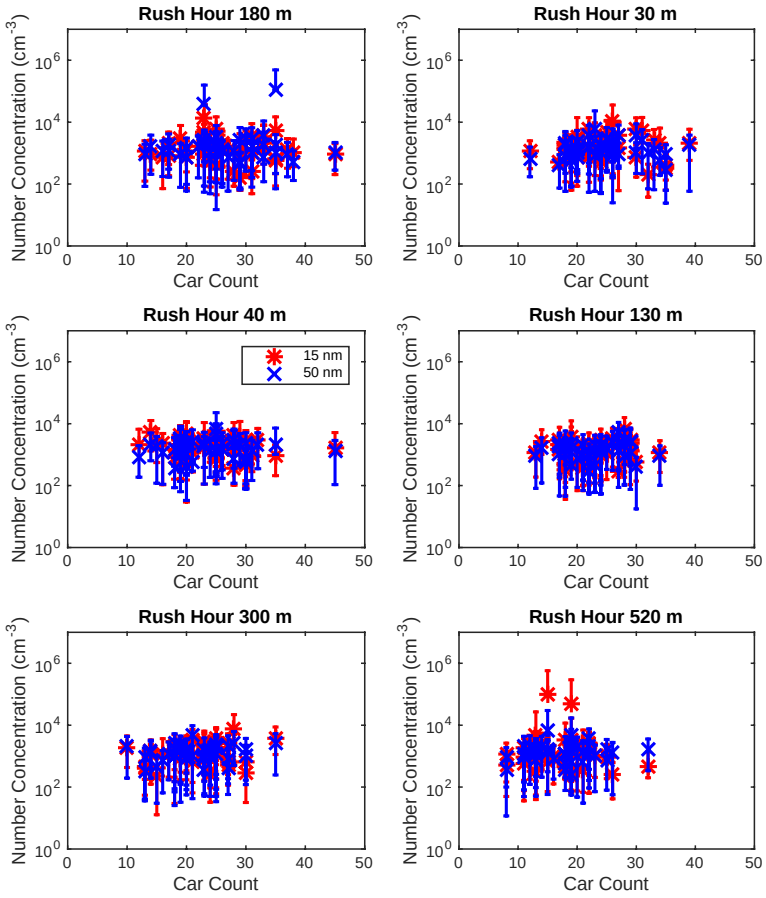

Figure 3-21. Mean 15 and 50 nm number concentration versus car counts during rush hour (07:30-09:00) at the six stationary locations (30, 40, 130, 180, 300, and 520 m from the center of I-81). Top and bottom bars correspond to maximum and minimum concentrations, respectively.

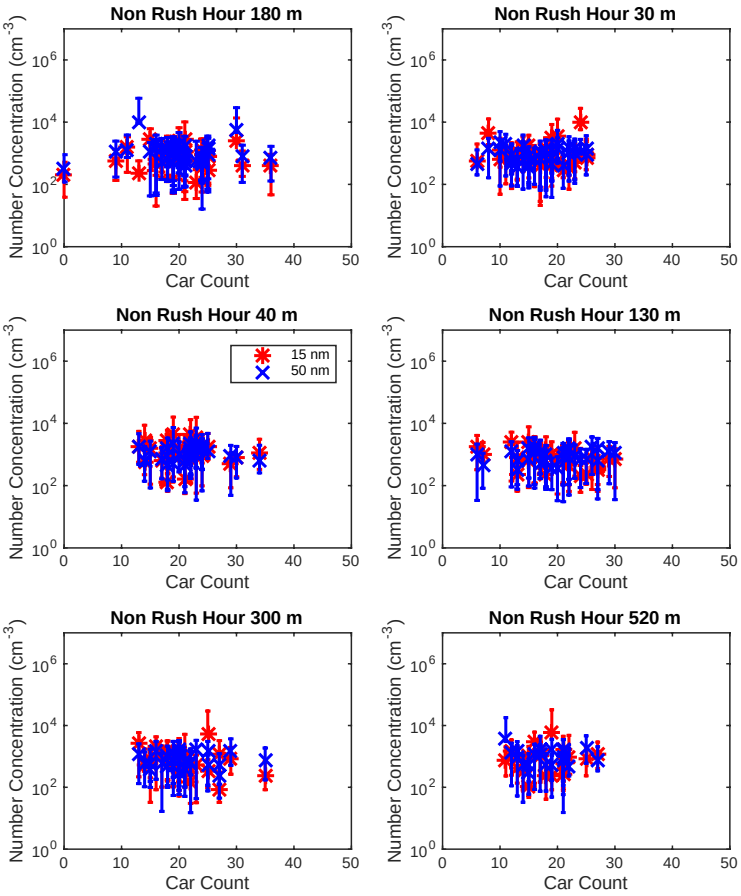

Figure 3-22. Mean 15 and 50 nm number concentration versus car counts during non-rush hour (1030-1200) at the six stationary locations (30, 40, 130, 180, 300, and 520 m from the center of I-81). Top and bottom bars correspond to maximum and minimum concentrations, respectively.

Similarly, no visible effects are noted when the number of HDDV is compared with the mean UFP concentration and variance around the mean during RH and NRH (Figs. 3-23, 3-24). Higher mean UFP concentrations are evident at several of the sampling locations during RH. In particular, at 520 m there are two points during RH that are an order of magnitude greater than the rest and NRH. Since the 15-nm number

concentrations appear elevated at 520 m during RH (Fig. 3-25) as well as total UFP, this indicates that the total UFP number concentration for the two outlying points is dominated by 15 nm particles that are often associated with vehicle emissions. Upon review of GoPro video footage, the 520 m sampling location often experienced HDDV school bus traffic during RH that was not present during NRH (Fig. 3-26). The increased number of school buses on the road at this time may explain the high concentration outliers during RH at 520 m, as school buses have been shown to emit high concentrations of UFP (Zhang et al., 2013; Zhang and Zhu, 2010).

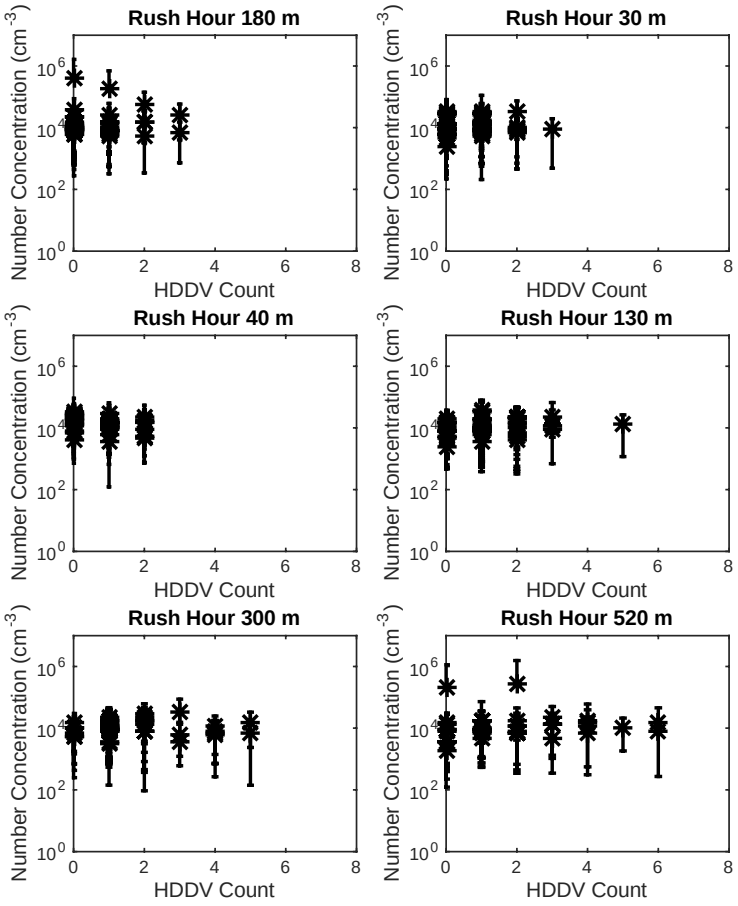

Figure 3-23. Mean total ultrafine particle number concentrations sampled by the number of heavy-duty diesel vehicles at the six stationary sampling locations (30, 40, 130, 180, 300, and 520 m from the center of I-81) during rush hour (07:30-09:00). Top and bottom bars correspond to maximum and minimum concentrations respectively.

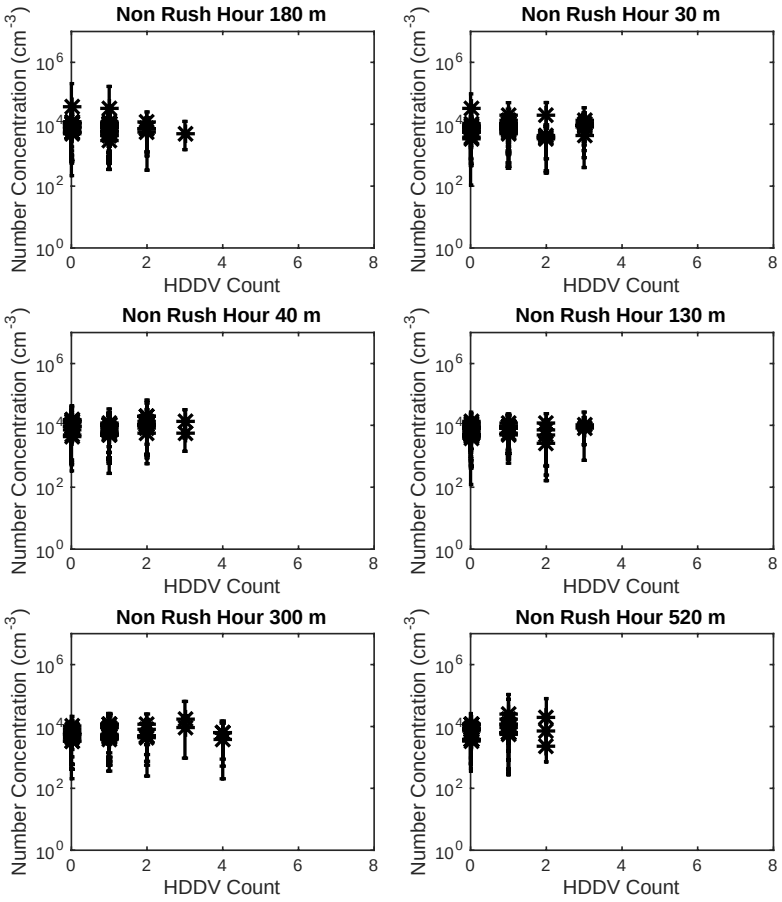

Figure 3-24. Mean total ultrafine particle number concentrations sampled by the number of heavy-duty diesel vehicles at the six stationary sampling locations (30, 40, 130, 180, 300, and 520 m from the center of I-81) during non-rush hour (10:30-12:00). Top and bottom bars correspond to maximum and minimum concentrations respectively.

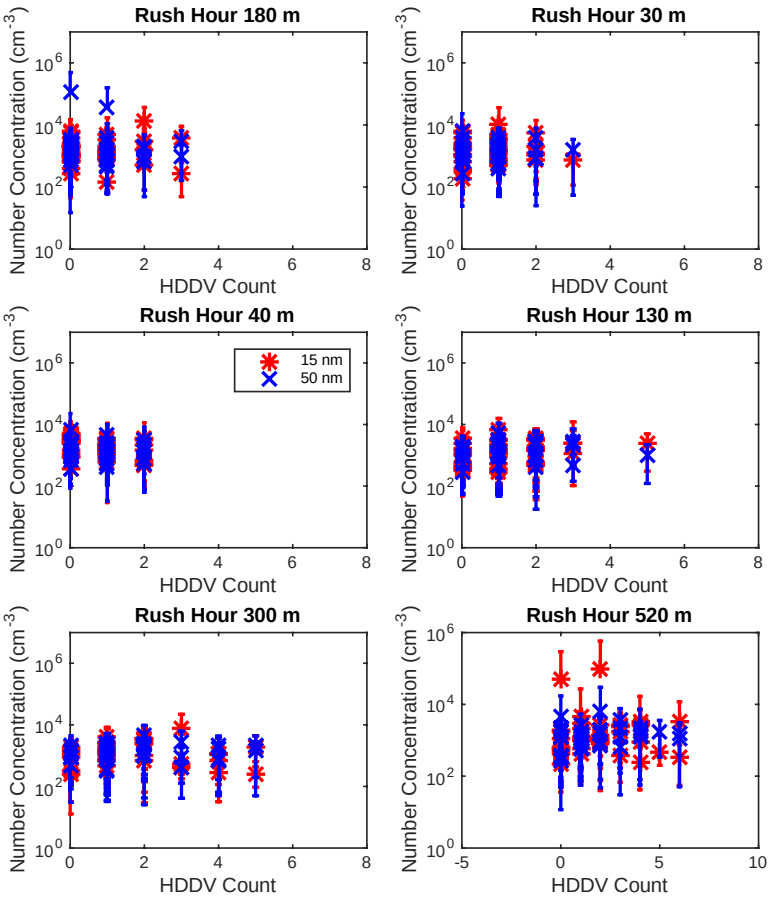

Figure 3-25. Mean 15- and 50-nm number concentrations sampled by the number of heavy-duty diesel vehicles at the six stationary sampling locations (30, 40, 130, 180, 300, and 520 m from the center of I-81) during rush hour (07:30-09:00). Top and bottom bars correspond to maximum and minimum concentrations respectively.

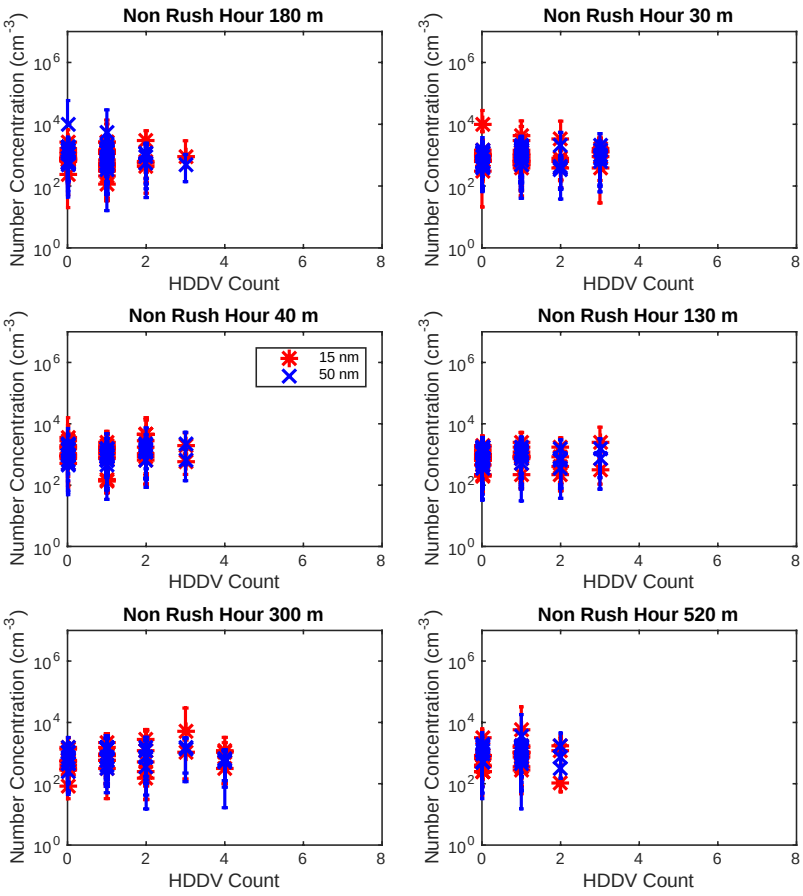

Figure 3-26. Mean 15- and 50-nm number concentrations sampled by the number of heavy-duty diesel vehicles at the six stationary sampling locations (30, 40, 130, 180, 300, and 520 m from the center of I-81) during non-rush hour (10:30-12:00). Top and bottom bars correspond to maximum and minimum concentrations, respectively

3.2.5 LME Analysis

LME analysis was undertaken to examine the role of different controls on UFP concentrations. Results from the LME analysis for RH are displayed in Table 3-4, and residuals are plotted in Figure 3-27. In order with *a priori* expectation, temperature and

distance from the center of I-81 significantly affect observed UFP concentrations. Both increasing temperature and distance decrease UFP concentrations. These results concur with those from other studies that have shown decreasing UFP concentrations with increasing distance from a source and/or temperature (Hagler et al., 2009; Janhäll et al., 2012; Reponen et al., 2003; Zhu et al., 2002a, 2002b). The result pertaining to temperature is especially relevant for northern or high elevation cities such as Syracuse that experience multiple months of cold weather, or for urban areas that experience large, diurnal changes in temperature, because cool mornings in combination with high-traffic time periods like RH could lead to short-term increases in UFP concentrations.

While only a weak relationship is observed between NRH UFP concentrations and distance from I-81 in section 3.2.3 (Fig. 3-14), of the five variables included in the LME, only distance from the center of I-81 is significant (Table 3-5). Just as in RH, increasing distance from I-81 is associated with decreasing UFP concentrations. Temperature is likely not significant because NRH samples were taken in a narrower range of warmer temperatures than RH (Fig. 3-1). Likewise, other variables such as wind speed may not have been significant for this dataset in either RH or NRH due to the relatively persistent, calm nature of the winds in Syracuse during the sampling period.

Plots of residuals ideally fall directly on the dashed y = 0 line (Figures 3-27 and 3-28). When that occurs, the LME is appropriate for the dataset. While residual plots shown in figures 3-27 and 3-28 generally adhere to this rule, they also indicate that another predictor variable not included in the dataset is likely also influencing UFP concentrations. Previous studies (Morawska et al., 2008) have identified relative humidity and atmospheric stability as predictors of UFP concentrations, and these

parameters were not included in this study. In addition, new particle formation events have been observed in other urban environments (Hofman et al., 2016, Pryor et al., 2011) and may have also occurred in Syracuse, which would contribute to the variability of UFP concentrations.

Table 3-4. Table of estimates and p-values for predictor variables included in the rush hour (07:30 -09:00) linear mixed effects model.

Coefficient	**Estimate**	**p-value**
Intercept	12028	8.6×10^{-35}
Local traffic count	94.927	0.72
Wind speed	-261.69	0.76
Wind direction	-367.82	0.66
Temperature	-4210.5	3.2×10^{-6}
Distance from center of I-81	-967.96	9.8×10^{-5}

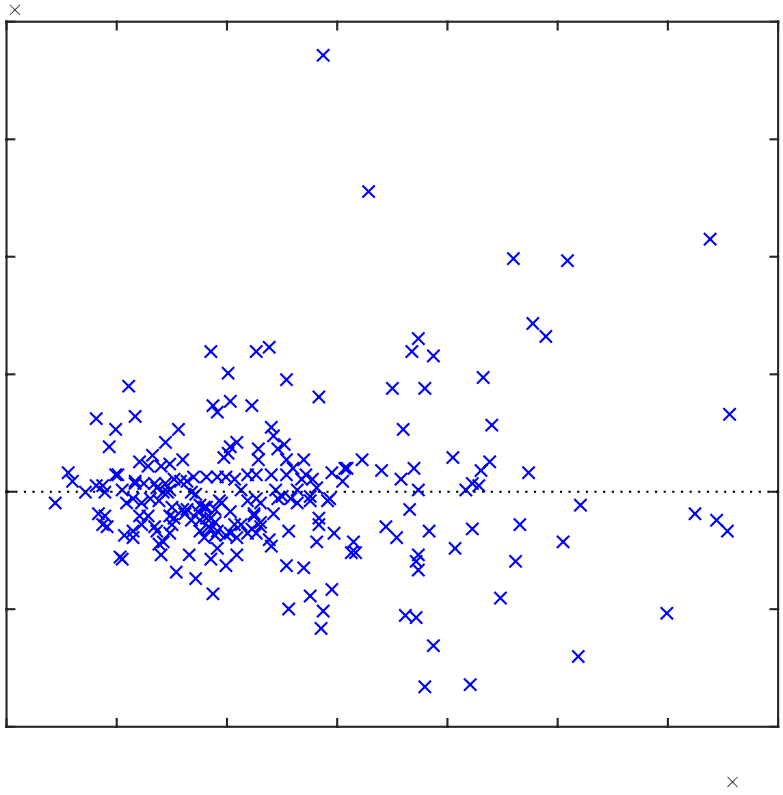

Figure 3-27. Plot of residuals for the rush hour (07:30 -09:00) linear mixed effects model.

Table 3-5. Table of estimates and p-values for predictor variables included in the non-rush hour (10:30 -12:00) linear mixed effects model.

Coefficient	**Estimate**	**p-value**
Intercept	7510.5	2.0×10^{-34}
Local traffic count	134.26	0.49
Wind speed	-49.547	0.92
Wind direction	-268.65	0.58
Temperature	-213.46	0.67
Distance from center of I-81	-682.16	2.8×10^{-4}

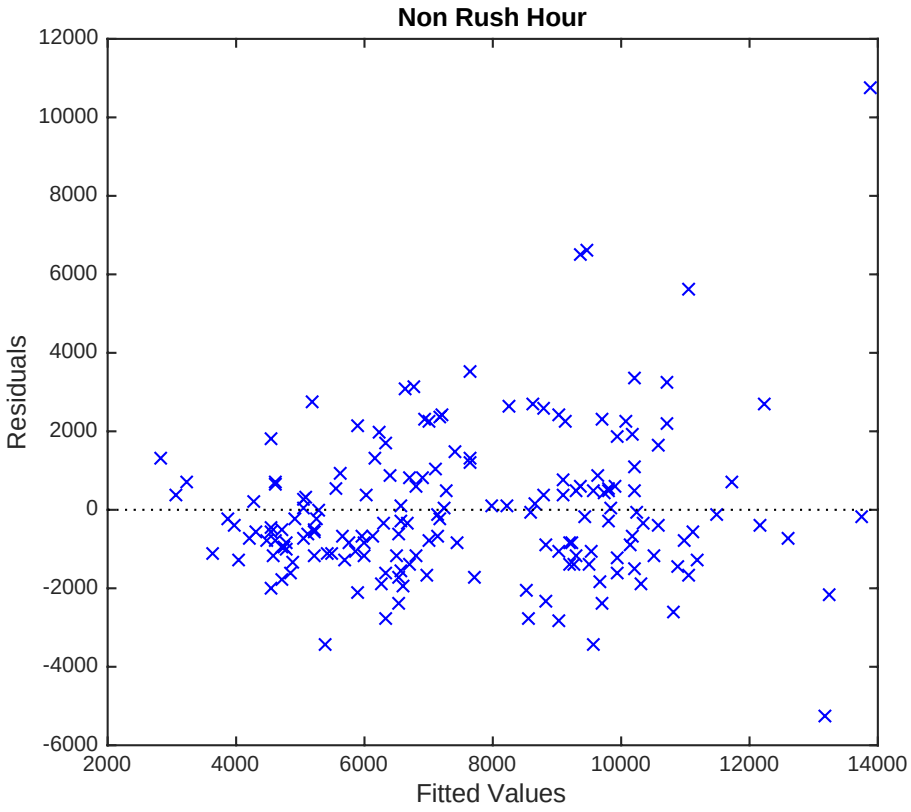

Figure 3-28. Plot of residuals for the non rush hour (10:30 -12:00) linear mixed effects model.

CHAPTER 4:CONCLUSIONS

This study successfully utilizes a TSI NanoScan SMPS in a mobile setting to measure UFP concentrations near an urban, elevated, high-traffic roadway (I-81 in Syracuse, NY). UFP concentrations generally decrease exponentially with distance from I-81, but results from individual transects are much more variable than those reported in previous studies, suggesting that UFP concentrations are more unpredictable in an urban environment when compared to near high-traffic roadways located in suburban or rural settings, and that the elevated structure may act to significantly impact the dispersion of UFP (Hagler et al., 2009; Zhu et al., 2002b, 2002a).

Daily mean $PM_{2.5}$ poorly relate to mean UFP concentrations during this study, highlighting the importance of using number-based monitoring techniques for UFP, rather than relying on pre-existing mass-based measurements from state-implemented PM monitoring programs.

UFP concentrations during NRH are significantly lower than during RH and exhibit more day-to-day variability. NRH UFP concentrations conform to exponential decay with distance from I-81 less often than during RH most likely because of lower NRH traffic volumes on I-81, higher temperatures, and differing wind conditions than those observed in RH. Mobile 15- and 50-nm particle concentrations are also higher during RH than NRH; however, only a weak exponential relationship exists between median normalized 15 nm particle concentrations and distance from the center of I-81.

UFP concentrations near I-81 are lower than what has been measured in previous near-road studies in other locations such as Los Angeles, California, Cincinnati, Ohio,

Raleigh, North Carolina, and Helsinki, Finland, but are reasonable given the traffic volume on I-81 and prevailing wind directions in relation to the sampling sites.

Local vehicle traffic is less influential on UFP concentrations than hypothesized, but school bus traffic at one sampling location (520 m from center of I-81) appears to have an effect on 15-nm particle concentrations.

According to LME analysis, of the variables recorded and analyzed during this study, distance from the center of I-81 is very influential in altering UFP concentrations near I-81 during RH and NRH. During RH, temperature is also influential, with colder temperatures being associated with higher UFP concentrations.

The elevated portion of I-81 in Syracuse will be undergoing substantial changes in the next several years. These changes are likely to come as a complete re-build of the highway, or as a replacement with a street-level boulevard and rerouting of through traffic outside of the city. If the street-level boulevard option is chosen, UFP concentrations near this roadway could significantly change and I recommend that this study be repeated for comparison and to evaluate whether the new design improves or worsens air quality in relation to the old highway design.

Additionally, I recommend that differences between UFP concentrations near elevated and ground level highways be studied further through direct comparison. An ideal set-up for a study such as this would be a highway with elevated and ground level portions in close proximity and with similar AADT. Methods used in this study to characterize the decay of UFP concentrations with distance from the highway could be used to determine if UFP concentrations decay differently from an elevated highway as opposed to a ground-level highway.

CHAPTER 5: REFERENCES

2010 Urban and Rural Classification - Geography - U.S. Census Bureau, 2010. https://www.census.gov/geo/reference/ua/urban-rural-2010.html (accessed 2.3.17).

Adachi, M., Romay, F.J., Pui, D.Y.H., 1992. High-efficiency unipolar aerosol charger using a radioactive alpha source. J. Aerosol Sci. 23, 123–137. doi:10.1016/0021-8502(92)90049-2

Allwine, K.J., Shinn, J.H., Streit, G.E., Clawson, K.L., Brown, M., 2002. Overview of URBAN 2000: A multiscale field study of dispersion through an urban environment. Bull. Am. Meteorol. Soc. 83, 521–536. doi:10.1175/1520-0477(2002)083<0521:OOUAMF>2.3.CO;2

Andersson, J.D., Wedekind, B.G.A., Hall, D., Stradling, R., Wilson, G., 2001. DETR/SMMT/CONCAWE Particulate Research Programme: Light Duty Results. doi:10.4271/2001-01-3577

Bagley, S.T., Baumgard, K.J., Gratz, L.D., Johnson, J.H., Leddy, D.G., 1996. Characterization of fuel and aftertreatment device effects on diesel emissions. Res. Rep. Health Eff. Inst. 1-75-86.

Benson, P.E., 1984. CALINE4 - A dispersion model for predicting air pollutant concentrations near roadways. Final report.

Buckley, S.M., Mitchell, M.J., McHale, P.J., Millard, G.D., 2016. Variations in carbon dioxide fluxes within a city landscape: Identifying a vehicular influence. Urban Ecosyst. 19, 1479–1498. doi:10.1007/s11252-013-0341-0

Buonanno, G., Morawska, L., Stabile, L., 2009. Particle emission factors during cooking activities. Atmos. Environ. 43, 3235–3242. doi:10.1016/j.atmosenv.2009.03.044

Carruthers, D.J., Holroyd, R.J., Hunt, J.C.R., Weng, W.S., Robins, A.G., Apsley, D.D., Thompson, D.J., Smith, F.B., 1994. UK-ADMS: A new approach to modelling dispersion in the earth's atmospheric boundary layer. J. Wind Eng. Ind. Aerodyn. 52, 139–153. doi:10.1016/0167-6105(94)90044-2

Carey, V.J., Wang, Y.G., 2001. Mixed-effects models in S and S-PLUS. J. Am. Stat. Assoc. 96, 1135-1136

Charlson, R.J., Langner, J., Rodhe, H., Leovy, C.B., Warren, S.G., 1991. Perturbation of the northern hemisphere radiative balance by backscattering from anthropogenic sulfate aerosols*. Tellus A 43, 152–163. doi:10.1034/j.1600-0870.1991.00013.x

Charlson, R.J., Schwartz, S.E., 1992. Climate Forcing by Anthropogenic Aerosols. Sci. Wash. 255, 423.

Charron, A., Harrison, R.M., 2003. Primary particle formation from vehicle emissions during exhaust dilution in the roadside atmosphere. Atmos. Environ. 37, 4109–4119. doi:10.1016/S1352-2310(03)00510-7

Chen, D.-R., Pui, D.Y.H., Hummes, D., Fissan, H., Quant, F.R., Sem, G.J., 1998. Design and evaluation of a nanometer aerosol differential mobility analyzer (Nano-DMA). J. Aerosol Sci. 29, 497–509. doi:10.1016/S0021-8502(97)10018-0

Choi, W., Paulson, S.E., 2016. Closing the ultrafine particle number concentration budget at road-to-ambient scale: Implications for particle dynamics. Aerosol Sci. Technol. 50, 448–461. doi:10.1080/02786826.2016.1155104

Choi, W., Ranasinghe, D., Bunavage, K., DeShazo, J.R., Wu, L., Seguel, R., Winer, A.M., Paulson, S.E., 2016. The effects of the built environment, traffic patterns, and micrometeorology on street level ultrafine particle concentrations at a block scale: Results from multiple urban sites. Sci. Total Environ. 553, 474–485. doi:10.1016/j.scitotenv.2016.02.083

Cimorelli, A.J., Perry, S.G., Venkatram, A., Weil, J.C., Paine, R.J., Wilson, R.B., Lee, R.F., Peters, W.D., Brode, R.W., 2005. AERMOD: A Dispersion Model for Industrial Source Applications. Part I: General Model Formulation and Boundary Layer Characterization. J. Appl. Meteorol. 44, 682–693. doi:10.1175/JAM2227.1

Climate Syracuse, meteoblue. https://www.meteoblue.com/en/weather/forecast/modelclimate/syracuse_united-states-of-america_5140405 (accessed 2.10.17).

Costabile, F., Birmili, W., Klose, S., Tuch, T., Wehner, B., Wiedensohler, A., Franck, U., König, K., Sonntag, A., 2009. Spatio-temporal variability and principal components of the particle number size distribution in an urban atmosphere. Atmospheric Chem. Phys. 9, 3163–3195.

Dallmann, T.R., Onasch, T.B., Kirchstetter, T.W., Worton, D.R., Fortner, E.C., Herndon, S.C., Wood, E.C., Franklin, J.P., Worsnop, D.R., Goldstein, A.H., Harley, R.A., 2014. Characterization of particulate matter emissions from on-road gasoline and diesel vehicles using a soot particle aerosol mass spectrometer. Atmos Chem Phys 14, 7585–7599. doi:10.5194/acp-14-7585-2014

Dockery, D.W., Schwartz, J., Spengler, J.D., 1992. Air pollution and daily mortality: Associations with particulates and acid aerosols. Environ. Res. 59, 362–373. doi:10.1016/S0013-9351(05)80042-8

Drewnick, F., Dall'Osto, M., Harrison, R., 2008. Characterization of aerosol particles from grass mowing by joint deployment of ToF-AMS and ATOFMS instruments. Atmos. Environ. 42, 3006–3017. doi:10.1016/j.atmosenv.2007.12.047

Durant, J.L., Ash, C.A., Wood, E.C., Herndon, S.C., Jayne, J.T., Knighton, W.B., Canagaratna, M.R., Trull, J.B., Brugge, D., Zamore, W., Kolb, C.E., 2010. Short-term variation in near-highway air pollutant gradients on a winter morning. Atmospheric Chem. Phys. Print 10, 5599–5626.

Fujita, E.M., Campbell, D.E., Arnott, W.P., Chow, J.C., Zielinska, B., 2007. Evaluations of the chemical mass balance method for determining contributions of gasoline and diesel exhaust to ambient carbonaceous aerosols. J. Air Waste Manag. Assoc. 57, 721-740.

Gibbons, J.D., Chakraborti, S., 2010. Nonparametric Statistical Inference, Fifth Edition. CRC Press.

Gidhagen, L., Johansson, C., Omstedt, G., Langner, J., Olivares, G., 2004. Model simulations of NOx and ultrafine particles close to a Swedish highway. Environ. Sci. Technol. 38, 6730–6740. doi:10.1021/es0498134

Giechaskiel, B., Ntziachristos, L., Samaras, Z., Scheer, V., Casati, R., Vogt, R., 2005. Formation potential of vehicle exhaust nucleation mode particles on-road and in the laboratory. Atmos. Environ. 39, 3191–3198. doi:10.1016/j.atmosenv.2005.02.019

Gramotnev, G., Brown, R., Ristovski, Z., Hitchins, J., Morawska, L., 2003. Determination of average emission factors for vehicles on a busy road. Atmos. Environ. 37, 465–474. doi:10.1016/S1352-2310(02)00923-8

Hagler, G.S.W., Baldauf, R.W., Thoma, E.D., Long, T.R., Snow, R.F., Kinsey, J.S., Oudejans, L., Gullett, B.K., 2009. Ultrafine particles near a major roadway in Raleigh, North Carolina: Downwind attenuation and correlation with traffic-related pollutants. Atmos. Environ. 43, 1229–1234. doi:10.1016/j.atmosenv.2008.11.024

Hagler, G.S.W., Lin, M.-Y., Khlystov, A., Baldauf, R.W., Isakov, V., Faircloth, J., Jackson, L.E., 2012. Field investigation of roadside vegetative and structural barrier impact on near-road ultrafine particle concentrations under a variety of wind conditions. Sci. Total Environ. 419, 7–15. doi:10.1016/j.scitotenv.2011.12.002

Hagler, G.S.W., Thoma, E.D., Baldauf, R.W., 2010. High-resolution mobile monitoring of carbon monoxide and ultrafine particle concentrations in a near-road environment. J. Air Waste Manag. Assoc. 60, 328–336. doi:10.3155/1047-3289.60.3.328

Heist, D., Isakov, V., Perry, S., Snyder, M., Venkatram, A., Hood, C., Stocker, J., Carruthers, D., Arunachalam, S., Owen, R.C., 2013. Estimating near-road pollutant dispersion: A model inter-comparison. Transp. Res. Part Transp. Environ. 25, 93–105. doi:10.1016/j.trd.2013.09.003

Hofman, J., Staelens, J., Cordell, R., Stroobants, C., Zikova, N., Hama, S., Wyche, K., Kos, G., Van Der Zee, S., Smallbone, K., Weijers, E., Monks, P., Roekens, E., 2016. Ultrafine particles in four European urban environments: Results from a new continuous long-term monitoring network. Atmos. Environ. 136, 68–81.

Hollander, M., Wolfe, D.A., Chicken, E., 2013. Nonparametric Statistical Methods. John Wiley & Sons.

Holmer, B., Postgård, U., Eriksson, M., 2000. Sky view factors in forest canopies calculated with IDRISI. Theor. Appl. Climatol. 68, 33–40. doi:10.1007/s007040170051

Huang, C., Lou, D., Hu, Z., Feng, Q., Chen, Y., Chen, C., Tan, P., Yao, D., 2013. A PEMS study of the emissions of gaseous pollutants and ultrafine particles from

gasoline- and diesel-fueled vehicles. Atmos. Environ. 77, 703–710. doi:10.1016/j.atmosenv.2013.05.059

Huang, L., Gong, S.L., Gordon, M., Liggio, J., Staebler, R., Stroud, C.A., Lu, G., Mihele, C., Brook, J.R., Jia, C.Q., 2014. Aerosol–computational fluid dynamics modeling of ultrafine and black carbon particle emission, dilution, and growth near roadways. Atmos Chem Phys 14, 12631–12648. doi:10.5194/acp-14-12631-2014

I81opportunities, https://www.dot.ny.gov/i81opportunities (accessed 12.13.16).

Janhäll, S., Molnar, P., Hallquist, M., 2012. Traffic emission factors of ultrafine particles: effects from ambient air. J. Environ. Monit. 14, 2488–2496. doi:10.1039/C2EM30235G

Juhn, Y.J., Qin, R., Urm, S., Katusic, S., Vargas-Chanes, D., 2010. The influence of neighborhood environment on the incidence of childhood asthma: A propensity score approach. J. Allergy Clin. Immunol. 125, 838–843.e2. doi:10.1016/j.jaci.2009.12.998

Kang, C.D., Cervero, R., 2009. From elevated freeway to urban greenway: land value impacts of the CGC project in Seoul, Korea. Urban Stud. 46, 2771–2794. doi:10.1177/0042098009345166

Kang, J.S., Lee, K.S., Lee, K.H., Sung, H.J., Kim, S.S., 2012. Characterization of a microscale cascade impactor. Aerosol Sci. Technol. 46, 966–972. doi:10.1080/02786826.2012.685115

Karjalainen, P., 2014. Vehicle nanparticle emissions under transient driving conditions. Tampere University of Technology. 1268

Keskinen, J., Pietarinen, K., Lehtimäki, M., 1992. Electrical low pressure impactor. J. Aerosol Sci. 23, 353–360. doi:10.1016/0021-8502(92)90004-F

Kittelson, D.B., Watts, W.F., Johnson, J.P., 2004. Nanoparticle emissions on Minnesota highways. Atmos. Environ. 38, 9–19. doi:10.1016/j.atmosenv.2003.09.037

Kristensson, A., Johansson, C., Westerholm, R., Swietlicki, E., Gidhagen, L., Wideqvist, U., Vesely, V., 2004. Real-world traffic emission factors of gases and particles measured in a road tunnel in Stockholm, Sweden. Atmos. Environ. 38, 657–673. doi:10.1016/j.atmosenv.2003.10.030

Kulkarni, P., Baron, P.A., Willeke, K., 2011. Aerosol Measurement: Principles, Techniques, and Applications. John Wiley & Sons.

Li, N., Sioutas, C., Cho, A., Schmitz, D., Misra, C., Sempf, J., Wang, M., Oberley, T., Froines, J., Nel, A., 2003. Ultrafine particulate pollutants induce oxidative stress and mitochondrial damage. Environ. Health Perspect. 111, 455–460.

Lohmann, U., Feichter, J., 2005. Global indirect aerosol effects: a review. Atmospheric Chem. Phys. 5, 715–737.

Mäkelä, J.M., Aalto, P., Jokinen, V., Pohja, T., Nissinen, A., Palmroth, S., Markkanen, T., Seitsonen, K., Lihavainen, H., Kulmala, M., 1997. Observations of ultrafine

aerosol particle formation and growth in boreal forest. Geophys. Res. Lett. 24, 1219–1222. doi:10.1029/97GL00920

Mehel, A., Murzyn, F., 2015. Effect of air velocity on nanoparticles dispersion in the wake of a vehicle model: Wind tunnel experiments. Atmospheric Pollut. Res. 6, 612–617. doi:10.5094/APR.2015.069

Menon, S., Hansen, J., Nazarenko, L., Luo, Y., 2002. Climate effects of black carbon aerosols in China and India. Science 297, 2250–2253. doi:10.1126/science.1075159

Miguel, A.H., Kirchstetter, T.W., Harley, R.A., Hering, S.V., 1998. On-road emissions of particulate polycyclic aromatic hydrocarbons and black carbon from gasoline and diesel vehicles. Environ. Sci. Technol. 32, 450–455. doi:10.1021/es970566w

Morawska, L., Ristovski, Z., Jayaratne, E.R., Keogh, D.U., Ling, X., 2008. Ambient nano and ultrafine particles from motor vehicle emissions: Characteristics, ambient processing and implications on human exposure. Atmos. Environ. 42, 8113–8138. doi:10.1016/j.atmosenv.2008.07.050

Napolitan, F., Zegras, P., 2008. Shifting urban priorities?: Removal of inner city freeways in the United States. Transp. Res. Rec. J. Transp. Res. Board 2046, 68–75. doi:10.3141/2046-09

Neumann, J., 1978. Some observations on the simple exponential function as a Lagrangian velocity correlation function in turbulent diffusion. Atmospheric Environ. 1967 12, 1965–1968. doi:10.1016/0004-6981(78)90132-4

Oberdörster, G., Sharp, Z., Atudorei, V., Elder, A., Gelein, R., Kreyling, W., Cox, C., 2004. Translocation of inhaled ultrafine particles to the brain. Inhal. Toxicol. 16, 437–445. doi:10.1080/08958370490439597

Olivares, G., Johansson, C., Ström, J., Hansson, H.-C., 2007. The role of ambient temperature for particle number concentrations in a street canyon. Atmos. Environ. 41, 2145–2155. doi:10.1016/j.atmosenv.2006.10.068

Paasonen, P., Kupiainen, K., Klimont, Z., Visschedijk, A., Denier van der Gon, H.A.C., Amann, M., 2016. Continental anthropogenic primary particle number emissions. Atmos Chem Phys 16, 6823–6840. doi:10.5194/acp-16-6823-2016

Park, S.S., Kozawa, K., Fruin, S., Mara, S., Hsu, Y.-K., Jakober, C., Winer, A., Herner, J., 2011. Emission factors for high-emitting vehicles based on on-road measurements of individual vehicle exhaust with a mobile measurement platform. J. Air Waste Manag. Assoc. 61, 1046–1056. doi:10.1080/10473289.2011.595981

Perry, S.G., Cimorelli, A.J., Paine, R.J., Brode, R.W., Weil, J.C., Venkatram, A., Wilson, R.B., Lee, R.F., Peters, W.D., 2005. AERMOD: A dispersion model for industrial source applications. Part II: model performance against 17 field study databases. J. Appl. Meteorol. 44, 694–708. doi:10.1175/JAM2228.1

Pirjola, L., Paasonen, P., Pfeiffer, D., Hussein, T., Hämeri, K., Koskentalo, T., Virtanen, A., Rönkkö, T., Keskinen, J., Pakkanen, T.A., Hillamo, R.E., 2006. Dispersion of

particles and trace gases nearby a city highway: Mobile laboratory measurements in Finland. Atmos. Environ. 40, 867–879. doi:10.1016/j.atmosenv.2005.10.018

Pryor, S.C., Barthelmie, R.J., Sørensen, L.L., McGrath, J.G., Hopke, P., Petäjä, T., 2011. Spatial and vertical extent of nucleation events in the Midwestern USA: insights from the Nucleation In ForesTs (NIFTy) experiment. Atmos Chem Phys 11, 1641–1657. doi:10.5194/acp-11-1641-2011

Pryor, S.C., Crippa, P., Sullivan, R.C., 2015. Atmospheric Chemistry, in: Reference Module in Earth Systems and Environmental Sciences. Elsevier. doi:10.1016/B978-0-12-409548-9.09177-6

Pryor, S.C., Joerger, V.M., Sullivan, R.C., 2016. Empirical estimates of size-resolved precipitation scavenging coefficients for ultrafine particles. Atmos. Environ. 143, 133–138. doi:10.1016/j.atmosenv.2016.08.036

Reponen, T., A. Grinshpun, S., Trakumas, S., Martuzevicius, D., Wang, Z.-M., LeMasters, G., E. Lockey, J., Biswas, P., 2003. Concentration gradient patterns of aerosol particles near interstate highways in the Greater Cincinnati airshed. J. Environ. Monit. 5, 557–562. doi:10.1039/B303557C

Ruths, M., von Bismarck-Osten, C., Weber, S., 2014. Measuring and modelling the local-scale spatio-temporal variation of urban particle number size distributions and black carbon. Atmos. Environ. 96, 37–49. doi:10.1016/j.atmosenv.2014.07.020

Schulz, H., Harder, V., Ibald-Mulli, A., Khandoga, A., Koenig, W., Krombach, F., Radykewicz, R., Stampfl, A., Thorand, B., Peters, A., 2005. Cardiovascular effects of fine and ultrafine Particles. J. Aerosol Med. 18, 1–22. doi:10.1089/jam.2005.18.1

Schauer, J.J., Kleeman, M.J., Cass, G.R., Simoneit, B.R.T., 1999. Measurement of emissions from air pollution sources. 2. C-1 through C-30 organic compounds from medium duty diesel trucks. Environ. Sci. Technol. 33, 1578-1587. doi:10.1021/es980081n

Seinfeld, J.H., Pandis, S.N., 2006. Atmospheric Chemistry and Physics: From Air Pollution to Climate Change. Wiley.

Snyder, M.G., Venkatram, A., Heist, D.K., Perry, S.G., Petersen, W.B., Isakov, V., 2013. RLINE: A line source dispersion model for near-surface releases. Atmos. Environ. 77, 748–756. doi:10.1016/j.atmosenv.2013.05.074

Stedman, D.H., Bishop, G.A., Aldrete, P., Slott, R.S., 1997. On-road evalutation of an automobile emission test program. Environ. Sci. Technol. 31, 927-931. doi: 10.1021/es960792q

Stölzel, M., Breitner, S., Cyrys, J., Pitz, M., Wölke, G., Kreyling, W., Heinrich, J., Wichmann, H.E., Peters, A., 2007. Daily mortality and particulate matter in different size classes in Erfurt, Germany. J. Expo. Sci. Environ. Epidemiol. 17, 458–467. doi:10.1038/sj.jes.7500538

Stommel, Y.G., Riebel, U., 2005. A corona-discharge-based aerosol neutralizer designed for use with the SMPS-system. J. Electrost., 10th International Conference on

Electrostatics10th International Conference on Electrostatics 63, 917–921. doi:10.1016/j.elstat.2005.03.061

Sullivan, R.C., Pryor, S.C., 2014. Quantifying spatiotemporal variability of fine particles in an urban environment using combined fixed and mobile measurements. Atmos. Environ. 89, 664–671. doi:10.1016/j.atmosenv.2014.03.007

Tai, A.P.K., Mickley, L.J., Jacob, D.J., 2010. Correlations between fine particulate matter (PM2.5) and meteorological variables in the United States: Implications for the sensitivity of PM2.5 to climate change. Atmos. Environ. 44, 3976–3984. doi:10.1016/j.atmosenv.2010.06.060

Takekawa, H., Minoura, H., Yamazaki, S., 2003. Temperature dependence of secondary organic aerosol formation by photo-oxidation of hydrocarbons. Atmos. Environ. 37, 3413–3424. doi:10.1016/S1352-2310(03)00359-5

Tammet, H., Mirme, A., Tamm, E., 2002. Electrical aerosol spectrometer of Tartu University. Atmospheric Res., Aerosol Number Concentration Measurement. International Workshop on Intercomparison of Condensation Nuclei and Aerosol Particle Counters 62, 315–324. doi:10.1016/S0169-8095(02)00017-0

Thorpe, A., Harrison, R.M., 2008. Sources and properties of non-exhaust particulate matter from road traffic: A review. Sci. Total Environ. 400, 270–282. doi:10.1016/j.scitotenv.2008.06.007

Tong, Z., Whitlow, T.H., MacRae, P.F., Landers, A.J., Harada, Y. 2015. Quantifying the effect of vegetation on near-road air quality using brief campaigns. Environ. Pollut., 201, 141-149. doi:10.1016/j.envpol.2015.02.026

Tritscher, T., Beeston, M., Zerrath, A.F., Elzey, S., Krinke, T.J., Filimundi, E., Bischof, O.F., 2013. NanoScan SMPS – A Novel, Portable Nanoparticle Sizing and Counting Instrument. J. Phys. Conf. Ser. 429, 12061. doi:10.1088/1742-6596/429/1/012061

TSI, Inc., 2015. Fast Mobility Particle Sizer Spectrometer Model 3091 Spec Sheet.

TSI, Inc., 2012a. Scanning Mobility Particle Sizer Spectrometer (SMPS) Model 3936 Spec Sheet.

TSI, Inc., 2012b. Condensation Particle Counter Model 3775 Spec Sheet.

TSI, Inc., 2012c. Nanoscan SMPS Nanoparticle Sizer Model 3910 Operation and Service Manual.

Underwood, E., 2017. The polluted brain. Science 355, 342. doi:10.1126/science.355.6323.342

United States Code, 2013 Edition, Title 42 - The Public Health and Welfare, Chapter 85 - Air Pollution Prevention and Control.

United States Department of Transportation, Federal Highway Administration. 2013. Highway Statistics, www.fhwa.dot.gov/policyinformation/statistics/2013/

Vogt, R., Scheer, V., Casati, R., Benter, T., 2003. On-Road measurement of particle emission in the exhaust plume of a diesel passenger car. Environ. Sci. Technol. 37, 4070–4076. doi:10.1021/es0300315

Wåhlin, P., Palmgren, F., Van Dingenen, R., 2001. Experimental studies of ultrafine particles in streets and the relationship to traffic. Atmos. Environ., Selected Papers Presented at the Venice Conference 35, S63–S69. doi:10.1016/S1352-2310(00)00500-8

Wang, Y.J., Nguyen, M.T., Steffens, J.T., Tong, Z., Wang, Y., Hopke, P.K., Zhang, K.M., 2013. Modeling multi-scale aerosol dynamics and micro-environmental air quality near a large highway intersection using the CTAG model. Sci. Total Environ. 443, 375–386. doi:10.1016/j.scitotenv.2012.10.102

Wang, Y.J., Zhang, K.M., 2012. Coupled turbulence and aerosol dynamics modeling of vehicle exhaust plumes using the CTAG model. Atmos. Environ. 59, 284–293. doi:10.1016/j.atmosenv.2012.04.062

Zhai, W., Wen, D., Xiang, S., Hu, Z., Noll, K.E., 2016. Ultrafine-particle emission factors as a function of vehicle mode of operation for LDVs based on near-roadway monitoring. Environ. Sci. Technol. 50, 782–789. doi:10.1021/acs.est.5b03885

Zhang, K.M., Wexler, A.S., 2004. Evolution of particle number distribution near roadways—Part I: analysis of aerosol dynamics and its implications for engine emission measurement. Atmos. Environ., Contains Special Issue section on Measuring the composition of Particulate Matter in the EU 38, 6643–6653. doi:10.1016/j.atmosenv.2004.06.043

Zhang, Q., Fischer, H.J., Weiss, R.E., Zhu, Y., 2013. Ultrafine particle concentrations in and around idling school buses. Atmos. Environ. 69, 65–75. doi:10.1016/j.atmosenv.2012.12.015

Zhang, Q., Zhu, Y., 2010. Measurements of ultrafine particles and other vehicular pollutants inside school buses in South Texas. Atmos. Environ. 44, 253–261. doi:10.1016/j.atmosenv.2009.09.044

Zhu, Y., Hinds, W.C., Kim, S., Shen, S., Sioutas, C., 2002a. Study of ultrafine particles near a major highway with heavy-duty diesel traffic. Atmos. Environ. 36, 4323–4335. doi:10.1016/S1352-2310(02)00354-0

Zhu, Y., Hinds, W.C., Kim, S., Sioutas, C., 2002b. Concentration and size distribution of ultrafine particles near a major highway. J. Air Waste Manag. Assoc. 52, 1032–1042. doi:10.1080/10473289.2002.10470842

Zhu, Y., Yu, N., Kuhn, T., Hinds, W.C., 2006. Field comparison of P-Trak and condensation particle counters. Aerosol Sci. Technol. 40, 422–430. doi:10.1080/02786820600643321

Zielinska, B., Sagebiel, J., McDonald, J.D., Whitney, K., Lawson, D.R., 2004. Emission rates and comparative chemical composition from selected in-use diesel- and gasoline-fueled vehicles. J. Air Waste Manag. Assoc. 54, 1138-1150. doi:10.1080/10473289.2004.1047090973

APPENDIX A:

Atmospheric Environment 143 (2016) 133–138

Contents lists available at ScienceDirect

Atmospheric Environment

journal homepage: www.elsevier.com/locate/atmosenv

Short communication

Empirical estimates of size-resolved precipitation scavenging coefficients for ultrafine particles

S.C. Pryor*, V.M. Joerger, R.C. Sullivan

Department of Earth and Atmospheric Sciences, Cornell University, Ithaca, NY 14853, USA

HIGHLIGHTS

- Below-cloud scavenging coefficients derived from long-term particle measurements.
- Scavenging coefficients decline by three as diameter goes from 15 nm to 100 nm.
- Good agreement with empirical parameterization of Laakso et al. (2003).

ARTICLE INFO

Article history:
Received 10 June 2016
Received in revised form
21 July 2016
Accepted 9 August 2016
Available online 11 August 2016

Keywords:
Below-cloud
Particle removal
Wet scavenging
Observational
Aerosol particles

ABSTRACT

Below-cloud scavenging coefficients for ultrafine particles (UFP) exhibit comparatively large uncertainties in part because of the limited availability of observational data sets from which robust parameterizations can be derived or that can be used to evaluate output from numerical models. Long time series of measured near-surface UFP size distributions and precipitation intensity from the Midwestern USA are used here to explore uncertainties in scavenging coefficients and test both the generalizability of a previous empirical parameterization developed using similar data from a boreal forest in Finland (Laakso et al., 2003) and whether a more parsimonious formulation can be developed. Scavenging coefficients (λ) over an ensemble of 95 rain events (with a median intensity of 1.56 mm h^{-1}) and 104 particle diameter (D_p) classes (from 10 to 400 nm) indicate a mean value of 3.4×10^{-5} s^{-1} (with a standard error of 1.1×10^{-6} s^{-1}) and a median of 1.9×10^{-5} s^{-1} (interquartile range: -2.0×10^{-5} to 7.5×10^{-5} s^{-1}). The median scavenging coefficients for D_p: 10–400 nm computed over all 95 rain events exhibit close agreement with the empirical parameterization proposed by (Laakso et al., 2003). They decline from ~4.1×10^{-5} s^{-1} for D_p of 10–19 nm, to ~1.6×10^{-5} s^{-1} for D_p of 80–113 nm, and show an increasing tendency for $D_p > 200$ nm.

1. Introduction and motivation

Below-cloud scavenging of aerosol particles by hydrometeors plays an important role in defining their atmospheric lifetimes and in situ particle size distributions (Andronache, 2003; Pruppacher and Klett, 1997). Full numerical treatment of below-cloud scavenging in atmospheric chemistry models is computationally demanding and is subject to large uncertainties due to non-linear dependencies of scavenging efficiencies with hydrometeor diameter spectra and phase, precipitation intensity, atmospheric turbulence and particle diameters (Andronache, 2003; Pruppacher and Klett, 1997). Thus, some atmospheric chemistry models continue to use scavenging coefficients expressed as a function of rainfall rate for specific particle diameters or modes (Feng, 2007) to represent this process (e.g. the EMEP MSC-W Eulerian chemical transport model (Simpson et al., 2012), DEHM (Frohn et al., 2001), and MATCH (Robertson et al., 1999)).

A number of previous publications have explained the mechanisms and theorized dependencies of below-cloud scavenging (e.g. (Andronache, 2003; Pruppacher and Klett, 1997; Wang et al., 2010)), so they are described only briefly here. The rate at which particles are scavenged by rain droplets depends on the collision and collection efficiency (where the latter term is often assumed to be 1 for particles with diameters much smaller than the rain droplet diameter), and is thus a function of the rainfall intensity and rain droplet size distribution, as well as the size distribution and composition of the in situ particles. The collision efficiency

* Corresponding author.
E-mail address: sp2279@cornell.edu (S.C. Pryor).

http://dx.doi.org/10.1016/j.atmosenv.2016.08.036
1352-2310/

($E(D,D_p)$) between a falling raindrop of a given diameter (D) and an in situ particle (of diameter, D_p) is theorized to decrease with increasing particle diameter in the D_p range ~1–100 nm, to remain fairly constant (i.e. within a factor of approximately 2–5) in the D_p range ~100 nm to 1 μm, and then to exhibit a rapid increase with increasing D_p (Wang et al., 2010). $E(D,D_p)$ for the smallest D_p is dominated by Brownian diffusion with additional contributions from thermophoresis and electrostatic forces (Andronache, 2004), and atmospheric turbulence (Quérel et al., 2014). For larger D_p interception and impaction play a larger role in dictating collision efficiency (Pruppacher and Klett, 1997; Wang et al., 2010). $E(D,D_p)$ increases with D, so given rainfall events with lower intensities (rainfall rates) are typically characterized by smaller rain droplet diameters than those with higher intensities (Marshall and Palmer, 1948), the *a priori* expectation is that higher rainfall rates are typically associated with a larger number of larger rain droplets, and thus higher particle scavenging efficiencies. This expectation has largely been realized in observational analyses e.g. (Castro et al., 2010; Chate, 2005; Laakso et al., 2003; Maria and Russell, 2005; Volken and Schumann, 1993; Zhao et al., 2015). However, there are large event-to-event and site-to-site variations in experimentally derived scavenging efficiencies (Andronache et al., 2006). Of the observational studies of below-cloud scavenging of ultrafine particles (UFP, particles with diameters (D_p) less than 100 nm) that have been conducted to date, only two (Laakso et al., 2003; Zikova and Zdimal, 2016) have considered sufficient rain event sample sizes ($n \approx 100$) to generate statistically robust estimates of size-resolved scavenging coefficients, and only one (Laakso et al., 2003) sought to develop an empirical parameterization of size-resolved scavenging coefficients. Herein, we use a 30-month time series of measured near-surface UFP size distributions and precipitation intensity to explore the generalizability of the empirical parameterization of Laakso et al. (2003), and to evaluate whether alternative, more parsimonious formulations can be advanced.

2. Data and methods

The meteorological and particle size distribution (PSD) data analyzed herein were collected at an AmeriFlux site in southern Indiana (in the Morgan Monroe State Forest (MMSF), 39°19′ N, 86°25′ W, 275 m a.s.l (Schmid et al., 2000)) from December 2006 to April 2009. Precipitation at this site is fairly evenly distributed across the year and has an average occurrence of approximately 1 day in 3 (see précis description of the meteorological conditions in Fig. 1). Size-resolved particle number concentrations in 104 size classes over the D_p range: 10–400 nm were obtained using a TSI scanning mobility particle sizer (SMPS3936) system comprising an electrostatic classifier (TSI-3080), long differential mobility analyzer (TSI-DMA3081) and a condensation particle counter (TSI-3025A). A second SMPS3936 system was also operated on the same manifold and comprised an electrostatic classifier (TSI-3080), nano-DMA (TSI-DMA3085) and a condensation particle counter (TSI-3786) and for which particle concentrations for D_p in the range 6–100 nm are reported. The sampling protocol was such that air was drawn from a height of 46-m (above a forest canopy with a mean height ~26–28 m) through copper tubing for 10-min in each half-hour period, with sampling at two other heights via a common manifold in each 30-min period (Pryor et al., 2010). Copper was chosen for the sampling lines because it was available at very long sections reducing the number of connections to two, is malleable (meaning all bends could be relatively smooth) and is relatively inert and resistant to acquisition of charge, but with such long sampling lines particle losses are inevitable. Thus, transmission efficiencies derived experimentally (which for D_p = 10 nm are

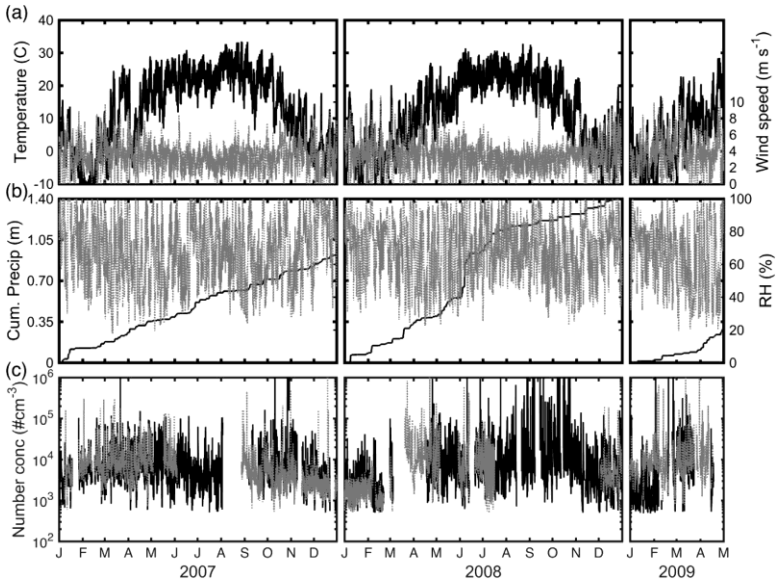

Fig. 1. Overview of meteorological conditions and particle number concentrations at MMSF during January 2007–April 2009. (a) Hourly average air temperature (°C) (black) and wind speed (m s^{-1}) (gray) at 46-m. (b) Cumulative precipitation (Cum. Precip, m) in each year (black) and hourly average relative humidity (RH, %) again at 46-m. (c) Total number particle concentrations (# cm^{-3}) at 46-m (Number conc) from an SMPS with a nano-DMA (D_p: 6–100 nm) (black) and an SMPS with a long-DMA (D_p: 10–400 nm) (gray).

below 0.3, but increase to over 0.5 for D_p > 20 nm) were used to determine empirical correction factors (Pryor et al., 2010) that have been applied to the observed PSD. We assume the particle losses in the copper sampling lines are independent of variations in humidity and other environmental conditions.

Rainfall rates derive from measurements using a Texas Electronics TE525 tipping bucket rain gauge also deployed at 46 m (Fig. 1b). Since this instrument is deployed without a wind-shield it is subject to under-capture during high wind events. The modal correction factor computed using the approach of Hildebrandt et al. (2007) and wind speed data from a sonic anemometer deployed at 46-m is ~1.1 (Fig. 2b). Frozen hydrometeors (snow, ice and hail) differ greatly from liquid droplets both in terms of the particle capture efficiencies (Sparmacher et al., 1993) and the accuracy of their measurement by tipping bucket rain gauges (Savina et al., 2012). To avoid inclusion of snow events in the analysis, METAR reports from the National Weather Service station KIND-Indianapolis, IN (located approximately 45 km to the north of MMSF) are used to screen out periods when snow or hail was observed. The procedure used is as follows; any event during which precipitation is reported by the TE525 at MMSF and for which snow/ice/hail were reported at KIND during that hour or the two hours prior to or subsequent to that time stamp are excluded from consideration. The resolution of the tipping bucket rain gauge is 0.254 mm (equal to one tip). To be consistent with the analysis of Laakso et al. (2003) and avoid inclusion of very light and comparatively poorly quantified rain events, events were only included in the analysis if the precipitation intensity ≥0.4 mm h^{-1}.

The in situ measured PSDs and rainfall rates are used to derive size-resolved scavenging coefficients ($\lambda(D_p)$) using:

$$\lambda(D_p) = -\frac{1}{t_1 - t_0}\ln\left(\frac{c_1(D_p)}{c_0(D_p)}\right) \quad (1)$$

where D_p is the particle diameter, $t_1 - t_0$ is the length of the rain event in seconds, and $c_0(D_p)$ and $c_1(D_p)$ are the average number concentration of particles in each size bin in the 30-min periods before and after the rain event, respectively.

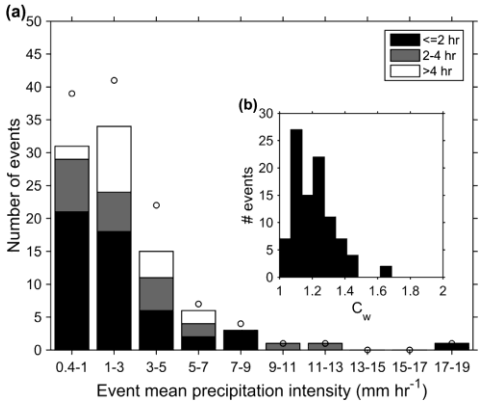

Fig. 2. (a) Summary of the intensity (in mm h^{-1}) and duration of the 95 rain events from which scavenging coefficients are computed for the SMPS3936 with the long-DMA (shown by the bars). Also shown are the intensities of the rainfall events (dots) included in the analysis of data from the SMPS with a nano-DMA (n = 121). (b) Histogram of the correction factor (C_w) for wind-related under-catch by the rain gauge computed from $C_w = exp[-0.001 \times \ln(R) - 0.0122 \times U \times \ln(R) + 0.034 \times U + 0.0077]$, where U is the wind speed (m s^{-1}), and R is the measured rainfall rate (mm h^{-1}) (Hildebrandt et al., 2007).

A premise of the empirical approach to determining size-resolved scavenging efficiencies is that with the exception of removal by below-cloud scavenging the particle population is stationary over the course of the rain event. To avoid strongly non-stationary conditions such as frontal passages or new particle formation occurrence, events are only included in the analysis if two criteria are met: (i) the wind direction (as measured using a 03001-5 R.M. Young Wind Sentry Set deployed at 46-m) at the start and end of the rain event did not differ by more than 90° and (ii) new particle formation (NPF) was not observed in the hour following cessation of rain (i.e. particle concentrations <1 × 10^3 cm^{-3} for D_p = 10–15 nm, inclusive and visual inspection of plots of the time evolution of PSD did not show evidence of NPF (see a detailed description of robust subjective and objective ways to detect NPF given in Kulmala et al. (2012)). To avoid unstable estimates of the concentration ratio, an individual diameter class was only included in the analysis of a specific rain event if both $c_0(D_p)$ and $c_1(D_p)$ exceeded 10 cm^{-3}.

Laakso et al. (2003) proposed the following functional form for the relationship between the median $\lambda(D_p)$ (for each of the 29 logarithmically distributed size channels (D_p) in the diameter space 10–500 nm) and precipitation rate:

$$\log_{10}\left(\frac{\lambda}{\lambda_0}\right) = a + b \times d_p^{-4} + c \times d_p^{-3} + d \times d_p^{-2} + e \times d_p^{-1} + f \times \left(\frac{p}{p_0}\right)^{0.5} \quad (2)$$

where λ_0 is 1 s^{-1}, $d_p = \log_{10}(D_p/D_{p0})$, D_{p0} = 1 m, p is the rain rate in mm hr^{-1}, p_0 is 1 mm h^{-1}, and *a*-*f* are the fitted coefficients.

In this analysis, we evaluate the degree of agreement between the empirical coefficients (*a*-*f*) as derived by Laakso et al. (2003) and observational estimates of $\lambda(D_p)$ as derived from the MMSF data set. We also use the framework described by (2) to develop least squares best-fit estimates from our observations. Our fitting procedure is as follows: the coefficient *f* (which describes the scaling term for precipitation intensity) is first derived by conditionally sampling the scavenging coefficients in three precipitation intensity classes (light (0.4–2 mm h^{-1}), moderate (2–5 mm h^{-1}), and heavy (>5 mm h^{-1})) in addition to treating the whole sample ensemble (i.e. all rainfall intensities). Then *f* and the median value of p is used with the estimates of $\log_{10}(\lambda/\lambda_0)$ as a composite dependent variable to generate the other fitting coefficients in Equation (2). Application of regression to fit complex (multi-predictor) equations (such as (2)) to small data sets can lead to model over-fitting. Hence we use stepwise regression to examine if a more parsimonious fit can be derived. In this analysis we use stepwise regression with a threshold minimum p-value of 0.1 for a term to be removed.

There are four primary potential sources of discrepancies between empirically derived $\lambda(D_p)$ from different studies:

a) Variations in the methodology used to select the cases (e.g. the stationarity criteria) and those used to compute the scavenging coefficients (e.g. the discretization of the precipitation data). The precipitation data at the MMSF site are reported with hourly discretization, while Laakso et al. (2003) had precipitation rates discretized at 15-min intervals and they included all events with a duration >0.5 h. The hourly discretization of precipitation data from MMSF will inevitably result in lower precipitation intensities than if

the precipitation data were discretized at higher frequency. Also, herein we compare UFP concentrations before and after rain events to capture the net effect of the precipitation event. That is we compare distributions at t = 0, prior to the commencement of precipitation, and at time t = n, after precipitation and thus each individual event results in a single estimate of λ for each particle diameter so each event is equally weighted in the estimation of median and mean $\lambda(D_p)$ regardless of the event duration. However, previous authors calculated λ from the UFP concentrations during rain events and thus compare the PSD at time t = 0, just prior to precipitation and at time = t + n, and at t + n and t + 2n, (where n is the temporal discretization of the PSD measurements) during the rain event (Laakso et al., 2003; Zikova and Zdimal, 2016).

b) Variations in the sampling system. Here we present data that were sampled well above a forest canopy to avoid local contamination of the PSD, and thus used long sampling lines that result in large corrections for tubing losses. Other sampling locations may not require use of long sampling lines.
c) Differences in particle instrumentation both in terms of operating principle (e.g. SMPS versus Fast Mobility Particle Sizers (Hornsby and Pryor, 2014)) and the discretization of the PSD. Also differences in instrument maintenance and deployment protocols (e.g. the presence of a wind shielding on, or heating of, rain gauges).
d) Differences in the type and intensity of precipitation and thus the rain droplet size distribution.

To address some of these sources of uncertainty we compute $\lambda(D_p)$ from two different SMPS3936 systems connected to the same sampling lines and manifold system. One SMPS was operated with a long-DMA in order to capture a wide range of particles diameters (10–400 nm), and one with a short-DMA to provide estimates of scavenging coefficients for D_p < 100 nm for a larger event sample (i.e. more rain events), and also undertake an assessment of $\lambda(D_p)$ for the diameter range 10–100 nm for rainfall events sampled by both SMPS systems.

3. Results

The rain events used to compute the scavenging coefficients from the SMPS3936 with a long-DMA exhibit a mean duration of almost 3 h (median of 2 h) and a mean intensity of 2.47 mm h^{-1} (median of 1.57 mm h^{-1}) (Fig. 2 and Table 1). Thus, the average rain intensities are higher than those reported in (Laakso et al., 2003) (median value of 0.8 mm h^{-1}), but cover the same range of values.

Although a substantial fraction of the scavenging coefficients (λ) from (1) are close to (or below) zero, the mean-λ is significantly different from zero and positive. We postulate that the negative λ values (that have also been observed in previous studies (Laakso et al., 2003; Zikova and Zdimal, 2016)) reflect causes such as the uncertainty in PSD measurements and inclusion cases where the PSD was non-stationary events (although the event passed our selection criteria). The empirical cumulative density function of λ over the ensemble of rain events and 104 diameter classes indicate a mean value of 3.4×10^{-5} s^{-1} (with a standard error of 1.1×10^{-6} s^{-1}), a median of 1.9×10^{-5} s^{-1}, and an interquartile range of -2.0×10^{-5} to 7.5×10^{-5} s^{-1} (Fig. 3a, Table 1). To provide further context for these estimates of λ an analysis was conducted in which number concentrations from the 104 size classes were sampled across 95 randomly sampled "no rain" events (that have the same characteristics in terms of duration and stationarity conditions applied above) and used to compute scavenging coefficients. The results indicate a mean value (computed over all diameters and all events) of 4.8×10^{-6} s^{-1} (with a standard error of 2.8×10^{-6} s^{-1}), and a median of -1.0×10^{-7} s^{-1} (interquartile range: -7.7×10^{-6} to 1.0×10^{-5} s^{-1}). Thus, the mean-λ for non-rain events is almost an order of magnitude below that obtained for our rain event ensemble, and the median is over an order of magnitude smaller than that computed for the rain events. This analysis thus further indicates that, while there is considerable event-to-event variability in derived λ estimates, the estimates derived herein are likely reflective of physical removal of particles by below-cloud scavenging. Further, although as in the study of Zikova and Zdimal (2016) the interquartile range of $\lambda(D_p)$ spans an order of magnitude for virtually all diameters considered (Fig. 3b), only two measured D_p exhibit mean-λ values that are negative and they are confined to diameters (10.9 nm and 399.5 nm) near the edges of the measured interval for this SMPS where the instrument has lower precision, and for the smaller diameter where the correction for tubing losses is largest.

The magnitude of median-$\lambda(D_p)$ agree with previously reported theoretical predictions (Wang et al., 2010) for the range of rainfall intensities represented in the data set. Also in accord with theoretical considerations and prior experimental research (Andronache et al., 2006; Wang et al., 2010), median scavenging coefficients by particle diameter computed over all 95 rain events decline from ~4.1×10^{-5} s^{-1} for D_p of 10–19 nm to ~1.6×10^{-5} s^{-1} for D_p of 80–113 nm, and then show an increasing tendency for D_p > 200 nm (Fig. 3b).

Scavenging coefficients for all D_p were conditionally sampled by rainfall intensity (Fig. 3a) to derive an estimate of the coefficient *f* in (2) as the slope of the fit between median-λ and rainfall intensity. The results indicate a value of 0.185 (versus 0.244984 in (Laakso et al., 2003)). The other coefficients in (2) were then determined by first averaging the median λ estimates across three size channels (so median $\lambda(D_p)$ is the average value of $\lambda(D_p(n-1))$, $\lambda(D_p(n))$, and $\lambda(D_p(n+1))$ and then fitting (2) using least squares regression (Fig. 4). The resulting fit has an adjusted variance explanation (adjusted-r^2) of 0.46, and all values of the coefficients have p-values <0.10. No more parsimonious model could be found using stepwise

Table 1
Summary of the data sets from which scavenging coefficients were computed for MMSF and the resulting statistics.

Statistic	Instrument			
	SMPS3936: Long-DMA	SMPS3936: Nano-DMA	Common events long-DMA	Common events nano-DMA
D_p range (nm)	10–400	6–100	10–100	
# Rainfall events	95	121	87	
Mean rainfall intensity (mm h^{-1}) (median)	2.47 (1.56)	2.46 (1.59)	2.55 (1.48)	
Mean-λ (10^{-5} s^{-1}) (standard error)	3.4 (0.11)	3.5 (0.32)	4.6 (0.25)	3.2 (0.28)
Median-λ (10^{-5} s^{-1}) (IQR)	1.9 (−2.0 to 7.5)	5.7 (−1.7 to 11)	2.6 (−1.5 to 8.8)	2.2 (−2.3 to 8.1)
RMSE of median-$\lambda(D_p)$ versus fit (10^{-5} s^{-1})	1.23	1.26		
RMSE of median-$\lambda(D_p)$ versus fit of Laakso et al., 2003 (10^{-5} s^{-1})	1.63	3.95		

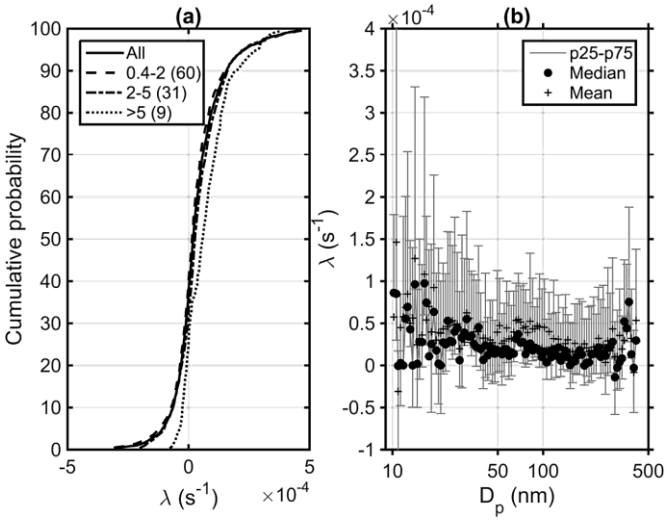

Fig. 3. (a) Empirical cumulative distribution plot of scavenging coefficients (λ) for each of the 104 diameters (D_p) reported by the SMPS3936 with the long-DMA for the ensemble of 95 rain events at MMSF (denoted by All in the legend). Also shown are cumulative distributions of λ values conditionally sampled by three rain intensity classes (in mm h^{-1}). The numbers shown in parentheses are the fraction of the total number of valid λ values in that rainfall intensity class. Thus, results from the highest rainfall intensity class are the least robust since they derive from a small sample size. (b) Mean, median and inter-quartile range of scavenging coefficients (λ) for each of the 104 diameters (D_p) reported by the SMPS fitted with the long-DMA.

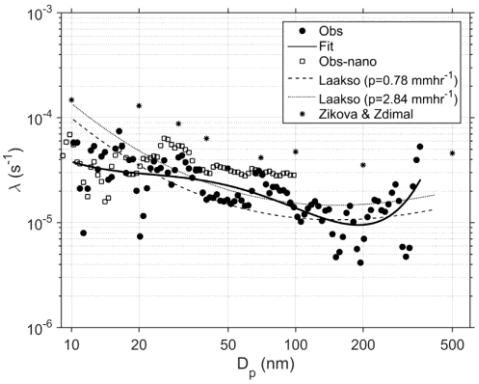

Fig. 4. Median scavenging coefficients (λ) as a function of particle diameter (D_p) at MMSF as used in the fitting procedure (i.e. averaged over three adjacent size classes) (Obs). Also shown is a fit from Equation (2) (the adjusted variance explanation (r^2) for this fit is 0.46), and the median scavenging coefficients as computed from the SMPS with the nano-DMA (Obs-nano). The lines denote results of the parameterization of Laakso et al. (2003) for two different precipitation rates (p = 0.78 mm h^{-1} and 2.84 mm h^{-1}). The asterisks show median scavenging coefficients as presented for 311 rain events by Zikova and Zdimal (2016) for selected particle diameters. The fitting coefficients for Equation (2) from MMSF and those from Laakso et al. (2003) (shown in parentheses in the format provided in the original reference) are as follows: a = 3.4549076 × 10^3 (274.35758), b = 1.0040252 × 10^7 (332839.59273), c = 5.484421066 × 10^6 (226656.57259), d = 1.12147496 × 10^6 (58005.91340), e = 1.01768617 × 10^5 (96588.38582), f = 0.185 (0.244984).

regression. Thus it appears that all the terms in Equation (2) contribute to the overall quality of the fit.

Although the fitting coefficients from MMSF exhibit marked discrepancies from those developed by Laakso et al. (2003), the median λ(D_p) values computed from the MMSF data set also exhibit good agreement with the parameterization of Laakso et al. (2003) (Fig. 4). The root mean squared error (RMSE) between λ from the fit derived herein and the observations for the 104 diameter classes is 1.23 × 10^{-5} s^{-1} (for the median precipitation intensity of 1.56 mm h^{-1}), while for the Laakso et al. (2003) parameterization is only slightly higher (1.63 × 10^{-5} s^{-1}). Thus, the parameterization of median λ(D_p) derived by Laakso et al. (2003) appears to be broadly applicable. Interestingly, in contrast to the convergence with estimates from the boreal forest site in Finland (Laakso et al., 2003), for all diameters data from MMSF indicate substantially smaller λ(D_p) than were derived using data from a site in the Czech Republic (Zikova and Zdimal, 2016) (Fig. 4). This discrepancy may reflect the occurrence of higher rainfall intensities at the site in the Czech Republic, differences due to the criteria used for event selection with regards to stationarity, and/or difference in the way in which scavenging coefficients are calculated (described above).

Median-λ(D_p) computed from the SMPS3936 with the nano-DMA for a larger set of rainfall events at MMSF (n = 121, see Table 1) generally exceed those from the SMPS with a long-DMA (Fig. 4). The λ estimates from the nano-DMA SMPS data set at MMSF are also smaller than those from the site in the Czech Republic, but by a lower margin than those from the SMPS with a long-DMA (Fig. 4). This may be in part due to the inclusion of more summertime rainfall events in the sample used to compute λ(D_p) from the SMPS with the nano-DMA (see Fig. 1c). To provide a context for these results computed independently from the two SMPS systems at MMSF (over different rain events), λ estimates for

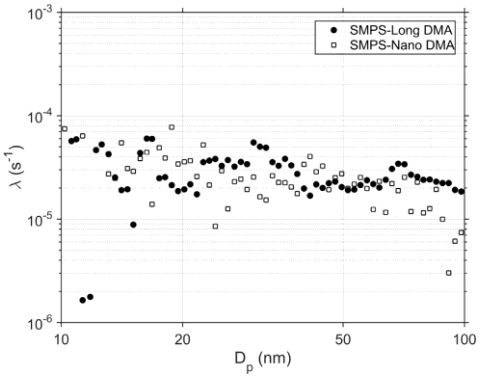

Fig. 5. Median scavenging coefficients (λ) as a function of particle diameter (D_p) for diameters between 10 and 100 nm, for all 87 events for which data from the SMPS with the Long-DMA (SMPS-Long DMA) and SMPS with nano-DMA (SMPS-Nano DMA) are both available. See Table 1 for the statistics of these events.

D_p 10–100 nm from the two systems for 87 common rainfall events were also computed. The results indicate relatively good agreement between $\lambda(D_p)$ estimates from the two systems (Table 1, Fig. 5) adding support to the inference that the discrepancies shown in Fig. 4 reflect differences in the nature of the rainfall events.

4. Concluding remarks

Below cloud scavenging is an important removal process for atmospheric aerosol particles and plays a key role in determining particle concentrations and size distributions. The magnitude of the effect remains uncertain in part because there remain very few robust observational data sets with which to evaluate numerical models of scavenging efficiencies. In situ measurements of particle size distributions and rainfall intensities collected over a 30-month period are used to develop a data set of rain events from which scavenging efficiencies for particle diameters between 10 and 400 nm are derived. The ensemble mean scavenging efficiency is 3.4×10^{-5} s^{-1} (and has a standard error of 1.1×10^{-6} s^{-1}), while the median is 1.9×10^{-5} s^{-1} (interquartile range: -2.0×10^{-5} to 7.5×10^{-5} s^{-1}). The median scavenging coefficients by particle diameter exhibit good agreement with the empirical expression formulated by Laakso et al. (2003).

Acknowledgments

This work was support by a grant to SCP from NSF (1517365). RCS acknowledges funding from NASA (14-EARTH14F-0207). The comments and suggestions of two reviewers and Prof. R. Barthelmie are gratefully acknowledged. The PSD data from MMSF analyzed herein can be downloaded from http://www.geo.cornell.edu/eas/PeoplePlaces/Faculty/spryor/ or can be requested by email (sp2279@cornell.edu). The AmeriFlux data used herein (available at: http://ameriflux.ornl.gov/) were collected under funding from the Office of Science, U.S. Department of Energy, and from the AmeriFlux Management Project, Lawrence Berkeley National Laboratory. Observations of meteorological conditions from the NWS station in Indianapolis are available from the National Centers for Environmental Information (ftp://ftp.ncdc.noaa.gov/pub/data/).

References

Andronache, C., 2003. Estimated variability of below-cloud aerosol removal by rainfall for observed aerosol size distributions. Atmos. Chem. Phys. 3, 131–143.
Andronache, C., 2004. Diffusion and electric charge contributions to below-cloud wet removal of atmospheric ultra-fine aerosol particles. J. Aerosol Sci. 35, 1467–1482.
Andronache, C., Grönholm, T., Laakso, L., Phillips, V., Venäläinen, A., 2006. Scavenging of ultrafine particles by rainfall at a boreal site: observations and model estimations. Atmos. Chem. Phys. 6, 4739–4754.
Castro, A., Alonso-Blanco, E., González-Colino, M., Calvo, A.I., Fernández-Raga, M., Fraile, R., 2010. Aerosol size distribution in precipitation events in León, Spain. Atmos. Res. 96, 421–435.
Chate, D.M., 2005. Study of scavenging of submicron-sized aerosol particles by thunderstorm rain events. Atmos. Environ. 39, 6608–6619.
Feng, J., 2007. A 3-mode parameterization of below-cloud scavenging of aerosols for use in atmospheric dispersion models. Atmos. Environ. 41, 6808–6822.
Frohn, L.M., Christensen, J.H., Brandt, J., Hertel, O., 2001. Development of a high resolution integrated nested model for studying air pollution in Denmark. Phys. Chem. Earth Part B Hydrol. Oceans Atmos. 26, 769–774.
Hildebrandt, A., Al Aufi, M., Amerjeed, M., Shammas, M., Eltahir, E.A.B., 2007. Eco-hydrology of a seasonal cloud forest in Dhofar: 1. Field experiment. Water Resour. Res. 43 (n/a-n/a).
Hornsby, K.E., Pryor, S.C., 2014. A laboratory comparison of real-time measurement methods for 10–100-nm particle size distributions. Aerosol Sci. Technol. 48, 571–582.
Kulmala, M., et al., 2012. Measurement of the nucleation of atmospheric aerosol particles. Nat. Protoc. 7, 1651–1667.
Laakso, L., Gronholm, T., Rannik, Ü., Kosmale, M., Fieldler, V., Vehkamaki, H., Kulmala, M., 2003. Ultrafine particle scavenging coefficients calculated from 6 years field measurements. Atmos. Environ. 37, 3605–3613.
Maria, S.F., Russell, L.M., 2005. Organic and inorganic aerosol below-cloud scavenging by suburban New Jersey precipitation. Environ. Sci. Technol. 39, 4793–4800.
Marshall, J.S., Palmer, W.M.K., 1948. The distribution of raindrops with size. J. Meteorol. 5, 165–166.
Pruppacher, H.R., Klett, J.D., 1997. Cloud chemistry. Microphysics of Clouds and Precipitation. Kluwer Academic Publishers, Dordrecht, pp. 700–791 (Chapter 17).
Pryor, S., Spaulding, A., Barthelmie, R., 2010. New particle formation in the Midwestern USA: event characteristics, meteorological context and vertical profiles. Atmos. Environ. 44, 4413–4425.
Quérel, A., Monier, M., Flossmann, A.I., Lemaitre, P., Porcheron, E., 2014. The importance of new collection efficiency values including the effect of rear capture for the below-cloud scavenging of aerosol particles. Atmos. Res. 142, 57–66.
Robertson, L., Langner, J., Engardt, M., 1999. An Eulerian limited-area atmospheric transport model. J. Appl. Meteorol. 38, 190–210.
Savina, M., Schäppi, B., Molnar, P., Burlando, P., Sevruk, B., 2012. Comparison of a tipping-bucket and electronic weighing precipitation gage for snowfall. Atmos. Res. 103, 45–51.
Schmid, H.P., Grimmond, C.S.B., Cropley, F., Offerle, B., Su, H.-B., 2000. Measurements of CO_2 and energy fluxes over a mixed hardwood forest in the mid-western United States. Agric. For. Meteorol. 103, 357–374.
Simpson, D., Coauthors, 2012. The EMEP MSC-W chemical transport model – technical description. Atmos. Chem. Phys. 12, 7825–7865.
Sparmacher, H., Fülber, K., Bonka, H., 1993. Below-cloud scavenging of aerosol particles: Particle-bound radionuclides—Experimental. Atmos. Environ. 27, 605–618.
Volken, M., Schumann, T., 1993. A Critical review of below-cloud aerosol scavenging results on Mt. Rigi. Water Air Soil Pollut. 68, 15–28.
Wang, X., Zhang, L., Moran, M.D., 2010. Uncertainty assessment of current size-resolved parameterizations for below-cloud particle scavenging by rain. Atmos. Chem. Phys. 10, 5685–5705.
Zhao, S., Yu, Y., He, J., Yin, D., Wang, B., 2015. Below-cloud scavenging of aerosol particles by precipitation in a typical valley city, northwestern China. Atmos. Environ. 102, 70–78.
Zikova, N., Zdimal, V., 2016. Precipitation scavenging of aerosol particles at a rural site in the Czech Republic. Tellus B 68, 27343 doi: 27310.23402/tellusb.v27368.27343.